UNIVERSITAT POLITÈCNICA DE CATALUNYA BARCELONATECH

Development of control systems and state observers for efficiency and durability improvement in PEM fuel cell based systems

Julio Alberto Luna Pacho

UNIVERSITAT POLITÈCNICA DE CATALUNYA

Programa de Doctorat:

AUTOMÀTICA, ROBÒTICA I VISIÓ

Tesi Doctoral

DEVELOPMENT OF CONTROL SYSTEMS AND STATE OBSERVERS FOR EFFICIENCY AND DURABILITY IMPROVEMENT IN PEM FUEL CELL BASED SYSTEMS

Julio Alberto Luna Pacho

Directors de tesi:
Dra. Maria Serra Prat i Dr. Attila Peter Husar

Gener de 2017

A mis padres

"The best thing for being sad," replied Merlin, beginning to puff and blow, "is to learn something. That's the only thing that never fails. You may grow old and trembling in your anatomies, you may lie awake at night listening to the disorder of your veins, you may miss your only love, you may see the world about you devastated by evil lunatics, or know your honour trampled in the sewers of baser minds. There is only one thing for it then — to learn. Learn why the world wags and what wags it. That is the only thing which the mind can never exhaust, never alienate, never be tortured by, never fear or distrust, and never dream of regretting. Learning is the only thing for you. Look what a lot of things there are to learn."

- T.H. White, The Once and Future King

Agradecimientos

En primer lugar, quisiera expresar mi más profundo agradecimiento a mis directores de tesis Maria Serra y Attila Husar por su orientación, soporte y ánimo durante estos últimos cuatro años. Especialmente agradecer a Maria por la confianza depositada en mi al inicio de mi etapa como investigador. Asimismo, quisiera agradecer con especial cariño a Jordi Riera, por su inestimable ayuda y por las constructivas conversaciones que mantuvimos a lo largo de este periodo.

En segundo lugar, agradecer a Elio Usai y Daniel Hissel, por permitirme realizar mis estancias en sus centros de investigación en Cagliari y Belfort respectivamente. También por las fructiferas colaboraciones resultantes de dichas estancias y las amistades forjadas durante esos periodos.

También quisiera agradecer a todo el personal del *Instituto de Robòtica i Informàtica Industrial (IRII)*, especialmente a todas las personas que forman o han formado parte del grupo de pilas de hidrógeno. Su amistad y profesionalidad han sido una gran fuente de motivación para mi.

Para finalizar, quisiera dar las gracias a mis padres, que me han apoyado constantemente durante todo mi periodo formativo y cuyo cariño y soporte ha sido indispensable para conseguir este logro. También a mi novia Vanoosheh, que ha sido una fuente de soporte incondicional durante esta fase de mi vida.

Soporte financiero: Esta tesis doctoral fue financiada por el *Ministerio de Economía y Competitividad* a través de la beca de Formación de Personal Investigador asociada al proyecto MESPEM (DPI2011-25649).

Julio Alberto Luna Pacho
Barcelona, enero de 2017

Resumen

Las pilas de combustible de membrana de intercambio protónico (PEM por sus siglas en inglés), las cuales utilizan hidrógeno como combustible, proporcionan altas densidades de potencia operando a bajas temperaturas, lo cual reduce el coste de los materiales y el mantenimiento. Las pilas de combustible de tipo PEM son apropiadas para un amplio rango de aplicaciones, tales como estacionarias, de ciclo combinado (CHP por sus siglas en inglés), sistemas portátiles y automoción. El rendimiento y la degradación en sistemas basados en pilas de combustible de tipo PEM están importantemente influenciados por las condiciones internas de la pila de combustible.

En la presente tesis doctoral, se realiza un extenso estudio de modelado y estrategias de observación y control en un sistema basado en pila de combustible de tipo PEM. El objetivo es obtener soluciones avanzadas de control que ayuden en la mejora de la durabilidad y el incremento de la eficiencia de las pilas de combustible. Estas soluciones de control tienen que tener en cuenta las condiciones internas de la pila de combustible, y utilizar esta información para operar el sistema bajo condiciones que garanticen que la degradación del sistema no se incrementa. Al mismo tiempo, los controladores deben garantizar que el sistema alcanza altas eficiencias, considerando las pérdidas por consumos parasíticos de los auxiliares del balance de la planta (BoP por sus siglas en inglés). Las soluciones de observación y control son evaluadas utilizando el perfil de conducción New European Driving Cycle (NEDC) como caso de estudio.

La primera parte de la tesis introduce la motivación tras el presente trabajo y la estructura del documento. Adicionalmente, se estudia en detalle el estado actual de la investigación referente a modelado, observadores de estados y estrategias de control para sistemas basados en pilas de combustible de tipo PEM. Tras este estudio del estado del arte, se presentan los objetivos de la presente tesis doctoral.

La segunda parte de la tesis está enfocada en el desarrollo, implementación y estudio de un modelo de sistema basado en pila de combustible de tipo PEM en un entorno de simulación.

El modelo considera derivadas espaciales de la pila de combustible para representar el comportamiento de la dinámica interna, la cual afecta la eficiencia y el grado de degradación del sistema. En la presente tesis, la degradación de la capa catalizadora se ve reflejada en la pérdida de superficie electroquímicamente activa (ECSA por sus siglas en inglés). La ECSA en la capa catalizadora del cátodo (CCL por sus siglas en inglés) se modela utilizando un modelo de agua de dos fases en el lado del cátodo de la pila con el objeto de representar fielmente su efecto en el voltaje de salida. Los auxiliares del BoP se consideran como consumos parasíticos que deben ser alimentados por la pila de combustible. El consumo parasítico más importante es el procedente del compresor, el cual está modelado para incluir su comportamiento dinámico en las estrategias de control.

Una vez que las ecuaciones del modelo son presentadas, observadores no-lineales de parámetros distribuidos (NDPOs por sus siglas en inglés) basados en modelo se desarrollan en la tercera parte del presente trabajo. Primero, las ecuaciones en derivadas parciales (PDEs por sus siglas en inglés) de la pila de combustible de tipo PEM son discretizadas y reformuladas para obtener el modelo de observación. Utilizando este modelo, se presentan y comparan dos novedosos enfoques de control por modos deslizantes (SMC por sus siglas en inglés) para la observación de las condiciones internas de la pila de combustible, utilizando para ello el perfil de corriente del NEDC como caso de estudio para las simulaciones.

La cuarta parte de la presente tesis está dedicada al control predictivo basado en modelos del sistema de pila de combustible de tipo PEM. En particular, se propone una estrategia de controlador predictivo no-lineal basado en modelo (NMPC por sus siglas en inglés) para la mejora de la eficiencia y a la vez, la mejora del ciclo de vida de la pila de combustible. El uso de los NDPOs en el esquema de control suministra información crítica acerca de las condiciones internas en la pila de combustible. Este hecho permite el diseño de objetivos de control avanzados que no serían realizables utilizando únicamente las limitadas mediciones que están disponibles en los sistemas basados en pilas de combustible de tipo PEM. Se diseña una función de coste multi-objetivo que prioriza entre los diferentes objetivos de control durante el proceso de optimización. Por último, se presenta la discusión de los resultados obtenidos comparando diferentes escenarios de simulación.

La quinta y última parte de la tesis está dedicada a la extracción de conclusiones a partir de los resultados obtenidos a lo largo del documento. Adicionalmente, se proponen distintas líneas de trabajo futuro para continuar la mejora y validación de las estrategias desarrolladas.

Palabras clave: pilas de combustible de membrana de intercambio protónico, observadores no lineales de parámetros distribuidos, control predictivo no lineal basado en modelo.

Resum

Les piles de combustible de membrana d'intercanvi protònic (PEM per les seves sigles en anglès), les quals utilitzen hidrogen com a combustible, proporcionen altes densitats de potència operant a baixes temperatures, reduint el cost dels materials i el manteniment. Les piles de combustible de tipus PEM són apropiades per a un ampli rang d'aplicacions, com ara estacionàries, de cicle combinat (CHP, per les seves sigles en anglès), sistemes portàtils i automoció. El rendiment i la degradació en sistemes basats en piles de combustible de tipus PEM estan importantment influenciats per les condicions internes de la pila de combustible.

En la present tesi doctoral, es realitza un extens estudi de modelatge i estratègies d'observació i control en un sistema basat en pila de combustible de tipus PEM. L'objectiu és obtenir solucions avançades de control que ajudin a la millora de la durabilitat i a l'increment de l'eficiència de les piles de combustible. Aquestes solucions de control han de tindre en compte les condicions internes de la pila de combustible, i utilitzar aquesta informació per operar el sistema sota condicions que garanteixin que la degradació del sistema no s'incrementa. Al mateix temps, els controladors han de garantir que el sistema aconsegueix altes eficiències, considerant les pèrdues per consums parasítics dels auxiliars del balanç de la planta (BoP per les seves sigles en anglès). Les solucions d'observació i control són avaluades utilitzant el perfil de conducció New European Driving Cycle (NEDC) com a cas d'estudi.

La primera part de la tesi introdueix la motivació darrere del present treball i l'estructura del document. Addicionalment, s'estudia en detall l'estat actual de la investigació referent a modelatge, observadors d'estats i estratègies de control per a sistemes basats en piles de combustible de tipus PEM. Després d'aquest estudi de l'estat de l'art, es presenten els objectius de la present tesi doctoral.

La segona part de la tesi està enfocada en el desenvolupament, implementació i estudi d'un model de sistema basat en pila de combustible de tipus PEM en un entorn de simulació. El model considera derivades espacials de la pila de combustible per representar el comportament de la dinàmica interna, la qual afecta l'eficiència i el grau de degradació del sistema. En la present tesi, la degradació de la capa catalitzadora es veu reflectida en la pèrdua de

la cuperfície electroquímicament activa (ECSA per les seves sigles en anglès). La ECSA a la capa catalitzadora del càtode (CCL per les seves sigles en anglès) es modela utilitzant un model d'aigua de dues fases en el costat del càtode de la pila amb l'objecte de representar fidelment el seu efecte en el voltatge de sortida. Els auxiliars del BoP es consideren com a consums parasítics que han de ser alimentats per la pila de combustible. El consum parasític més important és el procedent del compressor, el qual està modelat per incloure el seu comportament dinàmic en les estratègies de control.

Una vegada que les equacions del model són presentades, observadors no-lineals de paràmetres distribuïts (NDPOs per les seves sigles en anglès) basats en model es desenvolupen a la tercera part del present treball. Primer, les equacions en derivades parcials (PDEs per les sigles en anglès) de la pila de combustible de tipus PEM són discretitzades i reformulats per obtindre el model d'observació. Utilitzant aquest model, es presenten i comparen dos nous enfocaments de control per modes lliscants (SMC per les seves sigles en ingllés) per a l'observació de les condicions internes de la pila de combustible, utilitzant per a això el perfil de corrent del NEDC com a cas d'estudi per a les simulacions.

La quarta part de la present tesi està dedicada al control predictiu basat en models del sistema de pila de combustible de tipus PEM. En particular, es proposa una estratègia de controlador predictiu no-lineal basat en model (NMPC per les seves sigles en anglès) per a la millora de l'eficiència i al mateix temps, la millora del cicle de vida de la pila de combustible. L'ús dels NDPOs en l'esquema de control subministra informació crítica sobre les condicions internes a la pila de combustible. Aquest fet permet el disseny d'objectius de control avançats que no serien realitzables utilitzant únicament les limitades mesuraments que estan disponibles en els sistemes basats en piles de combustible de tipus PEM. Es dissenya una funció de cost multi-objectiu que prioritza entre els diferents objectius de control durant el procés d'optimització. Finalment, es presenta la discussió dels resultats obtinguts comparant diferents escenaris de simulació.

La cinquena i última part de la tesi està dedicada a l'extracció de conclusions a partir dels resultats obtinguts al llarg del document. Addicionalment, es proposen diferents línies de treball futur per a continuar la millora i validació de les estratègies desenvolupades.

Paraules clau: piles de combustible de membrana d'intercanvi de protons, observadors no lineals de paràmetres distribuïts, control predictiu no lineal basat en model.

Abstract

Proton exchange membrane (PEM) fuel cells, which use hydrogen as fuel, provide high power densities while operating at lower temperatures, reducing the cost of materials and maintenance. PEM fuel cells are suitable for a broad range of applications, such as stationary, combined heat and power (CHP), portable systems and automotive. Performance and degradation in PEM fuel cell-based systems is greatly influenced by the internal conditions of the fuel cell.

In this doctoral thesis, an extensive study of modelling, observation and control strategies of a PEM fuel cell-based system is performed. The objective is to obtain advanced control solutions that aid to enhance the durability and improve the efficiency of fuel cells. These control solutions have to take into account the internal conditions of the fuel cell and use this information to operate the system under conditions that guarantee that the degradation rate of the fuel cell is not increased. At the same time, the controllers have to guarantee that the system achieves high efficiencies, considering the parasitic power consumption of the balance of plant (BoP) ancillaries. The observation and control solutions are evaluated using the New European Driving Cycle (NEDC) profile as a case study.

The first part of the thesis introduces the motivation of the present work and the structure of the document. Additionally, the current state of the research regarding modelling, state observers and control strategies for PEM fuel cell-based systems are studied in detail. After the study of the state of the art, the objectives of this doctoral work are presented.

The second part of the thesis is focused on the development, implementation and study in a simulation environment of a PEM fuel cell-based system model. The model considers spatial derivatives for the fuel cell in order to represent the internal dynamic behaviour, which affects the efficiency and degradation rate of the system. In this thesis, a special attention is given to the electrochemically active surface area (ECSA). The ECSA in the cathode catalyst layer (CCL) is modelled using a two-phase water model at the cathode side of the fuel cell to better represent its effect on the output voltage. The BoP ancillaries are considered as a parasitic power consumption that has to be delivered by the fuel cell. The

most relevant parasitic power consumption is that of the compressor, which is modelled to include its dynamic behaviour in the control strategies.

Once the model equations are presented, model-based nonlinear distributed parameters observers (NDPO) are developed in the third part of the thesis. First, the partial differential equations (PDE) of the PEM fuel cell-based system are discretised and reformulated to obtain the observation model. Using this model, two novel sliding mode control (SMC) approaches for the observation of the internal conditions of the fuel cell are presented and compared, using the NEDC current profile as the case study for the simulations.

The fourth part of the thesis is devoted to model-based predictive control of the PEM fuel cell-based system. In particular, a nonlinear model predictive control (NMPC) strategy is proposed to improve the efficiency and at the same time, enhance the lifetime of the fuel cell. The use of the NDPOs in the control scheme facilitates critical information about the internal conditions of the fuel cell. This allows to design advanced control objectives that would not be achievable if using only the limited measurements that are available in PEM fuel cell-based systems. A multi-objective cost function that can prioritise between the different objectives of the controller during the optimisation procedure is designed. Finally, a discussion of the results obtained comparing different prioritisation between control objectives is provided.

The fifth and last part of the thesis is devoted to extract conclusions from the results that were obtained through the document. Moreover, different future work lines are proposed in order to continue with the improvement and validation of the developed strategies.

Keywords: proton exchange membrane fuel cells, distributed parameters models, nonlinear distributed parameters observers, nonlinear model predictive control.

Contents

List of Figures

List of Tables

Nomenclature

Throughout this doctoral dissertation, spatial and discretised systems are treated, denoting the spatial variables as x, y and z. Subscript i denotes the i gas reactant species while subscripts n and j are associated to the y and z discretisation volumes. For instance, $c_{i,(j,n)}$ refers to the concentration value of the i-th gas at the j (z-direction) and n (y-direction) discretisation volumes. The superscripts are associated to an element of the PEM fuel cell, being A the anode, C the cathode and M the membrane. Moreover, the superscript k is used for equations valid both for the anode and cathode sides. All column vectors are denoted by bold style, e.g. $\mathbf{x}$. Matrices are denoted by bold upper case, e.g., $\mathbf{A}$. Scalars are denoted by non-bold style, e.g., B. Real numbers are denoted by $\mathbb{R}$. Observed variables are denoted by the caret symbol, e.g., $\hat{x}$. Discrete time is represented by k and the notation $x(k+i|k)$ will denote a future value (at time $k+i$) of the variable x which is assumed at time k [6].

Roman letters

A	Area	m^2
C	Volumetric electrical capacitance	F m^{-3}
C_p	Heat capacity	J K^{-1}
c_i	Concentration of i-th gas	mol m^{-3}
D_i	Diffusion coefficient of i-th gas	m^2 s^{-1}
D_W	Self-diffusion coefficient of water in the membrane	m^2 s^{-1}
E	Electromotive force	V
f^V	Surface enlargement factor	—
F	Faraday constant	C mol^{-1}
h	Molar enthalpy	J mol^{-1}
I	Electrical current	A
i	Current density	A m^{-2}
i_0	Exchange current density	A m^{-2}
K	Darcy's constant	m^2 s^{-1} Pa^{-1}
k	Thermal conductivity	W m^{-1} K^{-1}
L	Fuel cell length	m
L_x	Gas channel width	m
L_z	Gas channel depth	m
M	Molar mass	kg mol^{-1}
$\dot{m}$	Mass flow	kg s^{-1}
$\dot{n}_i$	y-direction flux of i-th gas	mol m^{-2} s^{-1}
$\dot{n}_{i,in}$	Inlet molar flux of i-th gas	mol m^{-2} s^{-1}
n	Number of electrons per molecule of H_2	—
n_c	Number of fuel cells in the stack	—
n_y	Number of y-direction discretisation volumes	—
n_z	Number of z-direction discretisation volumes	—
P	Electrical power	W
p	Pressure	Pa
q	Charge	C mol^{-1}
r	Reaction rate	mol m^{-2} s^{-1}
R	Gas constant	J mol^{-1} K^{-1}
t	Time	s

t_W	Water transport number in the membrane	—
T	Temperature	K
u	Specific internal energy	J kg^{-1}
v	Flow velocity	m s^{-1}
V	Voltage	V
W_{el}	Electrical work	J mol^{-1}
x	Space coordinate	m
X	Ion exchange capacity	mol kg^{-1}
y	Space coordinate	m
z	Space coordinate	m

Greek letters

α	Cathode charge transfer coefficient	—
δ	Thickness of layer in y-direction	m
ε	Porosity coefficient	—
κ	Electrical conductivity of the membrane	Ω^{-1} m^{-1}
λ	Stoichiometry ratio	—
Λ	Water content	$\frac{N(H_2O)}{N(\text{polymer})}$
μ	Electrochemical potential	J mol^{-1}
Φ	Electrical potential	V
ρ	Density	kg m^{-3}
σ	Membrane conductivity	Ω m^{-1}
ξ	Mole fraction	—

Subscripts, superscripts

A	Anode side
amb	Ambient conditions
C	Cathode side
$coolant$	Coolant
dry	Dry conditions
$evap$	Evaporated
gen	Generated
i	Component index on anode and cathode sides

in	Input flux
j	j-th discretisation volume along the z-direction
k	Anode side ($k = A$) or cathode side ($k = C$)
l	Liquid
M	Membrane
n	n-th discretisation volume along the y-direction
r	Chemical reaction term
ref	Reference value
S	Solid
v	Vapour

List of Acronyms

AFC	Alkaline Fuel Cell
BD	Back Diffusion
BoP	Balance of Plant
BPP	Bipolar Plate
CFD	Computational Fluid Dynamics
CHP	Combined Heat and Power
CL	Catalyst Layer
CCL	Cathode Catalyst Layer
DMFC	Direct Methanol Fuel Cell
DOB	Disturbance Observer
EDC	European Driving Cycle
EIS	Electrochemical Impedance Spectroscopy
EOD	Electro-Osmotic Drag
FCHS	Fuel Cell Hybrid Systems
GDL	Gas Diffusion Layer
HHV	Higher Heating Value
HOSM	Higher Order Sliding Mode
LHV	Lower Heating Value
MCFC	Molten Carbonate Fuel Cell
MAE	Mean Absolute Error
MEA	Membrane Electrode Assembly
MIMO	Multiple-input and Multiple-output
MPC	Model Predictive Control
NDPO	Nonlinear Distributed Parameter Observer

NEDC	New European Driving Cycle
NMPC	Nonlinear Model Predictive Control
PAFC	Phosphoric Acid Fuel Cell
PDE	Partial Differential Equation
PEM	Proton Exchange Membrane
PEMFC	Proton Exchange Membrane Fuel Cell
SISO	Single-input and Single-output
SMC	Sliding Mode Control
SOFC	Solid Oxide Fuel Cell
STA	Super-Twisting Algorithm

Part I

Preamble

Chapter 1

Introduction

1.1 Motivation

As energy consumption increases, society, industry and governments have become aware of the necessity to deploy new sustainable energy systems that can cut down the problems associated with the use of fossil fuels and other non-renewable energies. The use of these energy sources produces carbon emissions and is not sustainable on a long-term time horizon. Accomplishing this technological and social shift requires high amounts of investments and research efforts addressed to alternative and clean energy sources. Moreover, the problems of storage and transportability have to be taken into account when studying future sustainable energy generation solutions. Therefore, researchers [7, 8, 9] have pointed out that it is necessary for future energy systems to make use of energy carriers that can be produced from renewable power sources.

Research studies [10, 11] have concluded that energy generation systems that use hydrogen can be a potential solution to satisfy the present and future energy demands without additional carbon emissions. Hydrogen as an energy vector has significant advantages compared to other power carriers and its use can aid to reduce gas emissions and to diversify the energy generation market [12]. This is mainly because hydrogen has the possibility to be produced from renewable primary energy sources (i.e. solar and eolic). Moreover, hydrogen can be burned directly (i.e. gas turbine) to obtain electricity producing only water and heat as by-products or may either be used to feed a fuel cell. Long-term storage is also a characteristic of hydrogen, making it perfect for long distance transport and mobile applications.

Proton exchange membrane (PEM) fuel cells, which use hydrogen as fuel and have high power densities while operating at low temperatures, are gaining increasing attention as clean and efficient energy conversion devices for a broad range of applications: automotive, stationary combined heat and power (CHP) and portable systems. Researchers from all over the world are dedicating a great effort to improve efficiency, reduce degradation and decrease the production costs of PEM fuel cell technology. In order to optimise their performance, PEM fuel cell systems require active control and therefore, in-depth knowledge of the system dynamics, which include multi-physics phenomena such as fluid mechanics, thermal dynamics and chemical kinetics.

To compete with other power generation systems, such as internal combustion engines for automotive applications, PEM fuel cells have to achieve a similar efficiency and cost. Cost reduction by means of materials improvement has already been achieved during the last decade [13]. Nevertheless, there is still room for improvement regarding the efficiency and durability of PEM fuel cells. Efficiency and durability are associated with the operating conditions of the system which are subject to changes due to cycling and current demand. Furthermore, the internal conditions of the PEM fuel cell also affect the performance and durability of the system.

An important subject when studying efficiency in a PEM fuel cell based system is the balance of plant (BoP), which is the study of all the subsystems that are needed to guarantee the proper operation of the fuel cell. When studying the efficiency of a fuel cell system, the majority of authors only consider to the actual PEM fuel cell efficiency. Nevertheless, important parasitic losses are caused by the elements of the BoP, making it necessary to include these losses when studying the efficiency of the system and when designing control strategies. Typically, a fuel cell system BoP includes the oxidant supply, fuel supply, heat management, water management, power conditioning and control subsystems [4].

Focusing on the fuel cell, a key aspect when studying its performance and efficiency is the understanding of the water transport mechanisms and the liquid and vapour water distribution along the different internal layers of the system. The correct water distribution is essential to obtain an optimum fuel cell performance. For instance, liquid water can obstruct the uniform distribution of reactants and cause uneven current densities over the active area of the fuel cell [14, 15]. However, online measuring of the internal water distribution in a PEM fuel cell is technologically impossible nowadays. Therefore, proper models for the

estimation of internal liquid and vapour water content in the fuel cell are required. Using the aforementioned estimations, control strategies may be able to manage the water content in a PEM fuel cell to improve their performance through a better water distribution and membrane humidification. The temperature of the system and the relative humidity of the injected gases can be used as manipulated variables to regulate the water content and its distribution in the fuel cell.

Concerning degradation, the lifetime of PEM fuel cells is mainly reduced as a result of catalyst metal degradation and carbon-support corrosion. Both of these degradation mechanisms are linked and supplement each other [16, 17, 18] because the platinum (Pt) catalyses the oxidation mechanism of the carbon-support, accelerating the carbon loss. At the same time, the loss of carbon releases carbon-supported Pt particles and therefore, active surface area loss. Three degradation categories can be distinguished [19]: baseline degradation, cycling degradation and incident-induced degradation. The baseline degradation is caused due to long-term material degradation and it is irreversible and unavoidable (it exists as long as the fuel cell is operating). Moreover, degradation mechanisms are accelerated by cycling conditions [19]. Finally, severe degradation occurs when the fuel cell is subjected to a unexpected incident which may cause, for example, global or local reactant starvation. Controllers can aid to avoid starvation and thus, reduce the impact of cycling as well as the impact of unexpected operating changes.

Modelling plays a key role in the research areas of control and health monitoring of PEM fuel cells. In fact, in order to develop control strategies that aid to improve efficiency and enhance the durability of PEM fuel cell systems, mathematical models are necessary. Effects of the operating conditions on the fuel cell performance have been studied by several authors with different experimental approaches. However, while experimental analysis gives back reliable information about the performance of the system, it can be exceedingly expensive and inaccurate (not being able to represent the internal dynamics of the fuel cell). Mathematical models aid to reduce experimentation costs. Moreover, models can be used to develop control and observation techniques that study aspects of the fuel cell that can not be analysed conveniently through experimental measurements.

While control-oriented models of PEM fuel cells have been historically characterised to be simple and efficient, the improvement of computational capacity allows to develop more detailed and complex models designed with control purposes in mind. Specifically, distributed

parameters models that represent the spatially distributed variables of PEM fuel cells have gained importance over the last years. These spatially distributed variables are associated with the performance of the system, thus making it necessary to study distributed parameters models of PEM fuel cells.

Estimation of internal states and performance variables in PEM fuel cell systems is a topic directly related with the implementation of advanced control techniques to improve efficiency and durability. While a certain amount of measurements are feasible using the existing sensor technology, there are parts of the system that are inaccessible because of its structure. Distributed parameter models combined with model-based state estimation techniques is a novel solution to study the internal conditions in PEM fuel cells, with the possibility of using this information in a control strategy. Additionally, the use of mathematical observation tools is directly related with the reduction of the number of sensors and their associated cost [20], hence state observation tools can aid in the reduction of the overall cost of PEM fuel cell systems.

In order to contribute to improve the state of the art of the described fuel cell research topics, this doctoral thesis is focused on combining nonlinear distributed parameter models of PEM fuel cells with novel nonlinear model-based estimation and control strategies. This approach will aid to increase the efficiency of the PEM fuel cell considering the BoP subsystems and enhance the fuel cell durability. Following the preceding discussion, the implemented distributed parameter model has to be accurate enough and include state-of-the-art water transport and water content dynamic models to better represent the real behaviour of the fuel cell.

1.2 Outline of the Thesis

This doctoral thesis is structured in five main parts: Preamble, Modelling, State Observation, Control and Concluding Remarks. The summary of the contents of each chapter is as follows:

Preamble

Chapter 2: State of the Art

A review of the literature related with PEM fuel cell modelling, estimation and control is provided in this chapter. First, a general introduction to PEM fuel cells and their behaviour is presented. Then, the state-of-the-art models for PEM fuel cells are analysed. Afterwards, nonlinear state observation techniques are introduced with special focus on state estimation in PEM fuel cells. Finally, model-based control techniques for PEM fuel cells of the literature are studied.

Chapter 3: Objectives

After analysing the current state of the art, the objectives of this doctoral thesis are defined considering the possible improvements and contributions that can be made to science. First, the general objective of the research is described. From this general objective, the specific objectives regarding the different topics within this doctoral dissertation are depicted.

Modelling

Chapter 4: PEM Fuel Cell System Modelling

In this chapter, the equations for the selected simulation PEM fuel cell model are given: a *1+1D nonlinear distributed parameters* model with a *two-phase water* model. The *distributed parameters* condition of the model will aid to develop state observers that can estimate internal variables of the system that can not be measured but affect the performance and durability. The aim of the *two-phase water* model is to represent with detail the water dynamics that happen in PEM fuel cells when subjected to a wide set of operating conditions, which have an important effect on the fuel cell voltage. The simulation model considers the *nonlinear* dynamics of the PEM fuel cell.

After the mathematical simulation model of the PEM fuel cell is presented, the rest of auxiliary subsystems of the BoP are introduced, including the compressor that feeds the PEM fuel cell with pressurised air. Besides the compressor, the secondary BoP elements include the thermal management subsystem, the coolant and hydrogen recirculation pumps, the humidifier system and all the valves of the system.

The implementation issues of the simulation model are also studied in this chapter. Partial differential equations (PDE) are converted into ordinary differential equations (ODE) by means of a spatial discretisation. Moreover, the simulation framework is introduced briefly.

The case study used in the simulations is presented: the New European Driving Cycle (NEDC). This case study is used to test the observation and control strategies and to calibrate the parameters of the model through published experimental data. The NEDC is a standard driving cycle used by many authors to test engineering solutions and fuel economy strategies in passenger cars.

State Observation

Chapter 5: Observation Problem

In this chapter the observation problem is described and an *observation model* is selected from the discretised equations set presented in Chapter 4. This observation model is selected considering the future control objectives of durability enhancement and efficiency improvement of the PEM fuel cell system.

Chapter 6: Nonlinear Distributed Parameter Observer with Disturbance Estimation

To estimate the internal conditions of the PEM fuel cell system described in Chapter 4, first, a nonlinear distributed parameter observer (NDPO) with *disturbance estimation* is introduced.

This observer uses a model-based estimation strategy with a nonlinear disturbance observer (NDOB) in parallel. The observation model comes from the PDEs discretisation presented in Chapter 5. The reaction rates and water transport flows that cross the membrane of the PEM fuel cell are considered as disturbances of the observation model, henceforth the need of a NDOB implementation to estimate them.

Chapter 7: High Order Sliding Mode Observer

A second observation approach is studied in this chapter. A novel high order sliding mode (HOSM) estimation technique, based on the observation model from Chapter 5 is developed to estimate the internal variables of the PEM fuel cell (states and disturbances).

Compared with the observer presented in Chapter 6, the HOSM observer includes the estimation of the reactions and water transport terms integrated within the observer structure, avoiding the requirement of an additional NDOB and improving the convergence time and accuracy of the observer.

Control

Chapter 8: Control Problem

In this chapter, the control model is presented. It has a similar structure as the observation model in Chapter 5. However, besides the PEM fuel cell PDEs, the control model also includes the air supply and thermal management subsystems presented in Chapter 4 in order to include efficiency improvement objectives in the cost function.

After the control model is described, the control problem is stated. Then, the control problem objectives are condensed in the nonlinear cost function that will be optimised in the control scheme described in Chapter 9.

Chapter 9: Nonlinear Model Predictive Control for PEM Fuel Cell Systems

This chapter presents the control solution proposed in this doctoral thesis in order to enhance the durability and improve the efficiency of the PEM fuel cell based system (including the parasitic losses of the BoP). The proposed control solution is based on nonlinear model predictive control (NMPC).

After studying the performance of the control strategy for three different cases for a NEDC current demand profile, results are presented and discussed. These results are obtained using the novel observation strategy from Chapter 7. The computational times needed to solve the closed-loop scheme are analysed to evaluate the feasibility of the proposed control solution implemented in real-time applications.

Concluding Remarks

Chapter 10: Conclusions and Future Work

In this chapter, the accomplishment of the objectives outlined in Chapter 3 is analysed. A relation of contributions derived from the research is presented. Moreover, conclusions and future lines of work are extracted from the results obtained during this doctoral dissertation.

Appendices

The appendices are devoted to display some additional information regarding this doctoral dissertation. The first appendix is related with the air feeding system model, which includes additional equations and parameters that are out of the scope of the main body of this work. The second appendix includes the numerical parameters used during the simulations.

1.3 Related Publications

Several works related with the described research topics have been published already or have been submitted in international journals and congresses. The updated (January 2017) relation of publications is included in this section.

1.3.1 International Journal Articles

The research activity has been disseminated in the following international journal articles:

- **[21]** J. Luna, C. Ocampo-Martinez and M. Serra. *Nonlinear predictive control for the concentrations profile regulation under unknown reaction disturbances in a fuel cell anode gas channel.* Journal of Power Sources, vol. 282, pages 129–139, 2015.
- **[22]** J. Luna, A. Husar and M. Serra. *Nonlinear distributed parameter observer design for fuel cell systems.* International Journal of Hydrogen Energy, vol. 40 (34), pages 11322–11332, 2015.
- **[23]** J. Luna, E. Usai, A. Husar and M. Serra. *Nonlinear observation in fuel cell systems: A comparison between disturbance estimation and high-order sliding-mode techniques.* International Journal of Hydrogen Energy, vol. 41 (43), pages 19737–19748, 2016.
- **[24]** J. Luna, S. Jemei, N. Yousfi-Steiner, A. Husar, M. Serra and D. Hissel. *Nonlinear predictive control for durability enhancement and efficiency improvement in a fuel cell power system.* Journal of Power Sources, vol. 328, pages 250–261, 2016.

Another journal article has been submitted and is currently under revision:

- **[25]** J. Luna, E. Usai, A. Husar and M. Serra. *Enhancing the efficiency and lifetime of a proton exchange membrane fuel cell using nonlinear model predictive control with nonlinear observation.* Submitted to the IEEE Transactions on Industrial Electronics.

1.3.2 Congress Communications

The following relation of national and international congress communications is also an outcome of this doctoral work:

- **[26]** J. Luna, C. Batlle, C. Kunusch, J. Riera, M. Sarmiento-Carnevali and M. Serra. *Observation of the internal states of a PEMFC anode gas channel.* In XXXIV Jornadas de Automática, Terrassa, Spain, 2013.
- **[27]** J. Luna, A. Husar and M. Serra. *State observers design for PEMFC systems.* In Ibero-American Conference on Hydrogen and Fuel Cells, Bellaterra, Spain, 2014.
- **[28]** J. Luna, C. Ocampo-Martinez and M. Serra. *Nonlinear predictive control for the concentrations profile regulation in a PEM fuel cell anode gas channel.* In European Control Conference, Strasbourg, France, pages 1807–1812, 2014.
- **[29]** J. Luna, E. Usai, A. Husar and M. Serra. *Distributed parameter nonlinear state observer with unmatched disturbance estimation for PEMFC systems.* In 6th International Conference on Fundamentals and Development of Fuel Cells, Toulouse, France, 2015.
- **[30]** J. Luna, E. Usai, A. Husar and M. Serra. *State Estimation in Fuel Cell Systems: A Sliding Mode Approach.* In V Iberian Symposium on Hydrogen, Fuel Cells and Advanced Batteries, Tenerife, Spain, 2015.
- **[31]** J. Luna, N. Yousfi-Steiner, S. Jemei, A. Husar and M. Serra. *Nonlinear model predictive control methodology for efficiency and durability improvement in a fuel cell power system.* In World Hydrogen Energy Conference, Zaragoza, Spain, 2016.
- **[32]** J. Luna, E. Usai, A. Husar and M. Serra. *Observation of the Electrochemically Active Surface Area in a Proton Exchange Membrane Fuel Cell.* In 42nd Annual Conference of IEEE Industrial Electronics Society, Firenze, Italy, 2016.

Chapter 2

State of the Art

This chapter provides an overview of previous research related to this doctoral thesis, which includes PEM fuel cell modelling, nonlinear state observation and nonlinear control. It introduces the general framework to design model-based observers and controllers for PEM fuel cell systems.

2.1 Fuel Cells and Hydrogen

Fuel cells are devices that deliver electric power from electrochemical reduction and oxidation reactions. They have a wide variety of potential applications including mobile, stationary, CHP and portable applications. The process of electric generation is performed in a continuous way while the fuel cell is fed with the enough quantity of reactants, namely fuel and oxidant. Fuel cell systems are in constant development and there is great expectancy in the industrial and automotive communities about the mass commercialisation of this technology.

A common classification of fuel cells is given by their electrolyte. In Table 2.1, the six most important fuel cell types available on the market are compared. The operating temperature is a key aspect when selecting a fuel cell technology, and it is possible to establish the difference between low temperature (AFC, PEM and DMFC) and high temperature (PAFC, MCFC, SOFC) fuel cells.

The most common fuel for fuel cells is hydrogen, an energy vector that can be obtained via electrolysis or reforming. One of the principal benefits of hydrogen fed fuel cells (over

TABLE 2.1: Fuel cell types [2]

Fuel cell type	Mobile ion	Operating temperature	Applications and notes
Alkaline (AFC)	OH^-	50-200°C	Used in space vehicles, e.g. Apollo, Shuttle
Proton exchange membrane (PEM)	H^+	30-100°C	Vehicles and mobile applications, and for lower power CHP systems
Direct methanol (DMFC)	H^+	20-90°C	Suitable for portable electronic systems of low power, running for long times
Phosphoric acid (PA)	H^+	220°C	Large numbers of 200 kW CHP systems in use
Molten carbonate (MCFC)	CO_3^{2-}	650°C	Suitable for medium to largescale CHP systems, up to MW capacity
Solid oxide (SOFC)	O^{2-}	500-1000°C	Suitable for all sizes of CHP systems, 2 kW to multi-MW

combustion engines for instance) is that the only by-products of the reaction are water and heat [4]. To reduce the emissions associated to hydrogen production to just water and heat, the electrolysis of the hydrogen needs to be performed from clean and renewable energies (i.e. wind turbines or solar panels). However, natural gas reforming is the first source of hydrogen currently.

While the advantages of fuel cells over other energy production methods are evident, some disadvantages exist as with any other technology. The major barrier for the mass market commercialisation of fuel cells is the cost. Nowadays fuel cell technology is only economically competitive in specialised applications. Another significant drawback is the power density (produced power per unit of volume or mass), where combustion engines outperform fuel cells [33]. Currently, researchers all over the world are working to improve fuel cell efficiency and durability and also reduce their manufacturing costs.

Multiple choices exist when selecting a fuel cell [2]. Among them, PEM fuel cells are attracting the most attention from researchers and industry because of their simplicity, viability and quick startup procedures. Particularly, PEM fuel cells are suitable for highly dynamic applications such as residential [34] and domestic CHP [35] and automotive systems [36].

Another advantage of fuel cells is their lack of moving parts, which allows to design very silent systems.

The multi-layer structure domain of a classic PEM fuel cell is shown in Figures 2.1a and 2.1b. The proton conducting membrane is located between the porous catalyst layers (CL), gas diffusion layers (GDL) and bipolar plates (BPP) on each side of the membrane. The flow channels are mechanised into the BPPs.

Figure 2.1c shows the schematic representation of the involved electrochemical reactions. At the anode side, the hydrogen diffuses from the channel through the GDL and reacts in the CL according to

$$2H_2 \rightarrow 4H^+ + 4e^-. \tag{2.1}$$

The membrane in a PEM fuel cell allows the transport of protons from the anode to the cathode catalyst layer. At the same time, it has to block the electrons, forcing them to travel through the external circuit between the anode and cathode, generating electrical current. The protons that travel through the membrane react with the oxygen in the cathode and the returning electrons, generating water and heat according to

$$O_2 + 4H^+ + 4e^- \rightarrow 2H_2O. \tag{2.2}$$

The generated water can leave the system through any gas channel. Moreover, it accumulate in the membrane or other parts of the cell. Water management is one of the most common problems when working with PEM fuel cells. Tools that perform water surveillance and management in order to increase the overall efficiency and decrease the degradation of PEM fuel cells are being developed [37, 38].

The overall reaction of a PEM fuel cell corresponds to the oxidation of hydrogen in the following exothermic reaction:

$$2H_2 + O_2 \rightarrow 2H_2O. \tag{2.3}$$

In a single cell at open circuit, approximately 1.2 V are generated. However, when a load is connected to the fuel cell, the cell voltage is decreased significantly, as will be seen in Section 2.1.6.

It is common to connect a certain amount of single cells in order to produce higher potentials. A group of PEM fuel cells connected in series is known as a PEM fuel cell stack. Figure 2.2

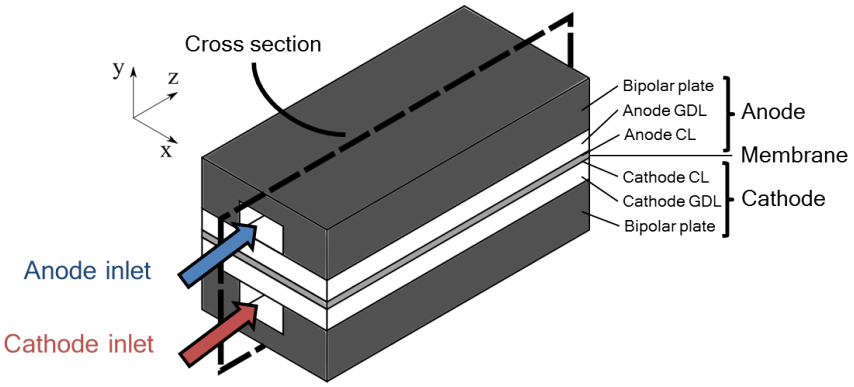

(A) Single-channel PEM fuel cell representation

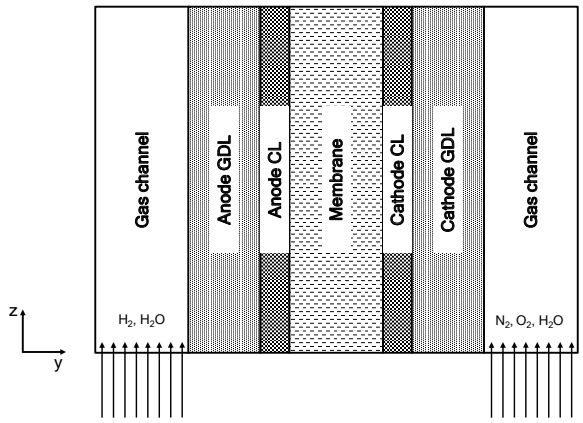

(B) PEM fuel cell modelling domain

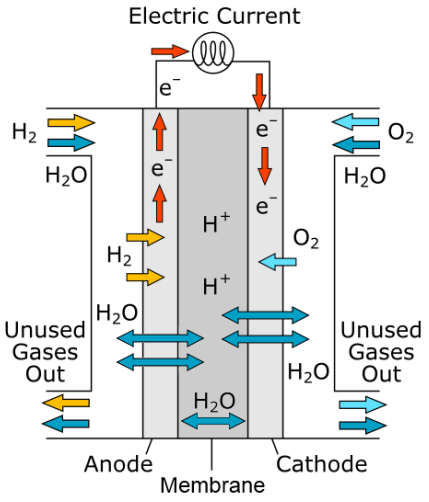

(C) PEM fuel cell electrochemical reactions

FIGURE 2.1: PEM fuel cell representation

shows a commercial stack built from interconnected single cells. The end plates in Figure 2.2 are used to maintain the structural balance of the stack by applying pressure on the cells. Moreover, they prevent the gases from escaping and they have inlet and outlet manifolds for the reactants.

2.1.1 Heat of Reaction

The reaction described by Equation (2.3) is the same as the reaction of hydrogen combustion. By definition, a combustion is an exothermic process, meaning that a certain amount of energy is released in the process. Rewriting Equation (2.3)

$$H_2 + \frac{1}{2} O_2 \rightarrow H_2O + \text{heat}. \tag{2.4}$$

FIGURE 2.2: PEM fuel cell stack [1]

To determine the amount of heat released during the combustion it is necessary to compute the difference between the heats of formation of products and reactants [4]. Applying this to the reaction in Equation (2.4) the resulting difference is

$$\Delta H = (h_f)_{H_2O} - (h_f)_{H_2} - \frac{1}{2}(h_f)_{O_2}. \tag{2.5}$$

In Table 2.2, the heats of formation at ambient pressure and 25°C for the reactants and products of Equation (2.4) are presented. Substituting the heats of formation in Equation (2.5) at ambient conditions (liquid water), it is obtained that

$$\Delta H = -286.02\,\text{kJ mol}^{-1} - 0 - 0 = -286.02\,\text{kJ mol}^{-1}. \tag{2.6}$$

By convention, the negative sign of a chemical reaction enthalpy means that heat is being released in the reaction. Rewriting the overall chemical reaction (2.4) it can be written that

$$H_2 + \frac{1}{2}\,O_2 \rightarrow H_2O\,(l) + 286.02\,\text{kJ mol}^{-1}, \tag{2.7}$$

which in this case the positive value of the heat means that it is a product of the reaction. Equation (2.7) is only valid at 25°C and atmospheric pressure, where water is in liquid form.

TABLE 2.2: Enthalpies and entropies of formation for fuel cell reactants and products at ambient pressure and 25°C [4]

	h_f [kJ mol^{-1}]	s_f [kJ mol^{-1} K^{-1}]
Hydrogen, H_2	0	0.13066
Oxygen, O_2	0	0.20517
Water [liquid], H_2O (l)	-286.02	0.06996
Water [vapour], H_2O (g)	-241.98	0.18884

2.1.2 Hydrogen HHV and LHV

The enthalpy of hydrogen combustion reaction obtained in Equation (2.7) is the maximum amount of energy that can be extracted from the reaction at 25°C and ambient pressure. It corresponds with the liquid water production. This enthalpy is also known as the hydrogen's higher heating value (HHV).

If there is an excess of oxygen, the combustion of the hydrogen will produce water in the form of vapour with a certain amount of unburned oxygen and other products if air is used in the reaction process. When vapour water is generated, the combustion equation can be written as

$$H_2 + \frac{1}{2} O_2 \rightarrow H_2O\,(g) + 241.98\,\text{kJ mol}^{-1}, \tag{2.8}$$

and the generated heat in this case is known as the hydrogen lower heating value (LHV).

The difference between HHV and LHV is the heat of evaporation of water at ambient pressure and 25°C

$$H_{fg} = 286.02\,\text{kJ mol}^{-1} - 241.98\,\text{kJ mol}^{-1} = 44.04\,\text{kJ mol}^{-1}. \tag{2.9}$$

2.1.3 Theoretical Electric Output

The final objective of a PEM fuel cell system is to produce electrical energy to feed a load connected to it. However, not all the energy of the reaction can be transformed into electrical energy. The portion of HHV that can be converted into electricity is known as Gibbs free energy and is expressed by the following equation:

$$\Delta G = \Delta H - T\Delta S, \tag{2.10}$$

meaning that some irreversible losses appear due to the creation of some entropy ΔS. In a similar manner as with the thermal energy in Equations (2.7) and (2.8), the difference between entropies of products and reactants is the magnitude ΔS, that can be expressed as

$$\Delta S = (s_f)_{H_2O} - (s_f)_{H_2} - \frac{1}{2}(s_f)_{O_2}. \tag{2.11}$$

The values of s_f for the products and reactants are presented in Table 2.2 and substituting them into Equations (2.10) and (2.11) it is obtained that, at 25°C, out of 286.02 kJ mol^{-1} of energy, 237.34 kJ mol^{-1} can be converted into electrical energy and the remaining 48.68 kJ mol^{-1} are converted into thermal energy (heat).

2.1.4 Theoretical Fuel Cell Potential

The ideal electrical work (W_{el}) is the product of the number of electrons participating in the reaction n, times the ideal potential of the cell (E_r) by the Faraday's constant (F) [4]

$$W_{el} = nFE_r, \tag{2.12}$$

moreover, as expressed in Equation (2.10), the maximum electrical energy that can be obtained from the reaction process is given by the Gibbs free energy (ΔG). Hence, it can be written that

$$W_{el} = -\Delta G. \tag{2.13}$$

Substituting Equation (2.12) into Equation (2.13), the value of the ideal potential of the cell can be computed

$$E_r = -\frac{\Delta G}{nF} = \frac{237.34 \text{ J}}{2 \cdot 96.485 \text{ C}} = 1.23 \text{ V}. \tag{2.14}$$

Which means that at 25°C, the theoretical voltage that a PEM fuel cell can offer is 1.23 V, justifying the need of a stack if higher voltages are required by the load.

2.1.5 Theoretical Fuel Cell Efficiency

As with any power generation system, the theoretical efficiency in PEM fuel cell systems is defined as the relation between the theoretical useful energy output and the total energy

input. In the case of a fuel cell without heat utilisation, the useful energy output is the electrical energy produced and the energy input is the enthalpy of hydrogen. Assuming an ideal case where there are no voltage drops and all the hydrogen is reacted, all the Gibbs free energy can be transformed into electrical energy, the theoretical fuel cell efficiency can be expressed as

$$\eta = \frac{\Delta G}{\Delta H} = \frac{237.34}{286.02} = 83\%. \tag{2.15}$$

The previous efficiency is valid at 25°C and atmospheric pressure. With other operating conditions, the value of η will vary. Moreover, in practical applications the efficiency is lower than the theoretical efficiency.

2.1.6 Fuel Cell Irreversibilities. Causes of Voltage Drop

If the fuel cell is not connected to an external circuit, which means that there is no external current, it would be expected that the potential was similar to the theoretical value presented in Equation (2.14). Nevertheless, in practice this potential (called the open circuit potential) is usually around 1 V, significantly less than the theoretical value. This fact suggests that voltage losses exist in the fuel cell even when no external load is connected to the system. In the literature [2], four causes of voltage drop are analysed.

1. **Fuel crossover and internal currents:** Despite the membrane being theoretically impermeable to reactant gases, a small amount of hydrogen will diffuse through the electrolyte from anode to cathode, reacting with the oxygen at the cathode side and producing the loss of two electrons for each diffused hydrogen molecule that will not travel through the external circuit, and thus, will not be used to generate potential. Internal currents is a similar concept as fuel crossover but in this case the electrons diffuse through the membrane to the cathode side of the fuel cell. In previous studies [4], fuel crossover and internal currents have been considered negligible because they are several orders of magnitude lower than other voltage drops in the system. Hence, it is usual not to include them in the polarization curve equation.

2. **Activation losses:** An initial voltage difference from equilibrium is needed in order to start the electrochemical reaction [4]. This effect is known as activation losses, which occur both at the anode and cathode sides of the fuel cell. However, the activation

losses are significantly higher at the cathode side since oxygen reduction is a slow reaction that requires higher activation overpotentials than the hydrogen oxidation at the anode side. Disregarding the effect of hydrogen oxidation, the Tafel equation, that expresses the total fuel cell activation losses, is as follows:

$$\Delta V_{act} = \frac{RT}{\alpha nF} \ln\left(\frac{i}{i_0}\right), \tag{2.16}$$

where α is the cathode charge transfer coefficient and i_0 the cathode current exchange density. Note that ΔV_{act} in Equation (2.16) increases with higher values of the demanded current density i. i_0 quantifies the rate of the chemical reaction at the CL in the absence of net electrolysis and zero overpotential. It is a function of the fuel cell temperature T, the oxygen pressure and the active catalyst surface at the CL [4].

3. **Ohmic losses:** Resistance of the flow of electrons through the electrically conductive components and resistance of the flow of ions through the membrane cause a voltage drop. Ohmic losses can be expressed by Ohm's law

$$\Delta V_{ohm} = iR_{ohm}, \tag{2.17}$$

where R_{ohm} is the total cell internal resistance, that includes ionic, electronic and contact resistance. Electronic and contact resistance can be considered constant parameters. However, the ionic resistance of the membrane depends on the membrane liquid water content and may change during operation of the fuel cell.

4. **Concentration losses:** When the reactant gases are consumed rapidly at the electrode by the electrochemical reaction, concentration gradients appear. Such gradients alter the partial pressure of the reactants and thus the fuel cell potential [4]. Concentration losses can be modelled with the expression

$$\Delta V_{conc} = \frac{RT}{nF} \ln\left(\frac{i_L}{i_L - i}\right), \tag{2.18}$$

where i_L is the limiting current density defined as the current density that causes oxygen exhaustion, which occurs when the oxygen is consumed faster than it can reach the catalyst surface during the electrochemical reaction, leaving this surface with a null reactant concentration.

2.1.7 Polarization Curve

Ohmic losses occur basically in the membrane of the PEM fuel cell, but activation and concentration voltage losses appear at both anode and cathode. Hence, the cell voltage is expressed as

$$V_{cell} = E_r - (\Delta V_{act} + \Delta V_{conc})^A - (\Delta V_{act} + \Delta V_{conc})^C - \Delta V_{ohm}, \tag{2.19}$$

where E_r is the ideal potential voltage of Equation (2.14). However, anode activation and concentration losses can be neglected ($(\Delta V_{act} + \Delta V_{conc})^A \approx 0$ [4]). Substituting Equations (2.16), (2.17) and (2.18) into Equation (2.19) a relationship between fuel cell potential and current density is obtained. This is known as the fuel cell polarisation curve and it follows the expression

$$V_{cell} = E_r - \frac{RT}{\alpha nF} \ln\left(\frac{i}{i_0}\right) - \frac{RT}{nF} \ln\left(\frac{i_{L,c}}{i_{L,c} - i}\right) - iR_{ohm}. \tag{2.20}$$

The polarization curve is shown in Figure 2.3. Note the difference between the theoretical fuel cell potential and the real potential curve, as expected from Equation (2.20). At low current densities there is a rapid initial fall in voltage caused by the activation losses. When the current is high enough, the predominant effect are the ohmic losses, as displayed by the linear behaviour of the voltage loss. When the current is higher (over 800 mA cm^{-2}), the concentration losses cause the voltage to fall rapidly.

2.1.8 Dynamic Behaviour

Some authors have studied the effect on stoichiometry (ratio between the reacted fuel and input molar flows) and current of PEM fuel cells [39] when considering rapid changes in the voltage, concluding that for high anode and cathode stoichiometry values, where there is an excess of reactants, no overshoot or undershoot dynamic behaviours in the output current were observed. From this study, it can be concluded that the response can be modelled with first order dynamic systems at high stoichiometries. For low stoichiometries, where the system shows fuel-starving conditions, the non-uniform distribution of the reactants causes the current response to behave like a pseudo-second-order dynamic system. Hence, it seems obvious that nonlinear models are needed to represent the full spectrum of the dynamics.

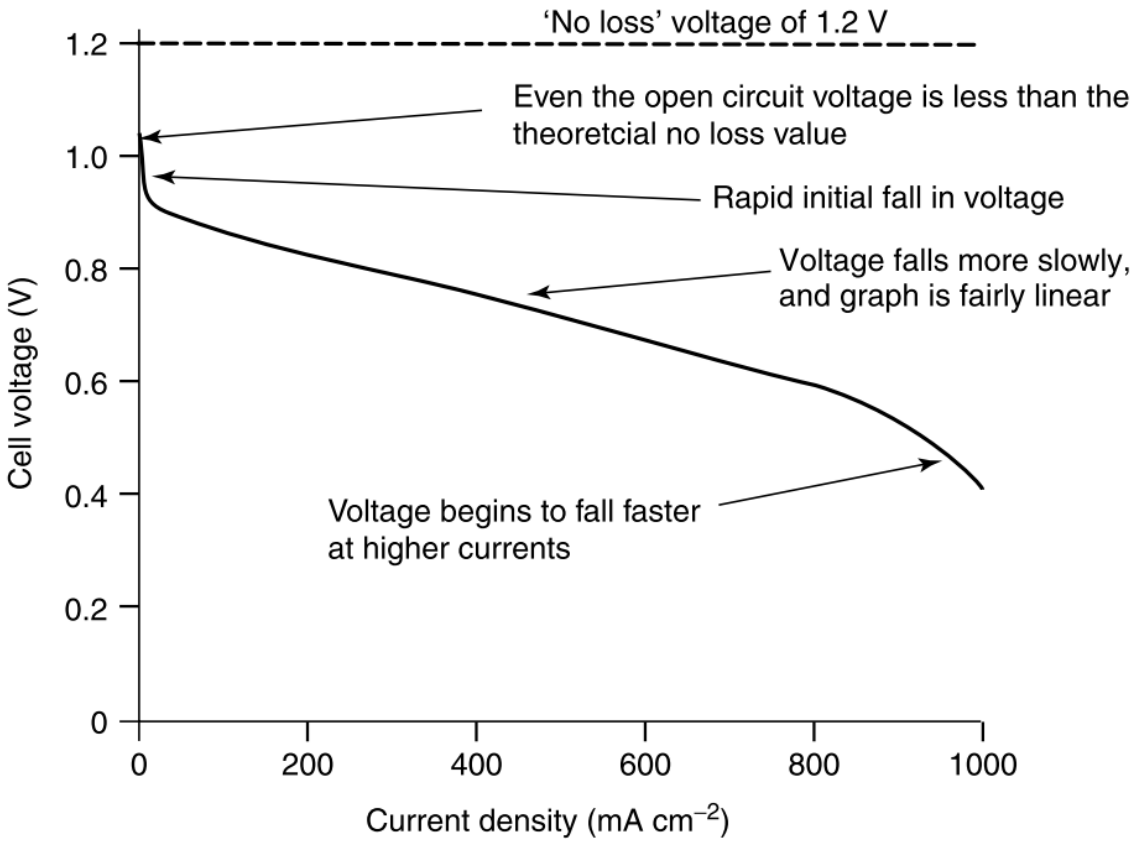

FIGURE 2.3: PEM fuel cell polarization curve [2]

Other works [40] study the effects of diverse operating conditions (i.e. different feed gas humidities, temperatures, air pressures, fluid dynamic variables, etc.). Humidity in both anode and cathode inlet gases have significant effects on the fuel cell performance. Temperature is also found to have a great repercussion in the dynamic behaviour of the system since increasing the temperature in the PEM fuel cell evaporates water, this produces dynamic changes in the response of the system.

2.2 PEM Fuel Cell Models

The use of PEM fuel cell simulation models allows to test, among others, different operation conditions (temperatures, gas molar inflows, etc.), geometric configurations of the systems and material properties without the need to use a real plant. Moreover, measuring internal variables in a real PEM fuel cell is virtually impossible due to its enclosed construction. Therefore, models are also needed to estimate the internal behaviour of the plant.

PEM fuel cell systems require highly complex multi-physics dynamic models. To model each of the physical phenomena that occurs during the operation, a representation based on mass, momentum and energy conservation, as well as electric current transport laws is proposed [4]. The following list enumerates the main phenomena modelled in the literature of PEM fuel cell based systems:

- Darcy's equation for fluid flow in gas channels and porous media
- Fick's Law for gas diffusion through porous media
- Stefan-Maxwell equation for multispecies diffusion through porous media
- Fourier's Law for heat conduction
- Faraday's Law to relate electrical current and reactant consumption in an electrochemical reaction
- Butler-Volmer equation to relate electrical current and potential
- Ohm's Law for electrical current conduction

When modelling PEM fuel cells, it is common to consider a series of assumptions and simplifications related to the gas properties, temperatures and membrane dynamic behaviour to reduce the computational complexity. Moreover, when implementing the model-based controllers, the models have to be used in real-time applications, thus, a trade-off between response-time and modelling accuracy has to be made.

Water transport modelling is crucial when studying the behaviour of PEM fuel cell systems since it plays a key role in the proton electrical conductivity and gas transport. Detailed water models are present in the literature. In [41] the membrane liquid water content is included as a state. In [42] a two-phase water transport model is included to study the effect of generation, evaporation and desorption rates on the performance of PEM fuel cells with different electrode pore size distributions.

When studying the literature, PEM fuel cell models are divided into different groups depending on the axis or section of study. Particularly, the most common models present in the bibliography are:

- Lumped parameter models
- 1D models perpendicular to the membrane

- 1+1D models
- 2D models or partial cross-section, yz or xz-direction
- 2D+1D models
- 3D models

In the 1D modelling domain, [43] studied the dynamic behaviour of the membrane and gas channels water transports of a PEM fuel cell with a distributed parameter model under isothermal conditions. In [44] a more advanced model which includes non-isothermal conditions is developed and compared with experimental data to investigate the effect of various design and operating conditions on the fuel cell performance. In [42] a multiscale 1D model of an open-cathode PEM fuel cell is developed, implementing a novel three-phase water model (liquid, vapour and membrane water content) that represents the variation of the ECSA with respect to the liquid to vapour ratio of water at the cathode catalyst layer.

Regarding more complex 2D and 1+1D models, recent research works [15] have succesfully developed distributed parameter models focused on control and estimation applications. In [45], a model that focuses on the fluid hydrodynamics and electrochemical kinetics of a PEM fuel cell is studied. These models are useful to represent more accurately than 1D models the dynamics of PEM fuel cells without the computational complexity of 3D models.

More complex 3D and 2D+1D models can also be found in the literature. However, the computational burden of these models is high and the optimization of the simulation procedures is a topic being studied by many researchers. Simplifications are usually common in 3D models to improve the simulation time. Computational Fluid Dynamics (CFD) research works such as [46] study the interactions between mass transport and the electrochemical kinetics of the system using a numerical model which is validated against published experimental data. In [47] a three-dimensional, two-phase and non-isothermal model is developed to simulate the behaviour of a PEM fuel cell. The model is then validated against real data. The parameter sensibility analysis of the aforesaid model is studied in [48] for a total of 11 major parameters that can influence the behaviour of the system.

The research of PEM fuel cell models is not only focused on the open-loop behaviour of the system; in [49] a 1D control-oriented model is developed to avoid fuel cell oxygen starvation with air flow controllers design. As it has been said, modelling the behaviour of the water

inside the system is a key aspect when studying the behaviour of a PEM fuel cell. Degradation, as introduced in Section 2.3, can be modelled as a reduction of the electrochemically active area (ECSA).

2.3 Degradation in PEM Fuel Cell Systems

While PEM fuel cell based systems are a promising technology, numerous countries, including the United States, Japan and Europe, are making noticeable economic efforts in order to extend their lifetime expectancy. The durability of PEM fuel cells represents one of the greatest technological challenges for their commercial implementation. The technical targets established by the United States Office of Energy Efficiency and Renewable Energy for PEM fuel cells are presented in Table 2.3.

Table 2.3: PEM fuel cells long-term targets [5]

Application	Efficiency	Durability (hours)
Transportation	60%	5.000
Stationary	40%	40.000
Consumer electronics ($< 50W$)	—	5.000
Auxiliary power unit ($3 - 30kW$)	40%	35.000

Different mechanisms of degradation affect the durability of PEM fuel cells [50]. Nevertheless, the lifetime of PEM fuel cells is mainly reduced as a result of catalyst metal degradation and carbon-support corrosion. Both of these degradation mechanisms are linked and supplement each other [16, 17, 18] because the platinum (Pt) catalyses the carbon-support oxidation. At the same time, the loss of carbon releases carbon-supported Pt particles and therefore it produces active surface area loss. In the literature, accelerated durability tests have been reported to describe degradation mechanisms in PEM fuel cells [51] and other types of fuel cells [52].

With respect to the degradation occurrence, three degradation categories can be distinguished [19]: baseline degradation, cycling degradation and incident-induced degradation. The baseline degradation is due to long-term material degradation and it is unavoidable (it

exists as long as the fuel cell is operating). Moreover, degradation is accelerated by cycling conditions [19]. Finally, severe degradation occurs when the fuel cell is subject to an unexpected incident which may cause global or local reactant starvation.

2.4 Hybridisation in PEM Fuel Cell Systems

Fuel cell hybrid systems (FCHS) are composed of a PEM fuel cell that acts a the primary power source and an energy storage system (ESS) that contributes to supply the power demand and stores the power generated by the fuel cell when there is a surplus between the demanded and the generated power. In general, ESSs in FCHSs are batteries or super-capacitor banks. A diagram with the PEM fuel cell, the auxiliary systems and the ESS is shown in Figure 2.4.

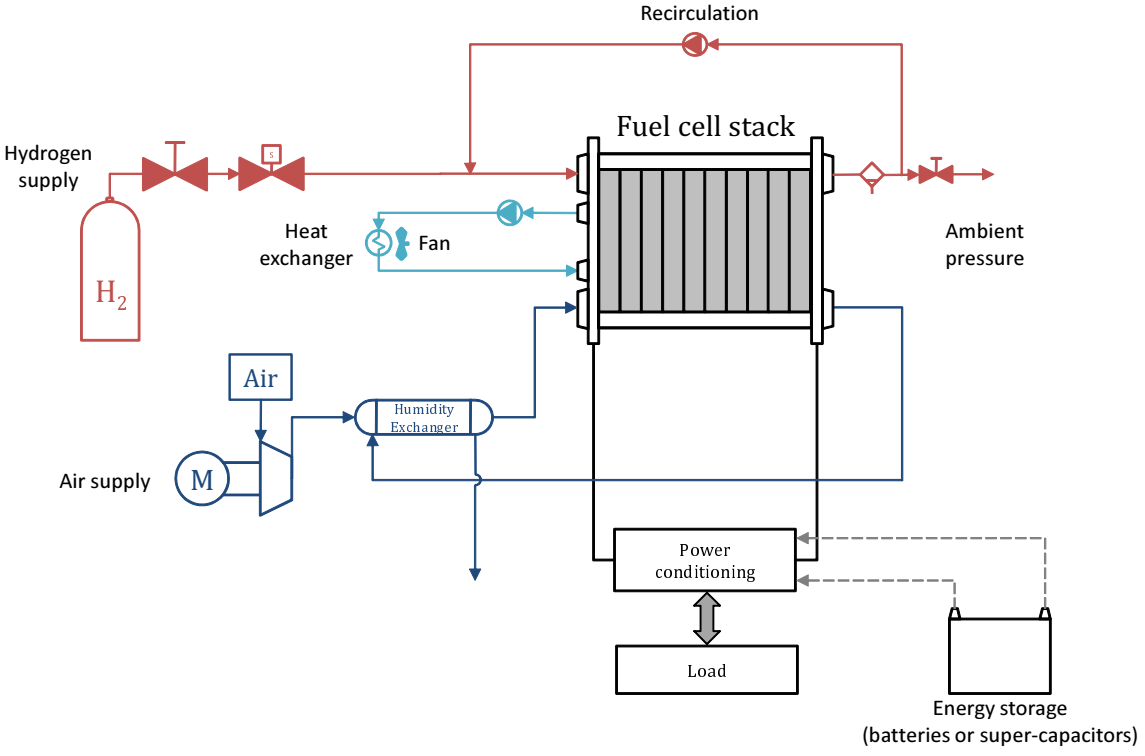

FIGURE 2.4: Scheme of a FCHS

The main advantage of using an ESS with the fuel cell is the ability to overcome the relatively slow fuel cell transient response [53], specially if the hydrogen comes from a reformer. This slow dynamic response also shortens the life expectancy of the fuel cell [54] due to active area loss when the system is submitted to cycling. Moreover, when introducing a battery or

a super-capacitor in parallel with the fuel cell, the additional element can store the surplus power and deliver it when necessary without increasing the fuel consumption, thus improving the hydrogen economy of the system. An additional advantage of FCHSs is the reduction of the warm-up time of the fuel cell system to reach full power [53].

Regarding the disadvantages of FCHSs, the inclusion of an ESSs increases the complexity of the system. For example, the scheme presented in Figure 2.4, requires additional power electronics to manage the power flows from and to the ESS. FCHSs also require more complex control strategies since the controller has to decide among the different operating modes of the hybrid system.

With respect to the operating modes of FCHSs, the addition of an ESS to the scheme allows the system to operate under four different energy flows [53]:

1. **Fuel cell supplying:** The fuel cell, being the primary power source, supplies the energy directly to the load.
2. **ESS charging:** If the power demanded by the load is lower than the power generated by the fuel cell system, it is possible to charge the ESS with the surplus energy.
3. **Regenerating:** In FCHSs, specially in automotive applications, the power demanded by the load can be negative, such as in the case of regenerative braking. This negative power demand can be redirected to the ESS to charge it with the energy from the load.
4. **Boosting:** A boosting energy flow can be supplied to the load using at the same time power from the fuel cell and from the ESS.

How to manage efficiently the energy flows is the objective of the energy management strategies (EMS). Different EMSs for fuel cell systems can be found in the literature [53, 55, 56].

The applications of FCHSs are mainly two: stand-alone residential applications and fuel cell hybrid vehicles [53].

Stationary applications have fast-changing load demands, e.g. turning on an oven. This makes it necessary to have an auxiliary ESS as well as a fuel cell to meet the power demands. Moreover, residential applications often generate the hydrogen with a reformer, which has slow dynamic responses to sudden changes of the load [57].

Regarding fuel cell hybrid vehicles, most of the major automotive manufacturers are interested in this technology [54]. Hydrogen fuel cells have been demonstrated to be a viable alternative to the conventional internal combustion engine vehicles. The use of ESS along with the fuel cell improves the hydrogen economy via recovering energy through regenerative braking and the batteries or super-capacitors can aid to supply the highly changing power demand associated with driving [53].

The focus of this doctoral thesis is on the fuel cell exclusively, disregarding the hybridisation. Nevertheless, the strategies developed in this work are focused on the low-level control of the fuel cell and they can be applied to hybrid systems.

2.5 State Estimation in PEM Fuel Cells

In the control theory community, nonlinear state observation and unknown input reconstruction is one of the most important research topics [58]. The linear case for concentrated parameter models is a well-studied problem for single-input and single-output (SISO) and multiple-input and multiple-output (MIMO) systems [59] and currently researchers are focusing their attention on the nonlinear outlook of the observation problem.

Added to the nonlinearities of the system, uncertainty conditions in the mathematical model and/or in the inputs, increase the complexity of the state reconstruction problem. Through the use of the dynamic representation of the plant, it is possible to implement techniques used in robust control, such as linear matrix inequalities [60], $\mathcal{H}_\infty$ [61] or sliding mode control (SMC) [62] to handle an hypothetical set of bounded uncertainties in the state estimation problem.

SMC is a nonlinear control method that applies a discontinuous signal to force the system to *slide* along a sliding surface. This sliding surface is chosen depending on the required dynamic response of the system. SMC is insensitive to model uncertainties and disturbances [63], making it an interesting tool to use in the design of observers and controllers for fuel cell-based systems. Moreover, SMC is not model-based, which is a desirable property in order to reduce the computational burden of the observation and control solutions in complex systems, such as is the case of fuel cells.

The discontinuous signal that SMC uses to slide along the desired sliding surface can not be used in all systems. This is because the switching motion can damage actuators, resulting in system stresses and oscillations. Because of this, second-order SMC is employed. Second-order and higher-order SMC is the generalisation of SMC to perform the control input with higher derivatives [64] of the sliding surface, reducing the switching effect that could damage the actuators [65].

A powerful tool to design controllers and observers for nonlinear systems is a variation of the second-order SMC technique: the super-twisting algorithm (STA) [66]. The main contribution of this technique in the case of nonlinear state observers is that it solves the estimation problem in finite time even in the presence of model and input uncertainties. Therefore, the STA approach facilitates the implementation in an actual real plant due to its inherent robustness and low computational burden [67], since it does not need the model of the plant to operate.

Two main categories of models are used in the literature to design model-based nonlinear estimators: lumped and distributed parameters models. Lumped (or concentrated) parameters models are mostly employed, either linear [68] and nonlinear [69]. In the case of the distributed parameters models approach of the problem, the development and implementation of the observers increases in complexity due to the discretisation technique. The observability analysis is also a complex issue in these models. Nevertheless, some research works are present in the literature that include observers for the estimation of distributed parameters models [70].

The subject of estimation of internal states and performance variables in PEM fuel cell systems is still marginally studied, but it has an increasing industrial interest, since its real implementation involves a better knowledge of the fuel cell and a reduction of the number of sensors and their associated cost. Furthermore, PEM fuel cells are highly nonlinear systems with fast dynamics. Henceforth, nonlinear state estimation in PEM fuel cell systems is an engaging research topic. Considering that water management is crucial when operating a PEM fuel cell system, addressing the estimation of the water content in the membrane is mandatory [71]. Other works present the nonlinear estimation of the inlet oxygen flows through the measurement of the output manifold partial pressures [72]. In other research publications, the estimated variables include the supply and return manifold oxygen pressures [73] and the hydrogen partial pressure in the anode channel [74].

In [75] an output-feedback control of a complete PEM fuel cell system is studied. The control objective is to regulate the oxygen excess ratio in the fuel cell. The estimation of the states is done measuring available physical quantities and employing a combination between second and third order sliding mode algorithms. It is demonstrated through simulation that the use of nonlinear observers allows to design novel controllers. The approach is successfully demonstrated in a simulation environment considering practical implementation issues such as parameter uncertainties and measurement noise.

2.6 Control Strategies for PEM Fuel Cells

Critical characteristics of PEM fuel cell based systems such as their robustness, efficiency and life expectancy are strongly related to their proper control. Controllers design is always based on some model of the system. Specifically, model-based controllers integrate a system model into the control algorithm. Control-oriented models require specific characteristics and obtaining them may be a difficult task.

In [76] and [77] control-oriented models are proposed. While [76] presents an accurate and validated control-oriented model, the high degree of complexity makes this model not immediately suitable for nonlinear control design. In [77], a three state air supply subsystem is explained and experimentally validated. The rest of the BoP is not included in this study.

To simplify the complex PEM fuel cell dynamics, in [78] a linear identification of the system time constants on an experimental PEM fuel cell system, under specific operating conditions, is obtained and a black box model of the overall system is developed. From this identification, a linear model of the PEM fuel cell-based system is developed and experimentally validated. A controller is designed in order to regulate the outputs to a desired reference value.

2.6.1 Control Objectives and Control Techniques for PEM Fuel Cells

Different control objectives and control techniques applied to PEM fuel cell systems can be found in the literature. The control of the anode and cathode stoichiometry, minimising input flow rates [49], control of temperature and water management are among the most frequent control objectives [76]. Other control objectives include the regulation of the stack power, the tracking of a desired voltage value and the improvement of the system efficiency.

The range of control techniques is wide; linear controllers, unfalsified controllers [79], predictive controllers and variable structure controllers are some of the most used control techniques as analysed in review works [80, 81]. As any real system, PEM fuel cells are plenty of fast dynamic behaviours and variables bounded by physical limits that should be considered when designing a control law, e.g., voltages, currents, flows. Moreover, the definition of several operational constraints, in the same way as the variable bounds, should be taken into account when formulating a closed-loop control scheme. The available manipulated variables in fuel cell-based systems include: the hydrogen and air inlet flow, the hydrogen and air inlet pressure, the fuel cell temperature, the reactants humidification, the coolant temperature and the coolant flow. Moreover, in PEM fuel cells a high degree of uncertainty exists due, for instance, to degradation mechanisms. Thus, the designed control laws have to be sufficiently robust.

2.6.2 Control of the Oxygen Excess Ratio

In a PEM fuel cell system the air supply is limited by the gas feeding dynamics and the air compressor dynamics. When the load demand changes abruptly, the oxygen in the PEM fuel cell cathode gas channel reacts instantaneously. If the oxygen level present in the channel can not guarantee a correct reaction due to the load demand change, the catalyst can be damaged. This phenomenon is known as oxygen starvation in the literature. To guarantee the sufficient oxygen supply is an important problem regarding the control of PEM fuel cells. The parameter that models the excess of oxygen in the cathode is known as the oxygen excess ratio (λ_{O_2}) [4] or oxygen stoichiometry

$$\lambda_{O_2} = \frac{\dot{n}_{O_2,in}}{\dot{n}_{O_2,react}}, \tag{2.21}$$

where $\dot{n}_{O_2,in}$ is the cathode inlet oxygen mass flow and $\dot{n}_{O_2,react}$ is the reacting oxygen mass flow. This reacting flow depends on the PEM fuel cell current I

$$\dot{n}_{O_2,react} = M_{O_2}\frac{n_c I}{4F}, \tag{2.22}$$

where M_{O_2} is the molar mass of the oxygen, n_c is the number of cells in the stack and F is the Faraday constant. Rewriting Equation (2.21)

$$\lambda_{O_2} = \frac{4F}{M_{O_2} n} \frac{\dot{n}_{O_2,in}}{I}. \tag{2.23}$$

Therefore, when the current demand increases, the oxygen stoichiometry is immediately reduced. To reduce CCL degradation, optimal λ_{O_2} values have to be guaranteed in order to avoid oxygen starvation situations.

In [82], a net power control strategy based on linear matrix inequalities (LMI) is proposed to track an optimal power demand while guaranteeing an optimal oxygen stoichiometry in an electrical vehicle. The optimal references are generated by a supervisor that takes into account the actual power demand and the actual value of the inlet air flow. A comparison with the internal control of a commercial PEM fuel cell is made and the results show improvement with the proposed control strategy. A comparison between linear and nonlinear PEM fuel cell models is made, remarking the differences in the dynamic response of the two modelling approaches. The linear model is used to design a controller and the simulation results are compared to real data from a Nexa internal control system.

On-line control implementation is an important issue in the literature. In [83] a self-tuning PID control strategy is proposed to regulate the oxygen excess ratio. The controller includes an artificial neural network model to update the control parameters in real time during the operation of the PEM fuel cell. Results show great regulation and disturbance rejection capabilities and the on-line implementation is feasible due to the simplicity of the controller.

In [84] a simplified mathematical model for calculating the oxygen excess ratio of a PEM fuel cell system in real time applications is presented. While it shows that these reduced models are suitable for certain applications, it is concluded that the model does not represent the full dynamics of a real PEM fuel cell system. Henceforth, additional studies to implement more advanced controllers have to be made for further improvement.

2.6.3 Control of the Hydrogen Supply

Hydrogen starvation is not as critical as oxygen starvation when feeding the system with pressurised hydrogen. Nonetheless, the use of pressurised hydrogen in dead-ended operation

can damage the membrane if the differential pressure between the anode and the cathode gas channels is too high. To avoid this, a purge valve can be installed at the anode output to reduce the pressure quickly in case of necessity and also remove excess of water [85] and cross-over nitrogen.

The problem of hydrogen starvation becomes more critical when the consumed hydrogen comes from an on-board fuel processor. These kind of reformers have relatively slow transitory responses and the consumption of hydrogen has to be controlled to guarantee that starvation does not occur in the CL. In [86] a dynamic model for hydrogen consumption of a PEM fuel cell stack is introduced. The model is used to investigate the dynamic characteristics of output voltage under hydrogen purge operation.

In [87] a control strategy to generate the requested power while minimising the fuel consumption is studied. The proposed controller actuates over the air pump voltage and a DC/DC switching converter to regulate the fuel cell current. The oxygen flow and stack current determine the minimum amount of required hydrogen flow, which is manipulated with a control valve. The proposed solution is experimentally validated contrasting the performance against a commercial PEM fuel cell stack internal control system.

2.6.4 Control of the System Efficiency

The output power of the PEM fuel cell has to meet the power demanded by the load through the appropriate manipulation of the control variables. Ideally, this has to be achieved with high efficiency values. It is generally accepted in the PEM fuel cell community that the air supply subsystem has a crucial role in the improvement of the performance of the system [88]. In particular, the air pressure and the oxygen excess ratio (2.21) have the greatest effect when studying the efficiency of the system.

The fuel cell polarisation curve and, therefore, the stack efficiency is mainly determined by the oxygen partial pressure in the catalyst layer of the cathode. This partial pressure is determined by the air pressure and the oxygen stoichiometry. In [89] a pressure control using second order sliding mode control is developed to guarantee an homogeneous pressure distribution along the anode and cathode gas channels to improve efficiency and reduce membrane degradation.

The total PEM fuel cell system net power is defined in [90] as the difference between the power produced by the fuel cell and the power consumed by the compressor to fed the air into the system. This work considers different load currents to study the trade-off between the maximum fuel cell voltage and minimum compressor consumption. The result of the study is the optimal oxygen flow rate (maximum net power) for each load current demand.

Actuating over other parameters of the PEM fuel cell system can aid to improve the efficiency. An important parameter for the correct performance of the fuel cell is the temperature of the system. Another is the humidification of the reactants. In [91] a proportional control for the coolant system is proposed. The effects of the temperature control on the dynamics and performance are studied. While improvement is achieved, the authors remark that the design of an observer for the internal parameters of the system is needed to implement advanced controls and real-time diagnosis.

2.6.5 Multi-objective Control

Until now, the analysed controllers presented single control objectives or control objectives regarding independent subsystems of the PEM fuel cell. The use of more advanced control techniques should allow the implementation of multi-objective control as stated in [92]. In this work different control strategies are studied to try to achieve different operational objectives at the same time. The controller developed includes the main control problems studied in PEM fuel cell systems: tracking of a desired output voltage, avoidance of starvation and maximisation of efficiency. A model based predictive approach is used to achieve these objectives.

A controllability versus efficiency analysis of a PEM fuel cell is studied in [93]. It considers the inputs to be the air compressor voltage and the hydrogen mass flow rate. The outputs are the stack voltage and the anode-cathode pressure difference. From a nonlinear model, a linearisation is made at selected operating points to perform the study. Diagonal control structures with PI controllers are implemented to improve the efficiency of the PEM fuel cell. A trade-off relation between the controllability and the efficiency of the PEM fuel cell was found in this work. Therefore, it is possible to find a balance between control objectives and the optimal efficiency of the system.

2.6.6 Models for Advanced Control of PEM Fuel Cells

Recently, more complex (with more detail) control-oriented models that reproduce the most influencing features of a laboratory PEM fuel cell system through ordinary nonlinear differential equations were presented. In [94] the control-oriented model is developed combining first principle physical laws and empirical analysis based on experimental data. This model is used for the design of advanced control algorithms such as SMC [95], linear parameter-varying control [96] and variable structure control [97].

In order to continue improving PEM fuel cells performance, distributed parameter models have acquired importance [14, 15]. This is due to the increasing concern about the effects of the variation of certain variables along the system. These effects include degradation of the CLs and the membrane as introduced in Section 2.3.

There are not many works in the literature that consider the efficiency improvement and reduced degradation aspects that were discussed in this chapter. In conclusion, advanced control strategies for PEM fuel cell-based systems should consider these two aspects in order to guarantee high efficiencies while extending the lifetime of the fuel cell. These control strategies have to be model-based in distributed parameters models in order to represent the internal dynamic behaviour that affects the cell efficiency and the degradation of the different fuel cell components.

2.7 Beyond State of the Art

This chapter introduces some fundamental notions regarding modelling, state estimation and control in PEM fuel cell systems. Moreover, it summarizes the state of the art of these research topics. Through the study of the state of the art, it has been concluded that, in order to implement more advanced control techniques that aid in the improvement of the PEM fuel cell technology, detailed models are needed. To make use of the full potential of these models, nonlinear state estimators have to be developed to implement multi-objective closed-loop control strategies.

In this doctoral dissertation, a *nonlinear distributed parameters model with two-phase water transport* has been chosen as the modelling framework for the PEM fuel cell description since

it efficiently deals with three main aspects of PEM fuel cells. Firstly, the *two-phase water transport* at the cathodic side allows for a better characterisation of the voltage generated by the stack. Secondly, the *distributed parameters* aspect of the model will allow to characterise the internal conditions of the system and use this information to avoid global and local starvation by means of nonlinear observation and control. Finally, the *nonlinear* framework allows to represent the conditions of the system in a wide range of operating points, where the fuel cell may naturally operate.

As mentioned beforehand, the estimation of the internal variables in PEM fuel cells is going to be achieved in this doctoral work through model-based nonlinear observation. In particular, novel *sliding mode* algorithms, based on the PEM fuel cell *nonlinear distributed parameter model*, are designed and tested in a simulation environment to estimate the internal conditions that greatly affect the performance and durability of PEM fuel cells.

Regarding the control aspect of this doctoral dissertation, in the corresponding chapters, *multi-objective nonlinear model predictive control* is proposed to improve the efficiency of PEM fuel cell based systems (considering the auxiliary subsystems) and at the same time, enhance the durability of the fuel cell. This control strategy also makes use of the aforementioned *nonlinear distributed parameters model*. Its combination with the *nonlinear observation strategies* are the main contribution of this doctoral work to the state of the art.

Chapter 3

Objectives

This doctoral thesis addresses model-based nonlinear control and observation applied to PEM fuel cells considering their related auxiliary subsystems. The novelty of the proposed observers and controllers is that they are based on a detailed distributed parameter model that represents the internal nonlinear dynamic behaviour of the PEM fuel cell.

3.1 General Objective

The objective of this doctoral thesis is to study advanced model-based estimation and control techniques and combine them to design strategies that aim to improve the global efficiency and enhance durability in PEM fuel cell based systems. It is expected that the developed strategies can be applied to a wide range of fuel cell systems and applications, such automotive, stationary and combined heat and power.

3.2 Specific Objectives

The above described general objective is divided in the following list of specific objectives:

1. Modelling and analysis of PEM fuel cell based systems

- To develop a nonlinear distributed parameters model of a PEM fuel cell that has enough detail to represent all the relevant nonlinear phenomena affecting efficiency, durability and dynamic response, which include:
  - Fluid, electrochemical and two phase water distribution consideration at the cathode side
  - Water distribution and transport along the different layers of the PEM fuel cell consideration
- To implement the developed model in a simulation environment
- To study the global efficiency of the PEM fuel cell based system considering the parasitic losses of the BoP
- To study the trade-offs between efficiency, durability and dynamic response of PEM fuel cell systems in order to state the control objectives and the variables to be observed

2. State observers design

   - To design nonlinear state observers that estimate critical unmeasurable variables that affect the efficiency and durability of the PEM fuel cell system. These observers should:
     - Be based on a distributed parameters PEM fuel cell model
     - Use sliding control approaches to implement the observers without increasing the complexity of the observation model
     - Have fast convergence to the real value of the variables

3. Controllers design

   - To design advanced model-based control techniques to achieve the following control objectives:
     - Enhance durability avoiding situations that cause PEM fuel cell degradation (i.e. cycling, local and global starvation, etc.)
     - Increase global efficiency of the system considering the BoP auxiliary elements
     - Guarantee the proper dynamic response of the plant

3.3 Methodology

To accomplish the aforementioned objectives the first step is to develop and implement, in a simulation environment, a PEM fuel cell model that represents its highly nonlinear and coupled dynamic behaviour. Moreover, this model has to have spatial derivatives that describe the internal conditions of the fuel cell, which greatly affect its performance and can not be measured using conventional sensors.

After the model implementation, the next step is to study the state of the art of control theory regarding nonlinear distributed parameters systems. The main focus of the study is going to be the observers and controllers that can be implemented using the distributed parameters PEM fuel cell simulation model as a substitute of a real plant.

Beyond state of the art controllers and observers are developed in this doctoral work to improve the efficiency and enhance durability of PEM fuel cell based systems while guaranteeing their reliability. While the experimental validation of the controllers and observers is not studied in this work, the New European Driving Cycle (NEDC) current profile is used to simulate a real automotive application in order to test and discuss the proposed strategies in a simulation environment.

Part II

Modelling

Chapter 4

PEM Fuel Cell System Modelling

4.1 Introduction

In this chapter, a simulation model of a PEM fuel cell is presented along with the model of the auxiliary BoP subsystems. The main characteristics of the model are:

- 1+1D or quasi-two dimensional representation of the gas and water transports [15]
- Two-phase multi-scale water transport mechanisms with mesoscopic filling effects model at the cathode side [42]
- Compressor model to feed the cathode with air [98]
- Dynamic stack temperature model [99] with statistical gradient model for each cell of the stack

During the development of this work, the simulation model has gone through several iterations. In the present chapter, the most complete version of the model is described. Moreover, in Parts III and IV the observation and control models are presented. These models make use of a simplified version of the simulation model as it will be explained in the corresponding chapters.

A crucial aspect of the simulation model is that it is detailed enough to represent the internal dynamic behaviour of the PEM fuel cell and at the same time it can be used efficiently in a model-based control strategy. This is the reason for the selection of the 1+1D model

[15] that is used in this doctoral work. In this model, the reactant gas flows are described by partial derivatives in one direction coupled to the transports through the membrane electrode assembly (MEA), which are represented as lumped parameters perpendicular to the gas flows, hence the 1+1D denomination of the model. Specifically, the gas flows are described with concentration partial derivatives along the gas channels. Figure 4.1 shows the input gas flows ($\dot{n}_{H_2,in}$, $\dot{n}_{O_2,in}$, $\dot{n}_{N_2,in}$ and $\dot{n}_{H_2O,in}$), the concentrations and the perpendicular transports ($\dot{n}_{H_2}$, $\dot{n}_{O_2}$, $\dot{n}_{N_2}$ and $\dot{n}_{H_2O}$) with their z-direction dependency.

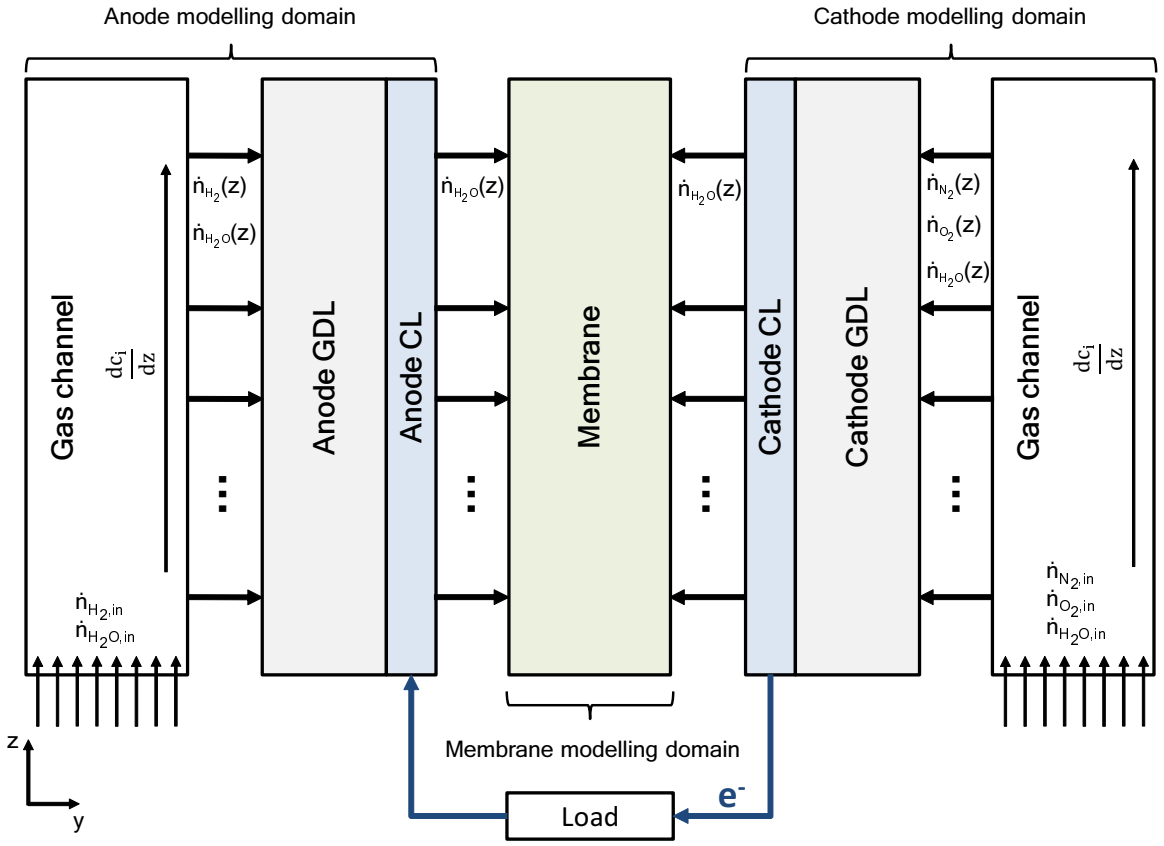

FIGURE 4.1: Input gas flows ($\dot{n}_{in}$) and spatially-dependant perpendicular transports ($\dot{n}$)

The effect of liquid water in the cathode CL is related with the catalyst activity and therefore, the oxygen reaction rate in the PEM fuel cell and the associated fuel cell voltage. Water vapour transports is considered in all the PEM fuel cell. Regarding liquid water transports, a liquid water model [42] is implemented only in the cathode side to better represent the stack voltage. This liquid water model incorporates mesoscopic pore filling effects in the cathode diffusion and catalyst layers.

Regarding the BoP auxiliaries, the main parasitic loss in a PEM fuel system is generated by the compressor (or equivalent air-feeding system). Recent studies have concluded that these

parasitic losses represent between 10 and 15% of the fuel cell total electric gross power [100]. The modelling of the compressor is essential to develop advanced control strategies that have as an objective to improve the efficiency of the system. In this doctoral work, the efficiency of the system takes into account the power consumption of the compressor as well as the rest of the secondary auxiliaries (e.g. valves, pumps, etc.).

The 1+1D model described in this chapter is used in the observation and control parts of this thesis work. This consideration allows to implement control strategies that take into account the internal concentration profiles of the fuel cell. This internal behaviour is often ignored in the literature to obtain simpler models. However, when operating PEM fuel cells, changes in the operating conditions can lead to local reactants starvation and water distribution that decrease the efficiency and durability of the system. Henceforth the use of a distributed parameters model is crucial to obtain advanced model-based control strategies that aim to avoid or mitigate starvation and improper water distribution inside the PEM fuel cell.

4.2 System Description

The system scheme considered in this work is presented in Figure 4.2. It contains four subsystems:

1. The PEM fuel cell stack and load
2. The hydrogen delivery, humidification and recirculation secondary auxiliaries
3. The air delivery and humidification auxiliaries
4. The refrigeration system

It is assumed that all the power is delivered by the fuel cell stack, henceforth, no additional power sources are considered. The hydrogen is stored in a high-pressure container and delivered to the anode through a pressure regulating valve. The cathode is air-fed with a compressor.

The PEM fuel cell stack is an assembly of n_c single-channel cells and each one of these is based on the fuel cell architecture presented in Figure 4.3. Each single cell has a channel

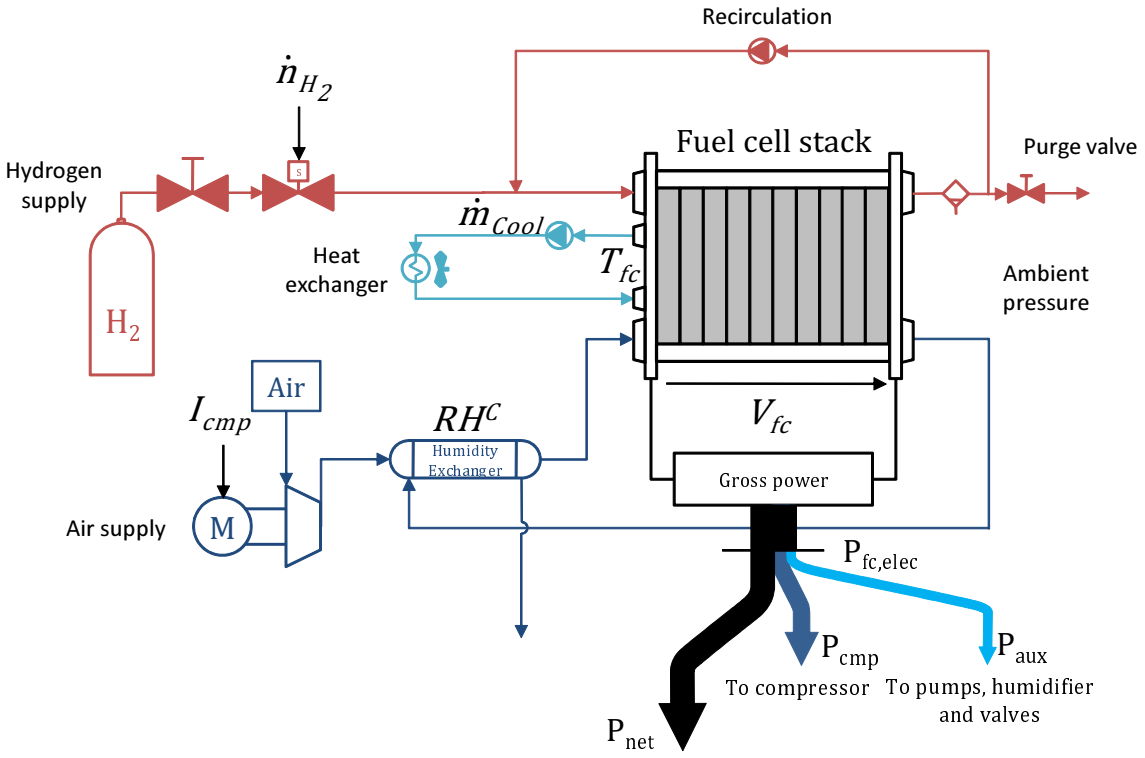

FIGURE 4.2: Scheme of the PEM fuel cell and BoP

length of 0.4 m, a channel width of 1 mm and a channel depth of 0.7 mm. The total surface area of the single cell A_{geo} is 25 cm^2.

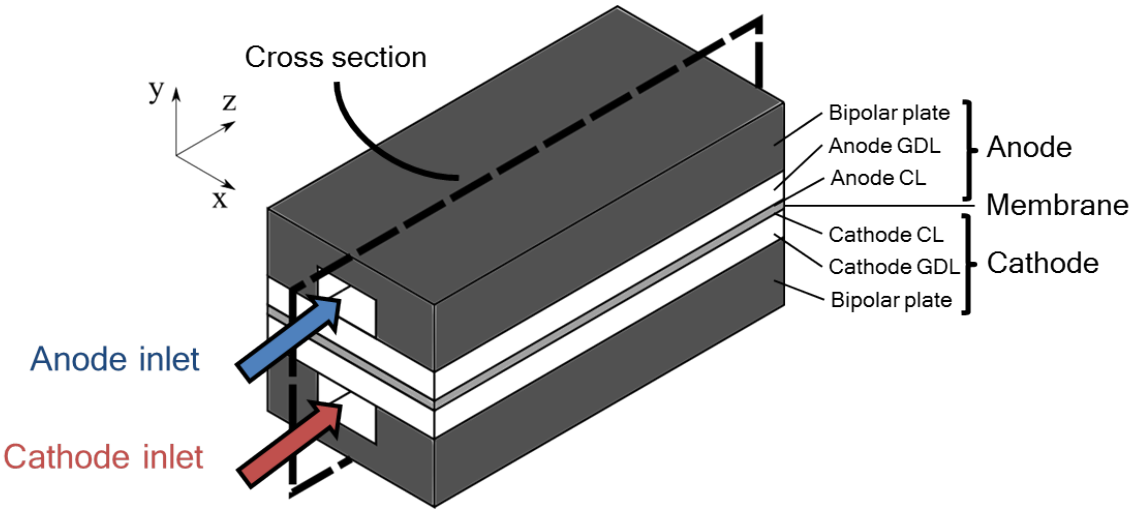

FIGURE 4.3: Single-channel PEM fuel cell representation

Part of the power delivered by the PEM fuel cell is used to feed the compressor and the rest of auxiliary subsystems. The net electrical power P_{net} is expressed as

$$P_{net} = P_{fc,elec} - P_{cmp} - P_{aux}, \tag{4.1}$$

where $P_{fc,elec}$ is the total electrical power generated by the fuel cell, P_{cmp} the power consumed by the compressor and P_{aux} the total power consumption by the rest of auxiliary systems (hydrogen recirculation, refrigeration pumps, heat exchanger fan and valves), which is characterised experimentally in Section 4.3.4.

4.3 System Model

The model presented in this section is the simulation model that emulates the fuel cell system to which the control and observation strategies are applied in Parts III and IV of this work. The observation and control models are derived from the simulation model, as developed in their respective chapters.

4.3.1 Fuel Cell Stack Model

4.3.1.1 Electrochemical Model

The total power generated by the PEM fuel cell can be modelled as the summation of the electrical and thermal power generation

$$P_{fc} = P_{fc,elec} + P_{fc,th}. \tag{4.2}$$

The fuel cell electrical power is expressed as

$$P_{fc,elec} = V_{fc} I_{fc}, \tag{4.3}$$

being V_{fc} the total fuel cell stack voltage and I_{fc} the total current delivered by the PEM fuel cell.

Considering that the fuel cell stack consists of n_c single fuel cells, the total fuel cell voltage in Equation (4.3) is denoted by

$$V_{fc} = \sum_{i=1}^{n_c} V_{fc,cell}, \tag{4.4}$$

where $V_{fc,cell}$ is the individual cell voltage for each cell.

The total current I_{fc} is used to obtain the current density i, which varies along the z-direction of the fuel cell. In this work it is assumed that the distribution of i depends on the partial pressure of oxygen p_{O_2} as denoted by the following expression:

$$i = i(z) = \frac{I_{fc}}{A_{geo}} \frac{p_{O_2}(z)/p_{O_2,ref}}{||p_{O_2}(z)/p_{O_2,ref}||_1}, \tag{4.5}$$

where A_{geo} is the single cell surface area of the electrode. This area is assumed to be the same for all the cells in the stack. The 1-norm in Equation (4.5) is defined as the sum of the absolute values along the z-direction:

$$\left|\left|\frac{p_{O_2}(z)}{p_{O_2,ref}}\right|\right|_1 = \sum \left|\frac{p_{O_2}(z)}{p_{O_2,ref}}\right|. \tag{4.6}$$

By obtaining i with Equation (4.5), the value is normalized to follow the partial oxygen pressure p_{O_2} profile at the cathode CL.

Each fuel cell voltage $V_{fc,cell}$ is computed using the Butler-Volmer equation [4]:

$$V_{fc,cell}(z) = E_r - \frac{RT_{cell}}{\alpha 2F}\left[ln\left(\frac{i(z)}{i_0(z)}\right) - ln\left(\frac{p_{O_2}(z)}{p_{O_2}^{ref}}\right)\right] - i(z)R_{ohm}(z), \tag{4.7}$$

where E_r is the ideal potential voltage of the fuel cell, T_{cell} is the individual temperature of each cell, i_0 is the cathode exchange current density and R_{ohm} is the internal resistance of the membrane that depends on the water content (see Section 4.3.1.6).

Note how in Equation (4.7) the z-direction dependence of the variables results in a fuel cell voltage that also changes along the z-direction. Since it is considered that the bipolar plates are perfect conductors, in Section 4.4, the computation of the total $V_{fc,cell}$ from the $V_{fc,cell}(z)$ values is explained.

As it was introduced in Chapter 2, in PEM fuel cell based systems, the exchange current

density i_0 at the anode is orders of magnitude larger than the one at the cathode [4], henceforth in this work only the cathode activation losses are considered. The cathode exchange current density i_0 is a function of the cell temperature T_{cell}, oxygen partial pressure and the electrochemically active area at the cathode catalyst site (ECSA)

$$i_0(z) = i_0^{ref} \frac{ECSA(z)}{A_{geo}} \left(\frac{p_{O_2}(z)}{p_{O_2}^{ref}} \right)^{0.5} e^{\left[-\frac{\Delta G^*}{RT_{cell}} \left(1 - \frac{T_{cell}}{T^{ref}} \right) \right]}, \tag{4.8}$$

being i_0^{ref} the intrinsic catalytic Pt activity at normal conditions (T^{ref} and $P_{O_2}^{ref}$) and ΔG^* the Gibbs activation energy for the oxygen reduction reaction at the CCL.

A two-phase water model [42] is introduced in Section 4.4.5. It describes the water transport mechanisms that affect the ECSA depending on the operating conditions of the system. While A_{geo} is the total surface area of the catalyst, the ECSA represents the active Pt area in the CCL and it is a function of the ratio of liquid volume to the total volume of void space in the porous CCL structure. This ratio is denoted by s_{CCL} at the cathode catalyst sites. As it is explained in Section 4.4.5, this ratio depends on the formation of liquid water in the CCL and the two-phase water flow model.

4.3.1.2 Gas Flow Model

The gas species flow dynamics are described by mass balance equations along the PEM fuel cell gas channels (see Figure 4.3)

$$\frac{\partial c_i(z)}{\partial t} = \frac{\partial}{\partial z} \left(v(z) c_i(z) \right) - \frac{\dot{n}_i(z)}{\delta} + S_i^g(z), \tag{4.9a}$$

$$v(z) = -K \frac{\partial p(z)}{\partial z}, \tag{4.9b}$$

$$p(z) = RT_{cell} \sum_i c_i(z), \tag{4.9c}$$

where subscript i represents the gaseous species, namely $i = H_2$ for hygrogen, $i = O_2$ for oxygen, $i = N_2$ for nitrogen and $i = H_2O$ for water vapour. The reaction and water molar transports from the MEA are modelled in $\dot{n}_i$ and they are defined as perpendicular to the gas channels in the y-direction [15]. The y-direction thickness of the anode and cathode gas channels is represented by δ. S_i^g is the evaporation rate of the liquid water in the cathode side of the PEM fuel cell (see Section 4.4.5) and is only valid when $i = H_2O$ at the cathode

($S_i^g = 0$ for any other gaseous species and the water at the anode side). As mentioned in the introduction, the effects of liquid water are only considered in the cathode side of the fuel cell as depicted by the source terms in Table 4.1.

The spatial derivatives in Equation (4.9) will be discretised in Section 4.4 to model the internal values of the gas concentrations in different sections along the gas channels.

4.3.1.3 Gas Diffusion Layers Model

Diffusion is the movement of a substance from a region of higher concentration to a region of lower concentration. In the PEM fuel cell, a concentration gradient of the reactants appears between the gas channels (high concentration) and the catalyst layers (low concentration), where the chemical reactions take place. The diffusion of the vapour water depends on the water vapour concentration difference between the PEM fuel cell layers. As shown in Figure 4.4, water can diffuse both ways along the y-direction.

Hydrogen, oxygen and vapour water diffuse from the gas channels through the GDLs and CLs in the y-direction due to the gradient of concentrations. Water usually diffuses backwards, from the membrane towards the gas channels. The diffusion model in the GDLs and CLs of the PEM fuel cell follows Fick's first law of diffusion [101]

$$J_i(y,z) = -D_i \frac{\partial c_i(y,z)}{\partial y}, \tag{4.10}$$

being J_i and D_i the diffusion flux and diffusion coefficient of the i-th gas species through the GDLs and CLs respectively, excluding nitrogen which does not react. In spite of the model being defined as a 1+1D model, in the cathode GDL and CL, a 2D model is implemented, Therefore, the values of the concentrations in the GDLs depend on the position along the y-direction (unlike the gas channels model in Section 4.3.1.2). Considering Equation (4.10), and the mass continuity equation

$$\frac{\partial c_i(y,z)}{\partial t} + \frac{\partial J_i(y,z)}{\partial y} = 0, \tag{4.11}$$

the gas concentrations at the boundary CLs after diffusing can be expressed as

$$\frac{\partial c_{i,CL}(y,z)}{\partial t} = D_i \frac{\partial^2 c_i(y,z)}{\partial y^2}. \tag{4.12}$$

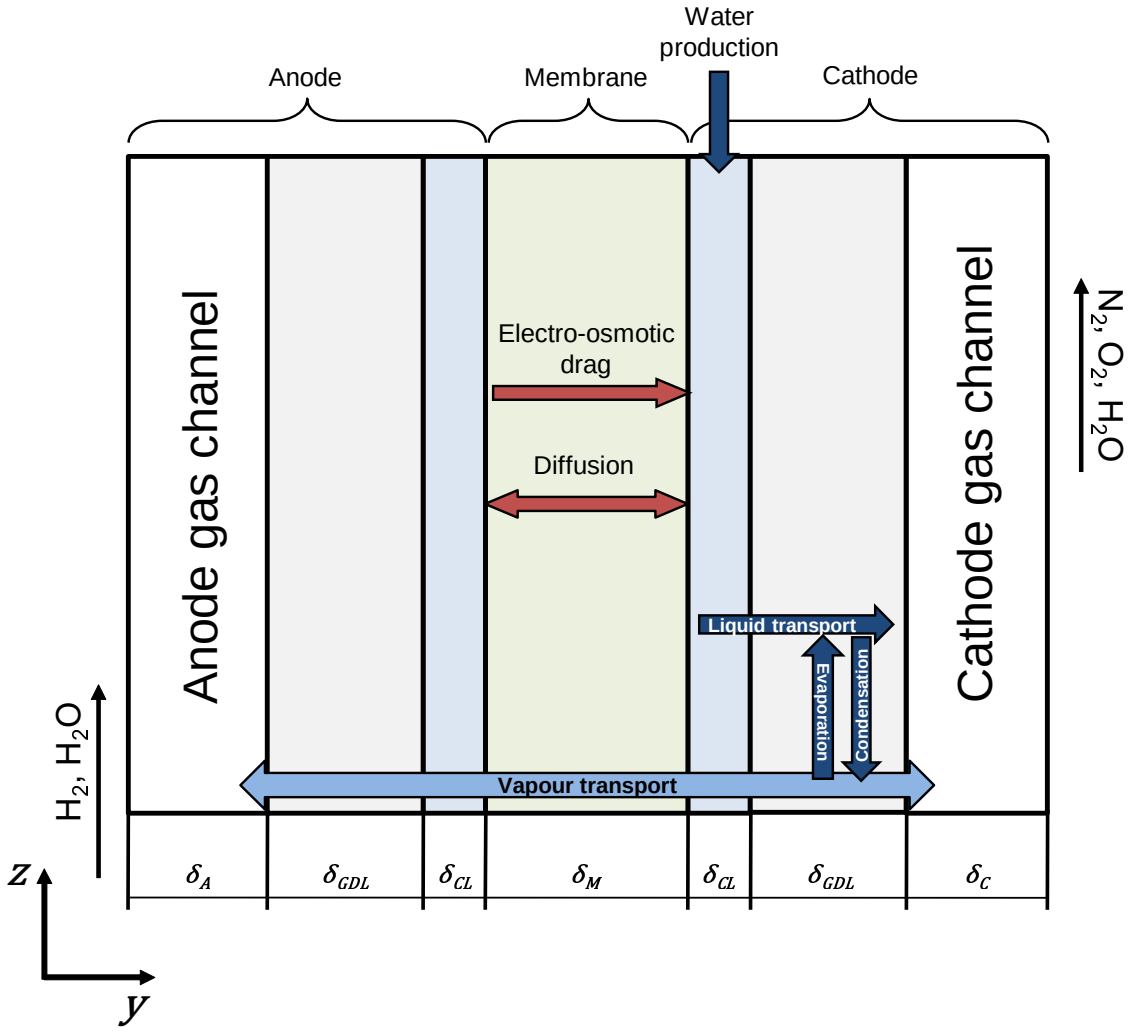

FIGURE 4.4: Two-phase water transport mechanisms in the fuel cell

4.3.1.4 Catalyst Layers Model

The electrochemical reactions take place at the catalyst sites after the reactants diffuse through the GDLs. The molar fluxes along the y-direction are a function of the anodic and cathodic reaction rates r^k. Here, $k = A$ denotes the anode side and $k = C$ the cathode side of the PEM fuel cell respectively. Henceforth, the hydrogen, oxygen and nitrogen molar fluxes are denoted as

$$\dot{n}^A_{H_2}(z) = r^A(z), \tag{4.13}$$

$$\dot{n}^C_{O_2}(z) = \frac{1}{2} r^C(z), \tag{4.14}$$

$$\dot{n}^C_{N_2} = 0. \tag{4.15}$$

In Figure 4.1 the y-direction molar flows and water transport terms are shown along with the input flows of the fuel cell. As expressed by Equation (4.15), nitrogen is not a reactant.

The anodic reaction rate r^A is formulated as

$$r^A(z) = f^V \frac{i_0^A(z)}{2F} \left[\exp\left(\frac{2F}{RT_{cell}} \left(\Delta\Phi^A(z) - \Delta\Phi^A_{ref} \right) \right) \frac{p^A_{H_2}(z)}{p^A_{H_2,ref}} - 1 \right], \tag{4.16}$$

being f^V a surface enlargement factor and $\Delta\Phi^A$ the electrical potential drop at the anode CL [15].

Regarding the cathodic reaction rate, the model is as follows:

$$r^C(z) = f^V \frac{i_0^C(z)}{2F} \exp\left(-\frac{\Delta G^*}{R} \left(\frac{1}{T_{cell}} - \frac{1}{T_{ref}} \right) \right) \frac{p^C_{O_2}(z)}{p_{O_2,ref}} \exp\left(-\frac{\alpha 2F}{RT_{cell}} \left(\Delta\Phi^C(z) - \Delta\Phi^C_{ref} \right) \right), \tag{4.17}$$

where $\Delta\Phi^C$ is the electrical potential drop at the cathode CL.

The potential differences at the anode ($\Delta\Phi^A$) and cathode ($\Delta\Phi^C$) CLs are modelled as

$$\Delta\dot{\Phi}^A(z) = \frac{i(z) - 2Fr^A(z)}{C^A \delta^{AC}}, \tag{4.18}$$

$$\Delta\dot{\Phi}^C(z) = \frac{2Fr^C(z) - i(z)}{C^C \delta^{CC}}, \tag{4.19}$$

being C^A and C^C the volumetric capacitance of the anode and cathode CL respectively. The y-direction thickness of the anode and cathode CLs is represented by δ^{AC} and δ^{CC}.

4.3.1.5 Two-phase Water Model

As introduced in Sections 4.1 and 4.3.1.2, the ratio of liquid water to the total volume of void space in the porous structure of the CCL, denoted by s_{CCL}, affects the ECSA (which influences i_0 and $V_{fc,cell}$). Since only cathode activation losses are considered in Equation (4.7), the two-phase water model is implemented only in the cathode side of the PEM fuel cell (see Figure 4.4), disregarding the effect of liquid water at the anode side.

The ECSA is modelled following mesoscopic pore filling effects for the CCL structure [42]:

$$ECSA(z) = \begin{cases} 4\pi\tau_{Pt}^2 n_p n_{Pt}, & \text{if } 2\tau_{Pt} < \tau_p \left(1 - \sqrt[3]{1 - s_{CCL}(z)}\right) \\ 2\pi\tau_{Pt}\tau_p n_p n_{Pt} \left(1 - \sqrt[3]{1 - s_{CCL}(z)}\right), & \text{else} \end{cases}, \tag{4.20}$$

where n_p is the number of pores in the CCL volume with a radius of τ_p for each pore, n_{Pt} is the number of Pt particles in the CCL, each one with a τ_{Pt} radius.

To be able to compute the ratio of liquid water in the CCL and cathode GDL, first the general expression for the dynamics of s is developed as introduced in [42, 102]:

$$\frac{\partial s(x,y,z)}{\partial t} = \frac{S^l_{H_2O}(x,y,z) - \nabla \cdot (-D_s \vec{\nabla} s(x,y,z))}{K^{sorp} \varepsilon \rho^l_{H_2O}}, \tag{4.21}$$

where D_s denotes the liquid water diffusivity throughout a layer with specific porosity of ε, $\rho^l_{H_2O}$ is the liquid water density, $S^l_{H_2O}$ the liquid water source term for the cathode side of the PEM fuel cell (see first row of Table 4.1) and K^{sorp} is the time constant for the sorption of water into the pores of the cathode GDL and CL. $\nabla \cdot \mathbf{F}$ and $\vec{\nabla} f$ denote the mathematical divergence and gradient respectively. Developing Equation (4.21):

$$\frac{\partial s(x,y,z)}{\partial t} = \frac{S^l_{H_2O}(x,y,z) + D_s \left(\frac{\partial^2 s}{\partial x^2} + \frac{\partial^2 s}{\partial y^2} + \frac{\partial^2 s}{\partial z^2}\right)}{K^{sorp} \varepsilon \rho^l_{H_2O}}. \tag{4.22}$$

Notice that in Equation (4.22) spatial derivatives in the x, y and z-directions appear. In [42] only the y-direction dependency was considered. In this work, the approach will be implemented for the y and z-directions. Therefore, disregarding the x-direction dependency, Equation (4.22) is expressed as

$$\frac{\partial s(y,z)}{\partial t} = \frac{S^l_{H_2O}(y,z) + D_s \left(\frac{\partial^2 s(y,z)}{\partial y^2} + \frac{\partial^2 s(y,z)}{\partial z^2}\right)}{K^{sorp} \varepsilon \rho^l_{H_2O}}. \tag{4.23}$$

To compute $S^{l}_{H_2O}$, the water generation ($S^{gen}_{H_2O}$), water evaporation ($S^{evap}_{H_2O}$) and water content at the membrane ($S^{M}_{H_2O}$) terms are needed [42]. These source terms are modelled as follows:

$$S^{gen}_{H_2O}(y,z) = \frac{ECSA(y,z)}{\forall_{CCL}} \frac{i(z)}{2F} M_{H_2O}, \tag{4.24}$$

$$S^{evap}_{H_2O}(y,z) = K^{evap} s(y,z) \frac{M_{H_2O}}{RT_{cell}} (p^{sat} - p^{v}(z)) \text{ if } p^{v}(z) < p^{sat}, \tag{4.25}$$

$$S^{M}_{H_2O}(z) = D_s \Lambda(z), \tag{4.26}$$

being $\forall_{CCL}$ the total volume of the CCL obtained from the geometric properties of the CCL, M_{H_2O} the molar mass of liquid water, K^{evap} the water evaporation rate constant and Λ the liquid water content at the membrane. An overview of the source terms is presented in Table 4.1. The evaporation source term in Equation (4.25) is a function of the vapour pressure p^{v} and the saturated vapour pressure p^{sat} at a given temperature T_{cell}

$$p^{sat}(T_{cell}) = 6.1121 e^{\left(18.678 - \frac{T_{cell}}{234.5}\right)\left(\frac{T_{cell}}{257.14 + T_{cell}}\right)}, \tag{4.27}$$

as proposed by [103].

Consequently, to obtain s_{CCL}, the source terms for the CCL in Table 4.1 are introduced in Equation (4.23). Then, s_{CCL} is used to obtain the value of ECSA in Equation (4.20).

Table 4.1: Water source terms

Source term	**Anode**		**Cathode**	
	GDL	CL	GDL	CL
$S^{l}_{H_2O}$	0	0	$-S^{evap}_{H_2O}$	$-S^{evap}_{H_2O} + S^{gen}_{H_2O} + S^{M}_{H_2O}$
$S^{g}_{H_2O}$	0	0	$S^{evap}_{H_2O}$	$S^{evap}_{H_2O}$

4.3.1.6 Membrane Model

The membrane separates both electrodes of the PEM fuel cell. Furthermore, it closes the electrical circuit internally by transporting the protons from the anode to the cathode side (see Figure 2.1c). As mentioned before, water plays a key role in the dynamics of the proton transport by means of affecting the electrical protonic conductivity. Henceforth, the water content of the membrane have to be included in its mathematical model.

Water content (Λ) in a PEM fuel cell membrane can be defined as the relation between the number of water molecules and the moles of polymer in the membrane [104]. It can be computed using the following isotherm curves [104]:

$$\Lambda(z) = \begin{cases} 0.3 + 10.8a_m(z) - 16.0a_m^2(z) + 14.1a_m^3(z), & \text{if } 0 < a_m(z) < 0.523 \\ \frac{(10.4-5.6)(T_{ref}-T_{cell})}{50} + 5.6\frac{(g(z)-3.589)}{5.6} + 3.589, & \text{else} \end{cases}, \quad (4.28)$$

being

$$g(z) = 0.3 + 10.8a_m(z) - 16.0a_m^2(z) + 14.1a_m^3(z), \quad (4.29)$$

where a_m is the water activity at the membrane, determined by the water partial pressures at the anode ($p^A_{H_2O}$) and cathode ($p^C_{H_2O}$) membrane boundaries

$$a_m(z) = \frac{p^A_{H_2O}(z) + p^C_{H_2O}(z)}{2p^{sat}}. \quad (4.30)$$

The anode and cathode partial pressures are obtained with Equation (4.9c).

Knowing the water content in the membrane it is possible to obtain the water concentration in the membrane $c^M_{H_2O}$, using the following expression [15]:

$$c^M_{H_2O}(z) = \Lambda(z)\rho^M(\Lambda(z))X^M(\Lambda(z)), \quad (4.31)$$

where ρ^M and X^M are the membrane density and the ion exchange capacity respectively. Both parameters are functions of the water content of the membrane and they are expressed as follows:

$$\rho^M(\Lambda(z)) = \frac{1 + \Lambda(z)M_{H_2O}X_{dry}}{\rho_{H_2O} + \Lambda(z)M_{H_2O}X_{dry}\rho_{H_2O}}, \quad (4.32)$$

$$X^M(\Lambda(z)) = \frac{X_{dry}}{1 + \Lambda(z)M_{H_2O}X_{dry}}, \quad (4.33)$$

being M_{H_2O} the water molar mass, X_{dry} the molar capacity of the dry membrane and ρ_{H_2O} the water density.

Moreover, from the water content Λ it is possible to obtain the mole fractions of water (ξ_{H_2O}) and protons (ξ_{H^+}) present in the membrane. These relations are the following [15]:

$$\xi_{H_2O}(\Lambda(z)) = \frac{\Lambda(z)}{\Lambda(z)+2}, \tag{4.34}$$

$$\xi_{H^+}(\Lambda(z)) = \frac{1}{\Lambda(z)+2}. \tag{4.35}$$

Two different physical transport mechanisms affect the water content in the PEM fuel cell. These mechanisms are [4]: back-diffusion (BD) and electro-osmotic drag (EOD). BD is defined as the diffusion of water from the cathode to the anode if the cathode side of the fuel cell holds more water. Nevertheless, water may diffuse from the anode to the cathode side of the fuel cell if the inverse situation arises. On the other hand, EOD is the effect of hydrogen protons generated by the reaction at the anode CL, dragging water molecules through the membrane to the cathode side.

Both BD and EOD water transport mechanisms are summed in order to give $\dot{n}_{H_2O}$ as seen in the following equation:

$$\dot{n}_{H_2O}(z) = \underbrace{-\frac{t_W(\Lambda(z))\kappa(\Lambda(z))}{F^2}\nabla\mu_{H_+}(z)}_{\text{EOD}} \overbrace{-\frac{D_W(\Lambda(z))c_{H_2O}}{RT_{cell}}\nabla\mu_{H_2O}(z)}^{\text{BD}}, \tag{4.36}$$

where D_W is the self-diffusion coefficient and t_W is a transport coefficient which depends on the membrane water content Λ. The detailed expressions for D_W and t_W in Equation (4.36) are extracted from [104]. The chemical potential gradients $\nabla\mu_{H_+}$ and $\nabla\mu_{H_2O}$ can be computed as follows:

$$\nabla\mu_{H_+}(z) = \frac{RT_{cell}}{\xi_{H_+}(\Lambda(z))}\nabla\xi_{H_+}(z) + F\nabla\Phi(z), \tag{4.37}$$

$$\nabla\mu_{H_2O}(z) = \frac{RT_{cell}}{\xi_{H_2O}(\Lambda(z))}\nabla\xi_{H_2O}(z), \tag{4.38}$$

being $\nabla\xi_{H_+}$ and $\nabla\xi_{H_2O}$ the water and hydrogen proton mole fraction gradients which are approximated by the mole fraction difference between the membrane and each one of the

CLs as expressed by [15]:

$$\nabla\xi_{H_2O}(z) = \frac{\xi_{H_2O}(\Lambda(z)) - \xi_{H_2O}(\Lambda^k(z))}{\delta^M/2}, \tag{4.39}$$

$$\nabla\xi_{H_+}(z) = \frac{\xi_{H_+}(\Lambda(z)) - \xi_{H_2O}(\Lambda^k(z))}{\delta^M/2}, \tag{4.40}$$

being $k = A$ when the mole difference is between the anode CL and the membrane and $k = C$ when the mole difference is computed between the cathode CL and the membrane. For each case, the water content Λ^k is calculated using Equation (4.28) but considering that the water activities for the anode and cathode sides are the following:

$$a_m^A = \frac{p_{H_2O}^A(z)}{p^{sat}}, \tag{4.41}$$

$$a_m^C = \frac{p_{H_2O}^C(z)}{p^{sat}}. \tag{4.42}$$

As mentioned before, the amount of accumulated liquid water in the membrane affects the total ohmic resistance R_{ohm} in Equation (4.7). The approximation taken is the one proposed in [105]:

$$R_{ohm}(z) = \frac{\delta^M}{\sigma^M(z)}, \tag{4.43}$$

where δ^M is the membrane thickness and σ^M is the membrane conductivity, which can be expressed as follows [104]:

$$\sigma^M(z) = \sigma(T_{cell} = 353\text{K})e^{\left[-E_{A,\sigma}(z)\left(\frac{1}{T_{cell}}+\frac{1}{T_{ref}}\right)\right]}, \tag{4.44}$$

being

$$\sigma(T_{cell} = 353\text{K}) = -0.0131556 + 0.00638558\Lambda(z) + 0.000167811\Lambda^2(z), \tag{4.45a}$$

$$E_{A,\sigma}(z) = 2640e^{(-0.6\Lambda(z))} + 1183, \tag{4.45b}$$

where $E_{A,\sigma}$ is the membrane activation energy for a given water content Λ.

4.3.1.7 Sign Criteria for the Reaction Terms and Water Fluxes

The geometric center of the membrane determines the sign change for the reaction terms in Section 4.3.1.4 and the water transport terms in Section 4.3.1.6. When approaching from the anode to the membrane, the reaction terms, gas fluxes and currents are positive. The same happens from the cathode side of the fuel cell. This is graphically represented in Figure 4.5.

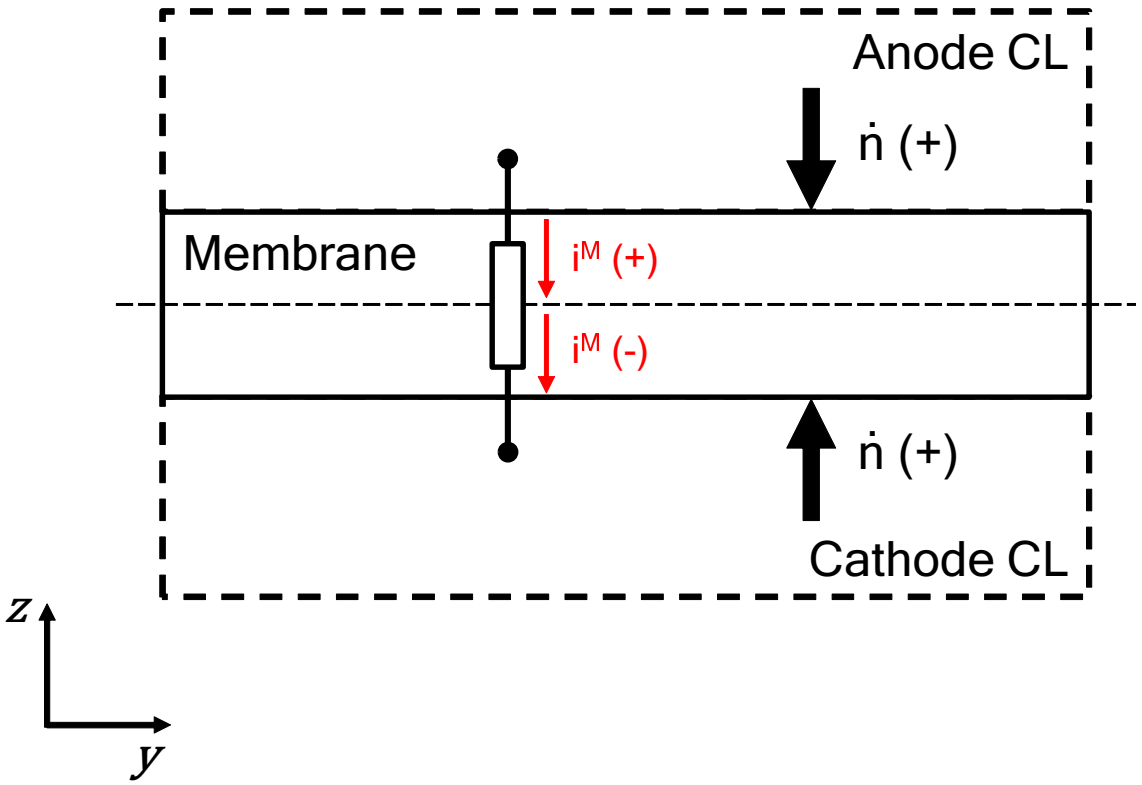

FIGURE 4.5: Sign criteria for the transversal (y-direction) flows

4.3.2 Thermal Model

In Figure 4.6 the thermal system modelled is represented. It consists of a coolant pump that circulates the coolant fluid (water) through a heat exchanger and the fuel cell. The temperature of the coolant is reduced in the heat exchanger by means of forced air convection using an electric fan.

4.3.2.1 Stack temperature model

The energy balance for the PEM fuel cell stack temperature T_{fc} is expressed as follows [99]:

$$MC_{fc}\frac{dT_{fc}}{dt} = \dot{E}_{tot} - \dot{E}_{fc,elec} - Q_{cool} - Q_{conv}, \tag{4.46}$$

being MC_{fc} the thermal mass of the fuel cell stack, E_{tot} the total energy of the hydrogen, $E_{fc,elec}$ the electrical potential generated by the fuel cell, Q_{cool} is the thermal energy dissipated by the coolant in the heat exchanger circuit and Q_{conv} is the convective heat transfer between the stack and the environment.

To complete Equation (4.46), the following set of equations is employed:

$$\dot{E}_{tot} = \frac{nI_{fc}}{2F}\Delta H, \tag{4.47a}$$

$$\dot{E}_{fc,elec} = V_{fc}I_{fc}, \tag{4.47b}$$

$$Q_{cool} = \dot{m}_{cool}C_{p,cool}\left(T_{cool,out} - T_{cool,in}\right), \tag{4.47c}$$

$$Q_{conv} = k_{conv}A_{stack}\left(T_{fc} - T_{amb}\right). \tag{4.47d}$$

where $\dot{m}_{cool}$ and $C_{p,cool}$ are the mass flow and heat capacity of the coolant fluid respectively. k_{conv} is the thermal conductivity coefficient for the stack assembly and A_{stack} is its surface area. The values for the coefficients in Equation (4.47a) are given in Appendix B. In order to simplify the thermal model, it is assumed that the difference $T_{cool,out} - T_{cool,in}$ is a constant value of 5 K.

The dynamic model presented in the previous section is used to compute the temperature of the stack (T_{fc}). But internally, fuel cells have temperature gradients as a result of the internal chemical reactions and heat generation at the CLs [106, 107].

In [108] the effect of the stack temperature is studied in static and dynamic operation. The temperature gradient between 10 single cells is analysed for different simulation scenarios. After achieving steady state, the thermal variation between the end plates and the middle point of the stack appears to be approximately 10 K for all the cases. In the present work, a probabilistic approach is applied to T_{fc} in order to represent the temperature gradient at the stack without increasing the complexity of the model. Assuming the normal probability

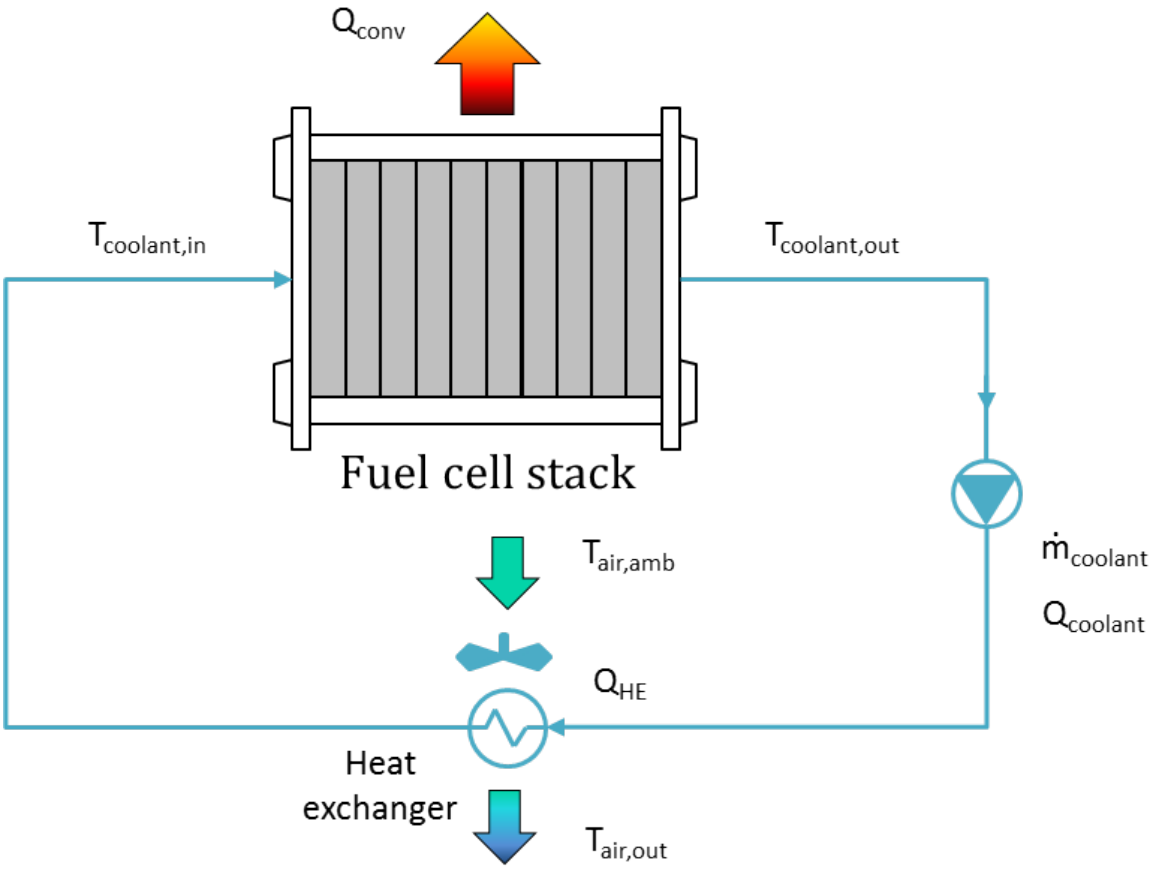

FIGURE 4.6: Fuel cell stack thermal system

distribution

$$f(x|\mu,\sigma^2) = \frac{1}{\sqrt{2\sigma^2\pi}} e^{-\frac{(x-\nu)^2}{2\sigma^2}}, \tag{4.48}$$

where μ is the mean of the distribution and σ is the standard deviation. Each cell temperature is computed as follows:

$$T_{cell} = T_{fc} + k_{dist} f(y|\mu,\sigma^2), \tag{4.49}$$

being k_{dist} the constant to model the total temperature gradient inside the stack. This way, the temperature varies along the different single cells of the stack. Figure 4.7 shows the temperature distribution of a 10 single-cell stack with a $T_{fc} = 353\ K$ and different values of k_{dist}.

For the simulations presented in Part IV, $k_{dist} = 50$, which gives a temperature gradient of approximately 10 K between the end plates and the middle point.

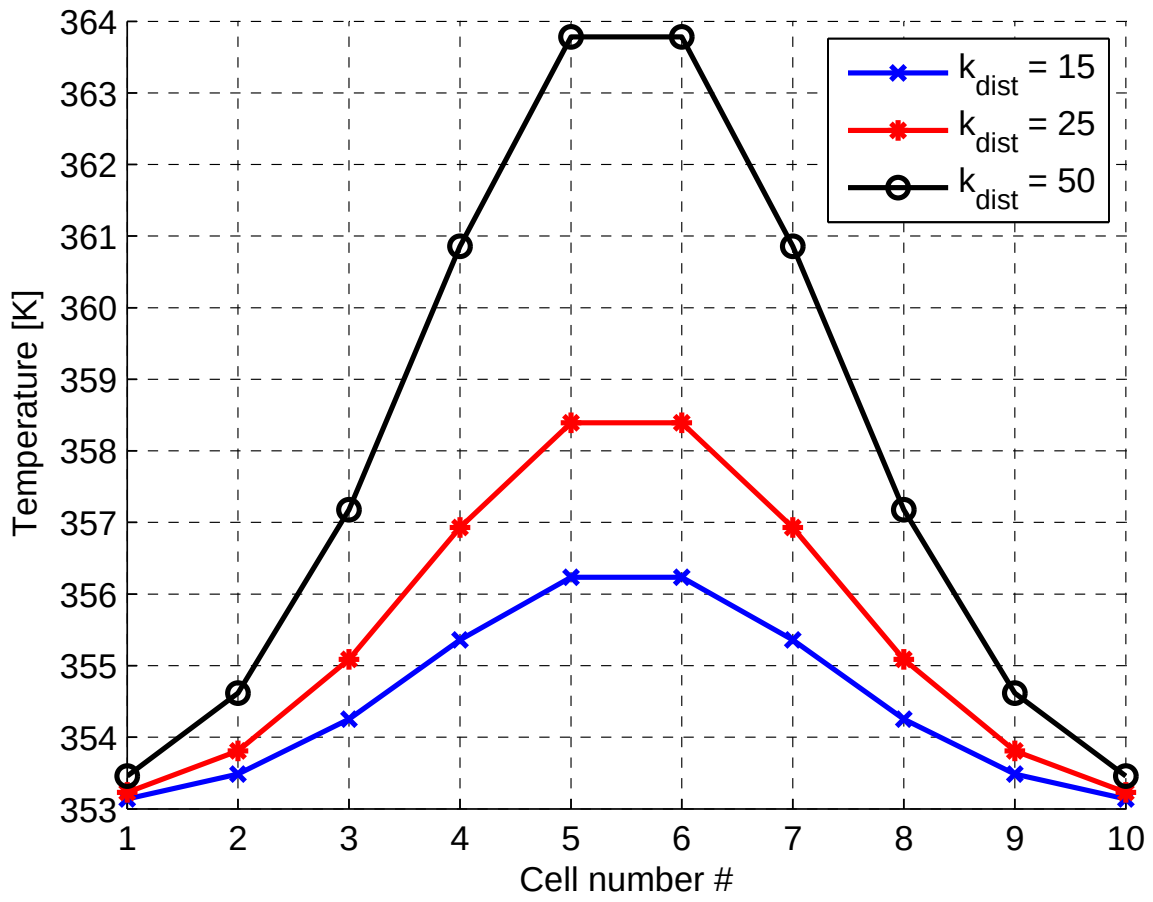

FIGURE 4.7: Fuel cell stack temperature distribution

4.3.3 Air Supply System Model

The air-feeding subsystem considered in this work takes air at ambient pressure and a compressor increases its pressure. The compressor is connected to an electric motor which is powered by the fuel cell. Figure 4.8 presents the scheme of the air supply system considered in this work.

The nonlinear dynamics of the system are described by the following set of ordinary differential equations [98]:

$$\dot{p}_{O_2} = d_1(p_{sm} - p_{O_2} - p_{N_2} - d_2) - \frac{d_3 p_{O_2}}{d_4 p_{O_2} + d_5 p_{N_2} + d_6} d_{17}\sqrt{p_{O_2} + p_{N_2} + d_2 - d_1 1} - d_7 I_{fc}, \tag{4.50a}$$

$$\dot{p}_{N_2} = d_8(p_{sm} - p_{O_2} - p_{N_2} - d_2) - \frac{d_3 p_{N_2}}{d_4 p_{O_2} + d_5 p_{N_2} + d_6} d_{17}\sqrt{p_{O_2} + p_{N_2} + d_2 - d_{11}}, \tag{4.50b}$$

$$\dot{\omega}_{cmp} = -d_9\omega_{cmp} - d_{10}\left[\left(\frac{p_{O_2}}{d_{11}}\right)^{d_{12}} - 1\right]\dot{n}_{O_2} + d_{13} I_{cmp}, \tag{4.50c}$$

$$\dot{p}_{sm} = d_{14}\left[1 + d_{15}\left[\left(\frac{p_{sm}}{d_{11}}\right)^{d_{12}} - 1\right]\right]\left[\dot{n}_{O_2} - d_{16}\left(p_{sm} - p_{O_2} - p_{N_2} - d_2\right)\right], \tag{4.50d}$$

where p_{O_2} and p_{N_2} are the oxygen and nitrogen partial pressures at the cathode inlet respectively, ω_{cmp} is the compressor angular speed and p_{sm} is the cathode channel supply manifold pressure. For simplicity, the constants of the compressor model, denoted by d_i, are defined in Appendix A.

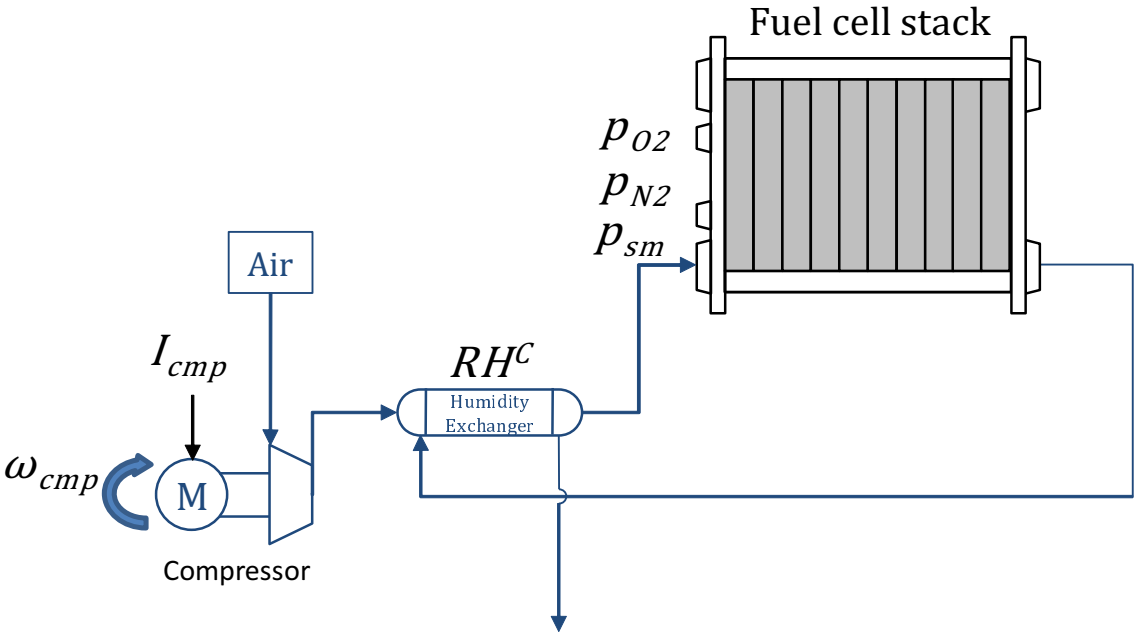

FIGURE 4.8: Air supply system scheme

The power consumed by the compressor (P_{cmp}) is

$$P_{cmp} = \tau_{cmp}\omega_{cmp}, \tag{4.51}$$

being τ_{cmp} and ω_{cmp} the torque and angular speed of the motor that powers the compressor respectively. P_{cmp} can also be expressed as a constant multiplied by the compressor current I_{cmp} and the angular speed ω_{cmp}

$$P_{cmp} = \eta_{cmp} k_t I_{cmp} \omega_{cmp}, \tag{4.52}$$

where η_{cmp} is the compressor efficiency and k_t the motor constant.

4.3.4 Secondary Auxiliaries Characterisation

Previously, the models for the PEM fuel cell and the compressor have been introduced. As seen in Figure 4.2, there are other systems that consume part of the power delivered by the fuel cell. In particular, these secondary auxiliary systems are the following:

- Refrigeration pump
- Heat exchanger fan
- Hydrogen recirculation pump
- Valves

The power consumption of the secondary auxiliaries is not as significant as the compressor losses [100] and they are fairly constant or on/off. Therefore, detailed modelling of the aforementioned subsystems can be simplified. Nevertheless, an experimental characterisation using a test bench is done to take into account the parasitic losses of the BoP when designing efficient control strategies. Since the auxiliaries will be powered only by the fuel cell, the total auxiliary consumed power can be expressed as

$$P_{aux} = V_{fc} I_{aux}, \tag{4.53}$$

being I_{aux} the current consumed by the secondary auxiliaries. As mentioned, Equation (4.53) does not include the compressor parasitic losses, which are modelled in Section 4.3.3.

To obtain this characterisation, a series of experiments are performed in a Bahia experiment bench [109]. This platform is equipped with sensors that can measure the power consumption

of the auxiliary systems as a function of the demanded load current. Using a NEDC [3] current profile as a case study (this driving cycle is introduced in detail in Section 4.5), the obtained parasitic losses are shown in Figure 4.9.

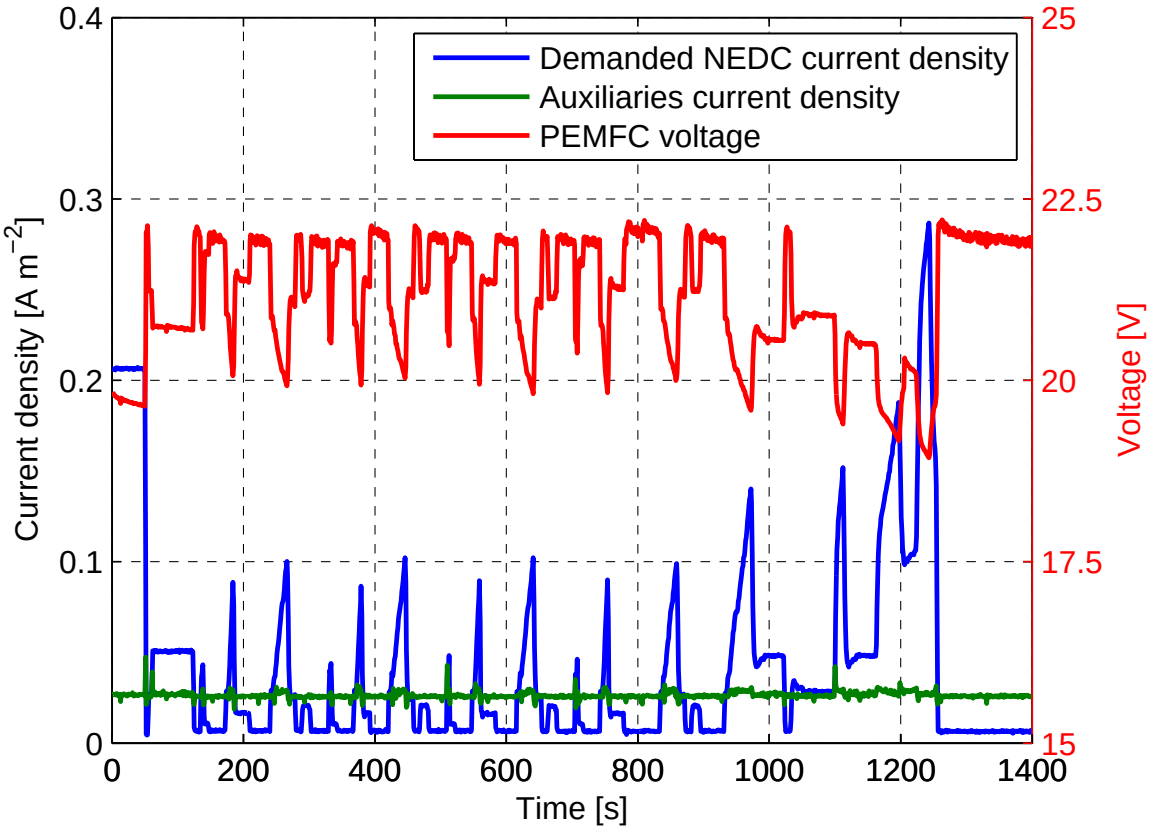

FIGURE 4.9: Auxiliaries current demand experiment

4.4 Model Implementation

The equations and experimental characterisation of the PEM fuel cell system model and its subsystems are introduced in Section 4.3. The proposed model is implemented in a Simulink framework, combined with MATLAB scripts to define the parameters of the system. The observation and control methodologies described in Parts III and IV are also implemented in Simulink. Discretisation methods are applied to numerically solve the PDEs.

4.4.1 Finite-difference Discretisation

In order to implement finite difference methods to solve numerically the first and second order spatial derivatives of the simulation model presented in Section 4.3, finite-difference discretisation procedures are proposed in this section.

In Figure 4.10, the detailed fuel cell model with the different discretisation directions is shown. All the fuel cell layers have z-direction dependencies that are going to be discretised in n_z volumes. Regarding the y-direction, only those variables that appear in the cathode CL and cathode GDL are going to be discretised in n_y volumes as shown in the detail at the bottom of Figure 4.10.

Finite-difference discretisation plays a special role when known boundary conditions are present in the problem. This is the case of the PEM fuel cell, where the model presents several known boundary conditions, such as the input molar fluxes or the external ambient pressure at the end of the gas channels. Henceforth, forward or backward differences will be applied to take advantage of the boundary conditions [110, 111].

Considering a function f at a certain point x, namely $f(x)$, the forward difference is expressed as

$$\frac{\partial f(x)}{\partial x} \approx \frac{\Delta_x[f](x)}{\Delta x} = \frac{f(x+\Delta x) - f(x)}{\Delta x}, \tag{4.54}$$

while the backward difference follows the expression

$$\frac{\partial f(x)}{\partial x} \approx \frac{\nabla_x[f](x)}{\Delta x} = \frac{f(x) - f(x-\Delta x)}{\Delta x}. \tag{4.55}$$

Finally, the central difference is

$$\frac{\partial f(x)}{\partial x} \approx \frac{\delta_x[f](x)}{\Delta x} = \frac{f(x+\frac{1}{2}\Delta x) - f(x-\frac{1}{2}\Delta x)}{\Delta x}. \tag{4.56}$$

For higher order derivatives the finite-difference discretisation is obtained in a similar way. For the same $f(x)$ function the forward second order difference is

$$\frac{\partial^2 f(x)}{\partial x^2} \approx \frac{\Delta_x^2[f](x)}{(\Delta x)^2} = \frac{f(x+2\Delta x) - 2f(x+\Delta x) + f(x)}{(\Delta x)^2}, \tag{4.57}$$

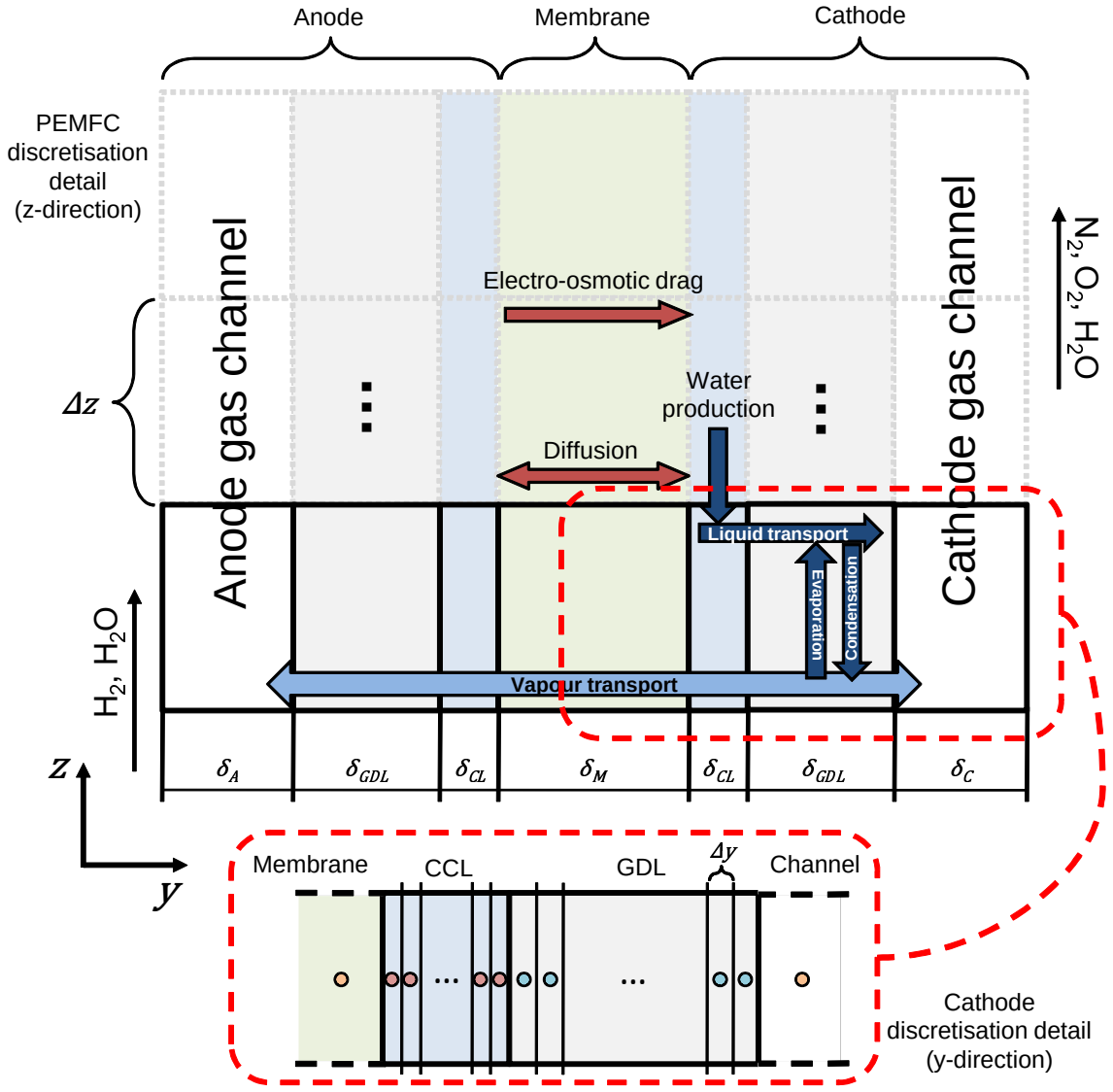

FIGURE 4.10: Two-dimensional discretisation volume and related two-phase water transport mechanisms in the fuel cell

the backward difference discretisation is expressed as

$$\frac{\partial^2 f(x)}{\partial x^2} \approx \frac{\nabla_x^2[f](x)}{(\Delta x)^2} = \frac{f(x) - 2f(x-\Delta x) + f(x-2\Delta x)}{(\Delta x)^2}, \tag{4.58}$$

and finally, the central difference follows the expression

$$\frac{\partial^2 f(x)}{\partial x^2} \approx \frac{\delta_x^2[f](x)}{(\Delta x)^2} = \frac{f(x+\Delta x) - 2f(x) + f(x-\Delta x)}{(\Delta x)^2}, \tag{4.59}$$

As explained, in the following section, the simulation model is discretised applying Equations (4.54)-(4.59) along the y and z directions of the fuel cell. Discretisation will also be

applied to the observation and discretisation models.

4.4.2 Discretised Electrochemical Model

Fuel cell voltage in Equation (4.7) depends on the oxygen partial pressure p_{O_2} which is a spatially distributed variable. Moreover, as shown in Equation (4.8), the current exchange density i_0 also depends on p_{O_2}. The spatially discretissed fuel cell voltage $V_{fc,cell,j}$ over n_z discretisation volumes can be expressed as

$$V_{fc,cell,j} = E_r - \frac{RT_{cell}}{\alpha 2F}\left[ln\left(\frac{i_j}{i_{0,j}}\right) - ln\left(\frac{p_{O_2,j}}{p_{O_2}^{ref}}\right)\right] - i_j R_{ohm,j}, \tag{4.60}$$

being $j \triangleq [1, \dots n_z]$ the discretisation volume subscript. It is assumed that

$$V_{fc,cell} \approx \overline{V_{fc,cell}} = \frac{\sum_{j=1}^{n_z} V_{fc,cell,j}}{n_z}. \tag{4.61}$$

Furthermore, the discretised current exchange $i_{0,j}$ is discretised as follows:

$$i_{0,j} = i_0^{ref}\frac{ECSA_j}{A_{geo}}\left(\frac{p_{O_2,j}}{p_{O_2}^{ref}}\right)^{0.5} e^{\left[-\frac{\Delta G^*}{RT_{cell}}\left(1-\frac{T_{cell}}{T^{ref}}\right)\right]}. \tag{4.62}$$

The discretised oxygen partial pressure $p_{O_2,j}$ (along with the rest of discretised gas species) is obtained from Equation (4.9c) and developed in the following section.

4.4.3 Discretised Gas Flow Model

Applying the forward and backward discretisation procedure introduced in Section 4.4.1, the gas flow model in Equation (4.9) can be expressed as:

$$\frac{\partial c_{i,j}}{\partial t} = \frac{v_{j-1}c_{i,j-1}}{\Delta z} - \frac{v_j c_{i,j}}{\Delta z} - \frac{\dot{n}_{i,j}}{\delta} + S_{i,j}^g, \tag{4.63a}$$

$$v_j = \frac{K}{\Delta z}\left(p_j - p_{j+1}\right) \tag{4.63b}$$

$$p_j = RT_{cell}\sum_i c_{i,j}, \tag{4.63c}$$

where Δz is the z-direction discretisation length, denoted by the division of the number of discretisation volumes by the total length of the gas channel L_z. Considering the boundary

condition for the hydrogen, oxygen, nitrogen and water given by [15]

$$v_{in}c_{i,in} = \dot{n}_{i,in} \triangleq u_i, \tag{4.64a}$$

$$p_{out} = p_{n_z} = p^{amb}, \tag{4.64b}$$

and a z-direction spatial discretisation over n_z finite volumes, the i-th concentration at volume j in Equation (4.63) can be expressed as:

$$\dot{c}_{i,j} = \begin{cases} \frac{u_i}{\Delta z} - \zeta_1 \Psi(j) - \frac{\dot{n}_{i,j}}{\delta_C} & \text{if } j = 1, \\ \zeta_1 \left(\Psi(j-1) - \Psi(j)\right) - \frac{\dot{n}_{i,j}}{\delta_C} & \text{if } 2 \leq j \leq n_z - 1, \\ \zeta_1 \Psi(j-1) + \Gamma(j+1) - \frac{\dot{n}^k_{i,j}}{\delta_C} & \text{if } j = n_z, \end{cases} \tag{4.65}$$

with

$$\Psi(j) = c_{i,j} \left(\sum_i c_{i,j} - \sum_i c_{i,j+1} \right), \tag{4.66a}$$

$$\Psi(j-1) = c_{i,j-1} \left(\sum_i c_{i,j-1} - \sum_i c_{i,j} \right), \tag{4.66b}$$

$$\Gamma(j+1) = \zeta_1 c_{i,j} \sum_i c_{i,j} + \zeta_2 c_{i,j}, \tag{4.66c}$$

being $\zeta_1 = KRT/\Delta z^2$ and $\zeta_2 = Kp^{amb}/\Delta z^2$.

4.4.4 Discretised Gas Diffusion Layers Model

The concentration of the reactants and water is then discretised through the GDLs and CLs y-direction following a spatial discretisation over n_y, using the diffusion law expressed in Equation (4.10) and the second order spatial difference from Equations (4.57) and (4.58)

$$\dot{c}_{i,(j,n)} = \begin{cases} \frac{D_i}{\Delta y^2} \left(c_{i,j} - 2c_{i,(j,n)} + c_{i,(j,n+1)} \right) & \text{if } n = 1, \\ \frac{D_i}{\Delta y^2} \left(c_{i,(j,n-1)} - 2c_{i,(j,n)} + c_{i,(j,n+1)} \right) & \text{if } 2 \leq n \leq n_y - 1, \\ \frac{D_i}{\Delta y^2} \left(c_{i,(j,n-1)} - c_{i,(j,n)} \right) & \text{if } n = n_y, \end{cases} \tag{4.67}$$

where $n \triangleq [1, \ldots n_y]$ is the discretisation volume subscript for the y-direction. Δy is the y-direction discretisation length, denoted by the division of the number of y-direction discretisation volumes by the total width of the GDLs and CLs.

Equation (4.67) is the general discretisation for the GDLs and CLs. Nevertheless, it will be particularised for a single volume in the anode (the liquid water model uses a n_y-volumes discretisation of the cathode GDL and an additional n_y-volumes discretisation of the CCL).

4.4.5 Discretised Two-phase Water Model

As presented in Equation (4.23), the PDE for the ratio of liquid water s depends spatially on the x and y directions. Applying the differentiation techniques presented in Section 4.4.1 it is possible to obtain the following discretised ratio of liquid water along the y and z directions, $s_{j,n}$

$$\dot{s}_{j,n} = \frac{S^l_{H_2O,(j,n)} + D_{s,(j,n)} f_{j,n}}{\varepsilon \rho^l_{H_2O}} \tag{4.68}$$

being

$$f_{j,n} = \begin{cases} \frac{s_{(j+1,n+1)} - s_{(j+1,n)} - s_{(j,n+1)} + 2s_{(j,n)}}{2\Delta y \Delta z} & \text{if } (j,n) = (1,1), \\ \frac{s_{(j+1,n+1)} - s_{(j+1,n)} - s_{(j,n+1)} + 2s_{(j,n)} - s_{(j-1,n)}}{2\Delta y \Delta z} & \forall (j,n) = (2,1), \ldots, (n_z - 1, 1), \\ \frac{s_{(j+1,n+1)} - s_{(j+1,n)} - s_{(j,n+1)} + 2s_{(j,n)} - s_{(j,n-1)}}{2\Delta y \Delta z} & \forall (j,n) = (1,2), \ldots, (1, n_y - 1), \\ \frac{-s_{(j+1,n)} + 2s_{(j,n)} - s_{(j,n-1)}}{2\Delta y \Delta z} & \text{if } (j,n) = (1, n_y), \\ \frac{s_{(j+1,n+1)} - s_{(j+1,n)} - s_{(j,n+1)} + 2s_{(j,n)} - s_{(j-1,n)} - s_{(j,n-1)} + s_{(j-1,n-1)}}{2\Delta y \Delta z} & \forall (j,n) = (2,2), \ldots, (n_z - 1, n_y - 1), \\ \frac{2s_{(j,n)} - s_{(j-1,n)} - s_{(j,n-1)} + s_{(j-1,n-1)}}{2\Delta y \Delta z} & \text{if } (j,n) = (n_z, 1), \\ \frac{-s_{(j,n+1)} + 2s_{(j,n)} - s_{(j-1,n)} - s_{(j,n-1)} + s_{(j-1,n-1)}}{2\Delta y \Delta z} & \forall (j,n) = (n_z, 2), \ldots, (n_z, n_y - 1), \\ \frac{-s_{(j+1,n)} + 2s_{(j,n)} - s_{(j-1,n)} - s_{(j,n-1)} + s_{(j-1,n-1)}}{2\Delta y \Delta z} & \forall (j,n) = (2, n_y), \ldots, (n_z - 1, n_y), \\ \frac{2s_{(j,n)} - s_{(j-1,n)} - s_{(j,n-1)} + s_{(j-1,n-1)}}{2\Delta y \Delta z} & \text{if } (j,n) = (n_z, n_y). \end{cases} \tag{4.69}$$

4.4.6 MATLAB and Simulink

MATLAB is a high-performance language for technical computing. It integrates computation, visualization, and programming in an easy-to-use environment where problems and solutions are expressed in familiar mathematical notation [112].

Simulink allows to implement models using a graphical programming interface. This modelling tool is specially useful to implement complex multi-physic systems, as is the case of PEM fuel cells. It allows to use all the analysis tools in MATLAB, therefore the simulation

results can be taken, analysed and visualised. While there are many predefined Simulink model blocks, the complex nonlinear dynamics of PEM fuel cells require the use of advanced code blocks. Simulink allows to write S-functions, which are blocks that can be programmed in MATLAB, C, C++, Ada or Fortran.

The complete list of parameter values for the MATLAB file and the model structure implemented in Simulink that is used to simulate the system and to develop the observers and controllers are included in Appendix B.

4.5 Case Study

Automobile manufacturers are investing in the development of fuel cell powered vehicles [113]. Fuel cell powered vehicles can offer good autonomy and quick refuelling times compared to battery electric vehicles. Nevertheless, this technology also faces important challenges such as high component costs, stack durability and the fact that the hydrogen infrastructure is almost non-existent. The objectives of this work are to increase the efficiency of fuel cells, reducing the cost per available kW and to increase the durability of the stack making use of advance control strategies.

Test driving cycles are used to certify the emissions levels for internal combustion engine vehicles in order to guarantee actual legislative norms [114, 115]. These driving cycles represent driving patterns for slow urban, rural roads and highway driving environments.

Different test cycles are used depending on the country. In the United States, Canada, Australia, Sweden and Switzerland a federal test procedure (FTP) or a variation is used. For the European Union (EU), the New European Driving Cycle (NEDC) is the test cycle used for the atmospheric pollutant emission certification in passenger vehicles [114].

Focusing on fuel cells and hybrid powered vehicles, automotive test driving cycles can be used to test performance of the vehicles and to assess novel control strategies that aid to improve this performance and enhance the durability of the system [3], one of the main challenges of the technologies nowadays.

The NEDC is used as the case study to test the performance of the observation and control strategies developed in Parts III and IV of this work.

4.5.1 The New European Driving Cycle

The NEDC consists of four repeated ECE-15 [116] urban driving cycles (UDC) and one extra-urban driving cycle (EUDC). The NEDC speed profile is shown in Figure 4.11: the four UDC occur between times 0 and 800 seconds, while the EUDC profile goes after time 800 until the end of the NEDC at 1200 seconds.

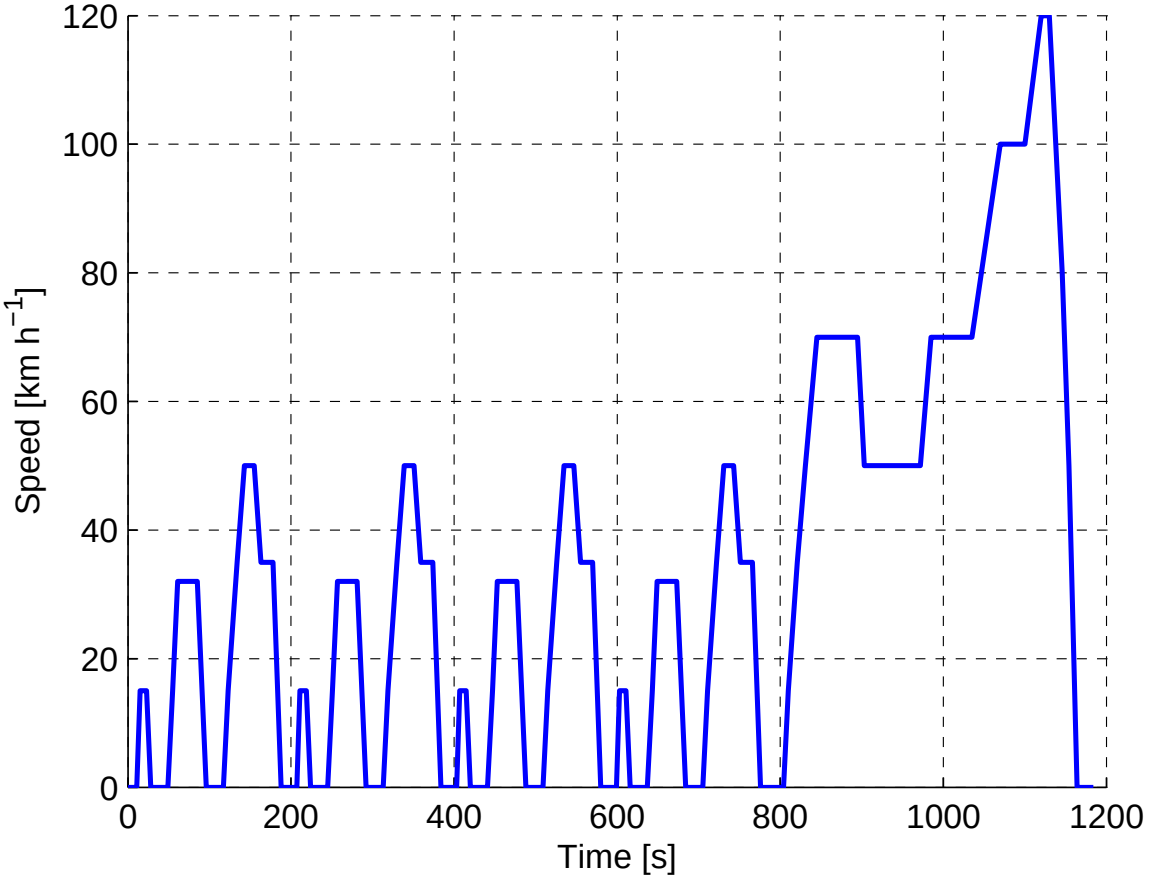

FIGURE 4.11: NEDC velocity profile

The procedure to transform the velocity profile in Figure 4.11 to the current density profile in Figure 4.12 is explained in [3], where a virtual car model is used to convert the velocity cycle to power cycle data, that can be transformed into power and current demand for the fuel cell system using its polarisation curve. In this work, the current profile from [3] is used as the scenario to test the observer and control strategies in Parts III and IV assuming no hybridisation, which means that all the power comes directly from the fuel cell. Even though this is not a very realistic scenario, the purpose of this assumption was to test the worst case scenario for the system.

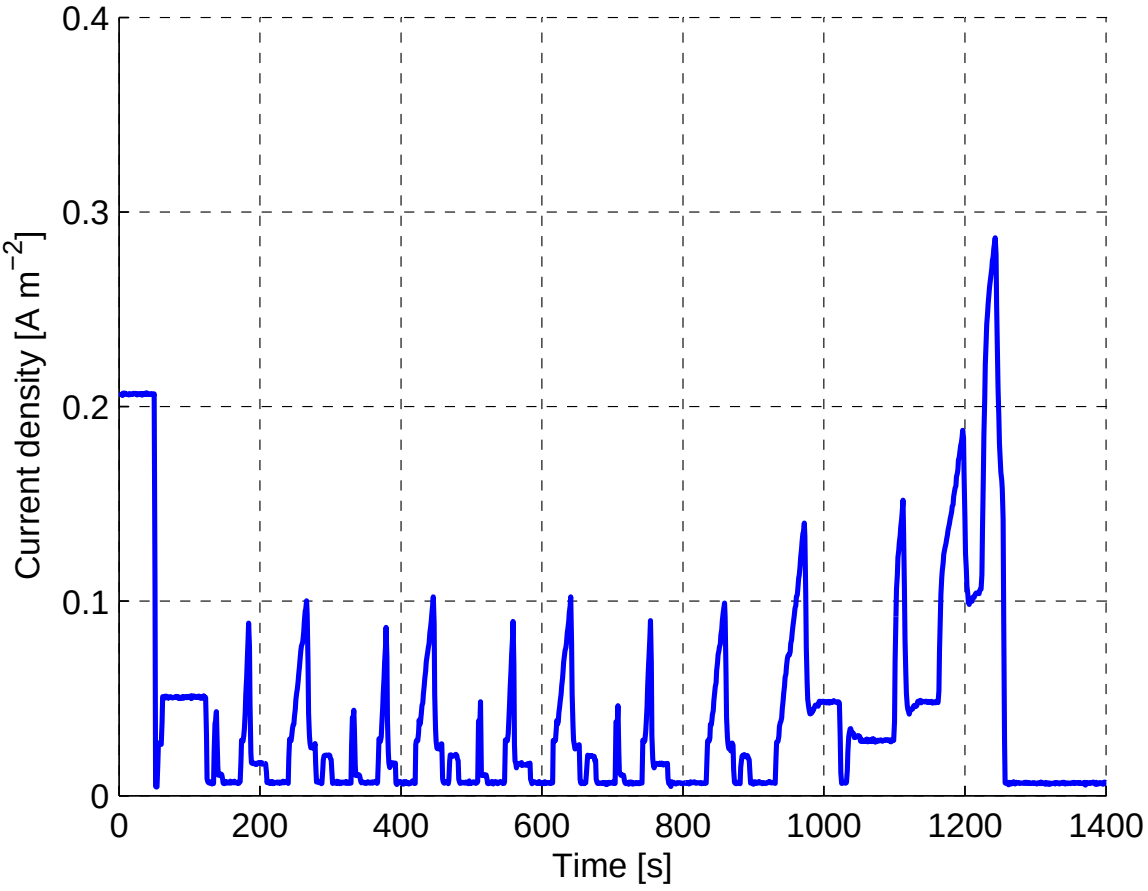

FIGURE 4.12: NEDC current density variation in a single cell

Part III

State Observation

The contents of this part have been published in the following articles:

- *J. Luna, E. Usai, A. Husar and M. Serra.* Observation of the Electrochemically Active Surface Area in a Proton Exchange Membrane Fuel Cell, IEEE Industrial Electronics Conference, 2016, Firenze
- *J. Luna, E. Usai, A. Husar and M. Serra.* Nonlinear observation in fuel cell systems: A comparison between disturbance estimation and high-order sliding-mode techniques, International Journal of Hydrogen Energy, 41(43): 19737-19748, 2016
- *J. Luna, A. Husar and M. Serra.* Nonlinear distributed parameter observer design for fuel cell systems, International Journal of Hydrogen Energy, 40(34): 11322-11332, 2015

Chapter 5

Observation Problem

5.1 Introduction

The internal conditions in fuel cells greatly affect their efficiency and durability. Examples of these internal variables are the local concentration of the reactants in the catalyst layers as well as local stoichiometries, which are directly related with efficiency and degradation. Moreover, the humidification of the membrane is also linked with the global efficiency and the degradation rate of the system. However, fuel cells are enclosed systems and the values of these internal variables are not available for measurement with the current sensor technology.

Therefore, in order to have a good knowledge of the fuel cell health state and be able to actuate properly with controllers, some of the system variables have to be estimated using state observation tools. Specifically, in this thesis work, state observers have been designed to estimate relevant internal variables that can be used in the control strategies developed in Part IV. The selection of the estimated variables follows the criteria of performance and durability improvement.

In this chapter, the basic concepts of state estimation in nonlinear systems are introduced, specially focusing on nonlinear observation for fuel cell systems. Then, the observation model, derived from the simulation model in Chapter 4, is presented along with additional considerations to develop and implement observation strategies in fuel cells. This observation model is used in Chapters 6 and 7 to develop two observation strategies for fuel cell based systems.

During the development of this doctoral work, the topic of full state estimation in a distributed parameter fuel cell was studied and published in [22], where the reaction terms at the anode and cathode sides were considered measurables. This simplification does not represent the real behaviour of fuel cells and it was removed from consideration and improved versions of the work were published in [29, 30, 31]. Prior to this doctoral work, this kind of observation strategy for fuel cells was not present in the literature, being one of the main contributions of this thesis.

5.2 Observability of Nonlinear Systems

Before introducing the observation model used to develop the state observers of this work, some concepts about observability and other theoretical principles about state reconstruction are introduced in this section.

5.2.1 The Lie Derivative

The gradient of a smooth (that has continuous partial derivatives of any order) scalar function h with respect a vector of states $\mathbf{x}$ is denoted by

$$\nabla h = \frac{\partial h}{\partial \mathbf{x}}. \tag{5.1}$$

In addition, for a given vector field $\mathbf{f}$, the Jacobian of $\mathbf{f}$ along the vector of states $\mathbf{x}$ is expressed as

$$\nabla \mathbf{f} = \frac{\partial \mathbf{f}}{\partial \mathbf{x}}, \tag{5.2}$$

which can be expressed in matrix form as a matrix of scalar elements

$$(\nabla \mathbf{f})_{ij} = \frac{\partial f_i}{\partial x_j}. \tag{5.3}$$

Given a scalar function $h : \mathbb{R}^n \to \mathbb{R}$ and a vector field $\mathbf{f} : \mathbb{R}^n \to \mathbb{R}^n$, the Lie derivative [117] of h with respect to $\mathbf{f}$ is a scalar function expressed by the vectorial product of the gradient of h and $\mathbf{f}$:

$$L_{\mathbf{f}} h = \nabla h \cdot \mathbf{f}. \tag{5.4}$$

Hence, the Lie derivative $L_{\mathbf{f}}$ is the directional derivative of h along the direction of the vector field $\mathbf{f}$. As any kind of derivative, the Lie derivative can be computed n times recursively for a given function along a vector field

$$L_{\mathbf{f}}^0 = h, \tag{5.5a}$$

$$L_{\mathbf{f}}^1 = L_{\mathbf{f}}(L_{\mathbf{f}}^0 h) = L_{\mathbf{f}} h, \tag{5.5b}$$

$$\dots$$

$$L_{\mathbf{f}}^n h = L_{\mathbf{f}}(L_{\mathbf{f}}^{n-1} h) = \nabla(L_{\mathbf{f}}^{i-1} h) \cdot \mathbf{f}. \tag{5.5c}$$

In an analogous manner, if $\mathbf{g}$ is another smooth vector field, then the product of Lie derivatives $L_{\mathbf{g}} L_{\mathbf{f}} h$ is expressed as

$$L_{\mathbf{g}} L_{\mathbf{f}} h = \nabla(L_{\mathbf{f}} h) \cdot \mathbf{g}. \tag{5.6}$$

When studying the state space representation of a mathematical model (where $h(\mathbf{x})$ depends on the state vector $\mathbf{x} \in \mathbb{R}^n$), the Lie derivative of $h(\mathbf{x})$ along the vector field $\mathbf{f}$ can be written as

$$L_{\mathbf{f}(\mathbf{x})} h(\mathbf{x}) = \begin{bmatrix} \frac{\partial h(\mathbf{x})}{\partial x_1}, & \dots, & \frac{\partial h(\mathbf{x})}{\partial x_n} \end{bmatrix} \begin{bmatrix} f_1(\mathbf{x}) \\ \vdots \\ f_n(\mathbf{x}) \end{bmatrix}. \tag{5.7}$$

All these definitions are essential for the nonlinear observability analysis and for the development of the state observers as it will be seen in the following sections of the present chapter.

5.2.2 Observability Definitions

When studying linear systems, a system can be classified as observable if the current state can be determined in finite time employing measured outputs and the model of the linear plant. The linear observability problem has been widely studied since 1965 [59] and several mathematical tools and indexes are available to perform the observability analysis of a system.

In the nonlinear case, the observability definition is not so straightforward; several definitions have to be presented to fully understand the concept of nonlinear observability [118]. These conditions include:

- Indistinguishability
- Global and local observability
- Local weak and weak observability

In the following sections, a brief introduction about these nonlinear observability concepts is given.

5.2.2.1 Indistinguishability

Two states x_a and x_b in $\mathcal{A}$, which is an open set of $\mathcal{X}$ ($\mathcal{A} \subseteq \mathcal{X}$), are said to be indistinguishable in $\mathcal{A}$ at t_0 if using the input u and considering the output variable y over the time interval $t_0 \leq t \leq t_1$, identical outputs result [117, 118]. This can formally be expressed as

$$y(\mathcal{X}(t_0, t, x_a)) = y(\mathcal{X}(t_0, t, x_b)), \quad t_0 \leq t \leq t_1. \tag{5.8}$$

For notation purposes, from now on the set of all points that are indistinguishable from a state x in a subset $\mathcal{A} \subseteq \mathcal{X}$ is determined by $\mathcal{I}(x)$. If the points are indistinguishable from a state x via trajectories in $\mathcal{U}$ is determined by $\mathcal{I}_{\mathcal{U}}(x)$

5.2.2.2 Global Observability

A nonlinear system is said to be observable or globally observable if there exists a time t_1 such that the initial state x_0 can be distinguished from any other state x using the input u and considering the output y in finite time over the time interval $t_0 \leq t \leq t_1$.

Formally speaking, a system is observable at x_0 if $\mathcal{I}(x_0) = x_0$, and is globally observable if $\mathcal{I}(x_0) = x_0$ for all x_0 [119].

5.2.2.3 Local Observability

Considering an open neighbourhood $\mathcal{U}$, a system is locally observable at x_0 if $\mathcal{I}_{\mathcal{U}}(x_0) = x_0$ via trajectories in $\mathcal{U}$ [117, 118, 119].

It has to be remarked that the concept of local observability is a stronger property than global observability because it involves the observability of the states in a neighbourhood or manifold, while in the global observability case the observation of the states can follow any trajectory not being bounded by a neighbourhood.

5.2.2.4 Weak Observability

The concept of weak observability is useful when it is sufficient to distinguish x_0 from the neighbours. This approach lends to an algebraic test that facilitates the task of analysing the observability of a nonlinear system [119].

A system is said to be weakly observable at x_0 if there exists a neighbourhood $\mathcal{U}$ whose intersection with the indistinguishable set of x_0 is equal to:

$$\mathcal{I}(x_0) \cap \mathcal{U} = x_0. \tag{5.9}$$

5.2.2.5 Local Weak Observability

Following a similar logic as in the definition of local observability, a system is said to be locally weakly observable at x_0 if there exists an open neighbourhood $\mathcal{U}$ of x_0 where $\mathcal{I}_{\mathcal{V}}(x_0) = x_0$ for every open neighbourhood $\mathcal{V} \subset \mathcal{U}$ [119].

In conclusion, the system is said to be locally weakly observable if it is possible to distinguish x_0 from its neighbours for all x_0.

5.2.2.6 Summary of Observability Definitions

The summary of the previous definitions and their dependencies is shown Figure 5.1. The relation between the conditions states again that local observability is the stronger and most restrictive condition.

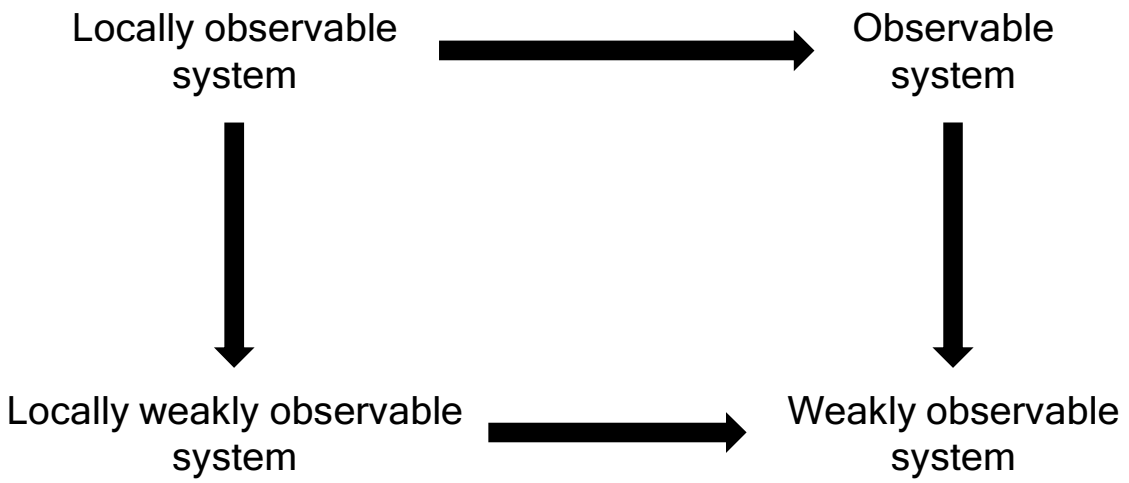

FIGURE 5.1: Nonlinear observability flow diagram

5.3 Observability Condition

A generic nonlinear system can be expressed as:

$$\dot{\mathbf{x}} = \mathbf{f}(\mathbf{x}), \tag{5.10}$$

$$\mathbf{y} = h(\mathbf{x}), \tag{5.11}$$

where $\mathbf{x} \in \mathbb{R}^n$ is the state vector and $\mathbf{y} \in \mathbb{R}^p$ the output vector. $\mathbf{f}$ and $\mathbf{g}$ are smooth vector fields.

In nonlinear systems, the observability condition is analysed from the observability matrix $\mathcal{O}$ that can be expressed as

$$\mathcal{O}(\mathbf{x}) = \frac{\partial}{\partial \mathbf{x}} \begin{bmatrix} h(\mathbf{x}) \\ L_{\mathbf{f}(\mathbf{x})} h(\mathbf{x}) \\ \vdots \\ L^{(n-2)}_{\mathbf{f}(\mathbf{x})} h(\mathbf{x}) \\ L^{(n-1)}_{\mathbf{f}(\mathbf{x})} h(\mathbf{x}) \end{bmatrix}, \tag{5.12}$$

where $L_{\mathbf{f}(\mathbf{x})}$ is the 1-repeated Lie derivative [117] which can be written as a tensor field formulated by

$$L_{\mathbf{f}(\mathbf{x})} h(\mathbf{x}) = \frac{\partial h(\mathbf{x})}{\partial \mathbf{x}} \mathbf{f}(\mathbf{x}). \tag{5.13}$$

Higher order Lie derivatives are expressed in Equation (5.5).

If the observability matrix (5.12) is non-singular, the full state vector $\mathbf{x}$ is locally weakly observable [120] at $\mathbf{x}_0$. Since $\mathcal{O}$ strongly depends on the state vector, the analytical computation of its rank is a demanding task. In all the simulations presented in this work, the observability condition study has been performed numerically. The computation of the rank has been done through the singular value decomposition of matrix $\mathcal{O}$. During the simulations presented in the next chapters, when $rank(\mathcal{O})$ was lower than the expected full rank, the observer was disconnected from the control loop until the observability condition (full rank) was recovered.

5.4 Observation Model

As mentioned before, degradation in fuel cells is linked with the reactants concentration in the CLs. Moreover, efficiency is related with the humidification of the membrane that separates the anode and cathode sides of the fuel cell. Reactants and water concentration values are states of the dynamic model that give information about the internal state of the system. These internal variables can be used to design controllers that aid to improve efficiency and enhance durability. Therefore, the observation of the gas species concentrations is going to be the main focus of the observers designed in the following chapters.

The observation model, based on simplified version of the simulation model in Chapter 4, will give back the full states profile along the z-direction of the fuel cell since it will maintain the distributed parameters characteristic of the simulation model. This is an essential feature in order to design and synthesise advanced controllers to improve the power quality and increase the performance of PEM fuel cells, taking into account the spatial variations of the variables.

Using the estimation of the reactants and water concentrations inside the PEM fuel cell, it is possible to derive the ECSA value at the CCL. As introduced in Chapter 4, the ECSA gives a quantitative measurement of the active surface where the reaction can occur and electric current is produced [42]. The ECSA affects the output voltage of the fuel cell and it depends on the Pt loading of the catalyst surface, the pore distribution and the state of hydration of the system. Pore distribution and Pt loading of the catalyst are specifications given by the PEM manufacturer. Moreover, these parameters degrade and fluctuate during the lifespan

of the fuel cell. The estimation of the ECSA will aid to design advanced control strategies in Part IV.

The observer model includes only the dynamic representation of the gas concentration states and the ECSA at the CCL. For the ECSA, the observer includes the discretised model of Section 4.4.2. Regarding the gas concentrations at the anode and cathode gas channels, GDLs and CLs, the observers include the discretised models presented in Sections 4.4.3 and 4.4.4.

5.4.1 Gas Flow Observation Model

Expressing Equation (4.65) for the observed i-th concentration species at each j discretisation volumes of the gas channels, it can be written that:

$$\dot{\hat{c}}_{i,j} = \begin{cases} \frac{u_i}{\Delta z} - \zeta_1 \Psi(j) - \frac{\dot{n}_{i,j}}{\delta_C} & \text{if } j = 1, \\ \zeta_1 \left(\Psi(j-1) - \Psi(j)\right) - \frac{\dot{n}_{i,j}}{\delta_C} & \text{if } 2 \leq j \leq n_z - 1, \\ \zeta_1 \Psi(j-1) + \Gamma(j+1) - \frac{\dot{n}^k_{i,j}}{\delta_C} & \text{if } j = n_z, \end{cases} \tag{5.14a}$$

with

$$\Psi(j) = \hat{c}_{i,j} \left(\sum_i \hat{c}_{i,j} - \sum_i \hat{c}_{i,j+1} \right), \tag{5.15a}$$

$$\Psi(j-1) = \hat{c}_{i,j-1} \left(\sum_i \hat{c}_{i,j-1} - \sum_i \hat{c}_{i,j} \right), \tag{5.15b}$$

$$\Gamma(j+1) = \zeta_1 c_{i,n_z} \sum_i c_{i,n_z} + \zeta_2 c_{i,n_z}. \tag{5.15c}$$

Note that in Equations (5.14) and (5.15), the states at the last discretisation volume ($j = n_z$) are known. c_{i,n_z} are actual values of the states at the output of the anode and cathode gas channels. The derivation of c_{i,n_z} from standard measurements in fuel cells is explained in Section 5.5.1.

5.4.2 Gas Diffusion Estimation Model

Regarding the concentrations diffusion along the y-direction of the fuel cell, taking into account Equation (4.67) the estimated gas concentrations at the GDLs can be expressed as

follows:

$$\dot{\hat{c}}_{i,(j,n)} = \begin{cases} \frac{D_i}{\Delta y^2}\left(\hat{c}_{i,j} - 2\hat{c}_{i,(j,n)} + \hat{c}_{i,(j,n+1)}\right) & \text{if } n = 1, \\ \frac{D_i}{\Delta y^2}\left(\hat{c}_{i,(j,n-1)} - 2\hat{c}_{i,(j,n)} + \hat{c}_{i,(j,n+1)}\right) & \text{if } 2 \leq n \leq n_y - 1, \\ \frac{D_i}{\Delta y^2}\left(\hat{c}_{i,(j,n-1)} - \hat{c}_{i,(j,n)}\right) & \text{if } n = n_y, \end{cases} \tag{5.16}$$

where $j \triangleq [1, \dots n_z]$ is the discretisation volume subscript for the z-direction and $n \triangleq [1, \dots n_y]$ is the discretisation volume subscript for the y-direction. Note that the term $\hat{c}_{i,j}$ when $n = 1$ in Equation (5.16) is the observed variable at the gas channel from Equation (5.14).

The use of Equation (5.16) allows to estimate the concentration values at the CLs without the use of additional measurements.

5.4.3 ECSA Estimation Model

The ECSA model presented in the previous chapter may be used to obtain of the estimation of the ECSA from the estimation of the concentration states at the CCL.

The local active surface area at the CCL j-volume ($ECSA_j$) is isolated from Equation (4.62)

$$ECSA_j = i_{0,j}\, A_{geo}\, (a_{O_2,j})^{-0.5}\, (i_{0,ref})^{-1} e^{\left(-\Delta G^* \left(1 - \frac{T_{cell}}{T_{ref}}\right) R^{-1} {T_{cell}}^{-1}\right)}, \tag{5.17}$$

being

$$a_{O_2,j} = \frac{p_{O_2,CCL,j}}{p_{O_2,ref}}. \tag{5.18}$$

As developed in Section 4.3.2, it is assumed that the fuel cell temperature T_{fc} is measured. From this value the temperature of each cell T_{cell} is obtained from a statistic distribution. Henceforth, the only unknowns in Equation (5.17) are the current exchange $i_{0,j}$ and the oxygen partial pressure at the CCL, $p_{O_2,CCL,j}$, for each one of the discretisation volumes.

From Equation (4.60), it is possible to calculate the estimate current exchange at the CCL knowing the fuel cell voltage

$$i_{0,j} = i \left(e^{\frac{-RT_{cell} \log\left(a_{O_2}\right) - 2\,\alpha F V_{fc,cell,j} + 2\,E_r \alpha F - 2\,i\,R_{ohm,j}\,\alpha F}{R\,T_{cell}}} \right)^{-1}, \tag{5.19}$$

which leaves the oxygen partial pressure as the only unknown parameter in Equation (5.17). Considering Equation (4.9c), the discretised partial oxygen pressure at the CCL can be expressed as

$$p_{O_2,CL,j} = RT_{cell} c_{O_2,CL,j}. \tag{5.20}$$

To obtain the oxygen concentration at the CCL, $c_{O_2,CL,j}$ and the rest of the gas species concentrations at the catalyst sites, two novel observation strategies are presented and developed in Chapters 6 and 7. Both strategies use the discretised gas flow and gas diffusion models presented in Sections 4.4.3 and 4.4.4.

5.5 Direct and Indirect Measurements in PEM Fuel Cell Systems

PEM fuel cell systems incorporate sensors to measure variables such as temperatures, pressures, concentration values, etc. These measurements provide a knowledge of the PEM fuel cell that is used to improve its operation. In the vast majority of systems, these sensors are located in accessible parts of the fuel cell, such as the inlet and outlet gas channels, where it is possible to install measurement devices. Furthermore, temperature sensors can be distributed around the exterior structure of the PEM fuel cell to measure the thermal behaviour of the system.

As it was introduced before, the measurement of internal variables is practically impossible in PEM fuel cell systems. One way to overcome this lack of internal measurements is to implement indirect measurement techniques such as dielectric spectroscopy, or EIS. In a fuel cell, the EIS is used to describe the electrochemical properties of the MEA through a frequency analysis to characterise the low frequency impedance and the ohmic resistance. From the experimental data extracted in EIS tests, researchers have developed tools to estimate some of the internal variables in PEM fuel cells. In [121], EIS is used to characterise the water transport events through the MEA. These techniques are out of the scope of this work.

Other internal variables can be derived through indirect measurements. A classic example in PEM fuel cells is the hydrogen reaction rate, which can be described as a function of the fuel cell current, a variable that can be easily measured.

Using direct and indirect measurements, observers may be designed to estimate states and internal variables of PEM fuel cells. As with any other dynamic system, the measurement of variables has two main objectives: to give information about the actual status of the overall system (state of health) and to use the information to steer the states to desired operation points (control). The development of advanced estimation techniques in this work is focused on the implementation of better control strategies that allow the system to perform in a reliable and efficient manner through all of its operating range.

5.5.1 Measurements for Full State Estimation in PEM Fuel Cell Systems

As introduced in Section 5.4.1, the concentration states at the last z-discretisation volume have to be known or measured to estimate the states corresponding to the discretised gas channels. From these values, the concentrations at the GDLs and CLs will be estimated using the equations presented in Section 5.4.2.

In this section, a method to derive the concentrations at the end of the anode and cathode gas channels using common measurements in fuel cells is explained.

Taking into account the generic nonlinear state space model

$$\dot{\mathbf{x}} = \mathbf{f}(t, \mathbf{x}, \mathbf{u}), \tag{5.21a}$$

$$\mathbf{y} = h(t, \mathbf{x}, \mathbf{u}), \tag{5.21b}$$

where $\mathbf{x} \in \mathbb{R}^n$ is the state vector, $\mathbf{y} \in \mathbb{R}^p$ the output vector and $\mathbf{u} \in \mathbb{R}^m$ the input vector of the observer model, the states are the gas species concentrations at each discretisation volume $c_{i,j}$ and the inputs are the inlet flows which are considered to be measured too.

Using the observation model in Section 5.4.1 and the nomenclature in Equation (5.21), $\mathbf{x} \triangleq c_{i,j}$, where i refers to the i-th gas concentrations and j to the z-direction discretisation volume. The input vector u includes the input molar flows $\dot{n}_{i,in}$, therefore $\mathbf{u} \triangleq \dot{n}_{i,in}$. As shown in Chapter 4, it is assumed that the PEM fuel cell cathode inlet is fed with air, therefore, nitrogen is considered as a state variable and the measured outputs used to obtain

the output concentrations vector $\mathbf{y}$ are expressed as

$$\mathbf{y} = \begin{bmatrix} h^A_{H_2}(\mathbf{x}) \\ h^A_{H_2O}(\mathbf{x}) \\ h^C_{N_2}(\mathbf{x}) \\ h^C_{O_2}(\mathbf{x}) \\ h^C_{H_2O}(\mathbf{x}) \end{bmatrix} = \begin{bmatrix} c^A_{H_2,n_z} \\ c^A_{H_2O,n_z} \\ c^C_{N_2,n_z} \\ c^C_{O_2,n_z} \\ c^C_{H_2O,n_z} \end{bmatrix}. \tag{5.22}$$

The measurement of the gas concentrations in the last discretisation volume is not a trivial task. Gas purity sensors are expensive and in general they operate under long response times, making them unfitting for the estimation function. However, it is possible to infer the aforementioned concentrations from other measurements present in a PEM fuel cell based system.

Knowing the output anode relative humidity and the water saturation pressure at the system temperature, it is possible to infer the water concentration value from the water partial pressure ($p^A_{n_z,H_2O}$) as derived from Equation (4.63c):

$$c^A_{H_2O,n_z} = \frac{p^A_{H_2O,n_z}}{RT_{cell}}. \tag{5.23}$$

Moreover, knowing the output pressure ($p^A_{n_z}$) of the anode gas channel is usual in the majority of the PEM fuel cell based systems. From this output pressure and using (5.23) it is possible to obtain the partial pressure of hydrogen, since

$$p^A_{n_z} = p^A_{H_2,n_z} + p^A_{H_2O,n_z}. \tag{5.24}$$

And following the same procedure as in Equation (5.23), the hydrogen concentration at the end of the anode gas channel is derived.

In the cathode side there is an additional gas in comparison with the anode side. Therefore, an additional equation is needed to obtain the output concentrations. Employing a humidity sensor, the output water concentration can be obtained. The pressure at the cathode output has to be measured as well.

Measuring the total current demanded by the load I, the total reacted oxygen flow rate (denoted by subscript r) is obtained [4]

$$\dot{n}^C_{O_2,r} = L_x L_z \frac{I}{4F}. \tag{5.25}$$

The input molar flows are considered as measured variables. This is accomplished using flow meters. Knowing the reacted oxygen (5.25) and the oxygen input molar flow $\dot{n}^C_{O_2,in}$, the total output oxygen molar flow is computed

$$\dot{n}^C_{O_2,n_z} = \dot{n}^C_{O_2,in} - \dot{n}^C_{O_2,r}, \tag{5.26}$$

which represents the flux of oxygen at the output of the cathode gas channel.

The oxygen concentration at the output of the cathode is obtained dividing $\dot{n}^C_{O_2,n_z}$ by the output gas flow velocity $v^C_{n_z}$. This velocity can be obtained applying Darcy-Weisbach principle [122]

$$\frac{\Delta p^C}{L_z} = f_D \frac{\rho_{air}}{2} \frac{v^2_{out}}{D^C}, \tag{5.27}$$

where Δp^C is the measured difference between the input and output cathode manifold pressures, ρ_{air} the air density, D^C the hydraulic diameter of the cathode gas channel and f_D is the friction factor. For fuel cells, the flow is considered to be laminar and therefore

$$f_D = \frac{64}{Re}, \tag{5.28}$$

being Re the Reynolds number

$$Re = \frac{v_{in} D^C}{\nu}, \tag{5.29}$$

where ν is the kinematic viscosity of air. Eq. (5.27) can be rewritten as

$$v^C_{out} = \sqrt{\frac{\Delta p}{L} \frac{2D}{f_D \rho_{air}}} \tag{5.30}$$

Therefore,

$$c^C_{O_2,n} = \frac{\dot{n}^C_{O_2,n_z}}{v^C_{out}}. \tag{5.31}$$

From Equation (4.63c), and knowing the output concentrations of water and oxygen, the

partial pressures can be obtained. Moreover, knowing $p^C_{H_2O,n_z}$, $p^C_{H_2O,n_z}$ and the total output pressure $p^C_{n_z}$, the nitrogen partial pressure at the end of the cathode gas channel is obtained. Finally, the nitrogen concentration is computed using the previous values.

Deriving the $c^C_{O_2,n}$ with Equations (5.25)-(5.31) would introduce a certain error due to the fact that the internal dynamics of the channel are disregarded in Equation (5.26). However, this fact would only affect the observation procedure during a short transitory period which can be neglected.

Henceforth, the following measurements are assumed to be available:

- Relative humidity at the end of both gas channels
- Pressures in the last discretisation volume both for the anode and cathode gas channels
- Input molar fluxes for all the gas species
- Temperatures in the fuel cell
- Total current

The measurement of the input molar fluxes and specially the measurement of the output relative humidities imply a time delay that can affect the behaviour of the proposed estimation techniques. Specifically, relative humidity sensors work with response times of less than 5 seconds to 90% of the final value and 10 seconds for the 100% [123]. Molar flow meters perform with response times around 1 second [124]. The effect of these delays and other robustness issues of the observers are studied in Chapter 7.

Chapter 6

Nonlinear Distributed Parameter Observer with Disturbance Estimation

6.1 Introduction

The theory of state observation of nonlinear systems was introduced in the previous chapter, including the concept of observability in nonlinear systems. Moreover, the observation model used in this work, derived from the simulation model in Chapter 4 was presented. The observation model aims to allow the design of observation strategies to estimate the internal conditions of the fuel cell, which are critical for its performance and durability.

Both the ECSA and the CCL exchange current i_0 affect the output voltage of the fuel cell. It was demonstrated that to obtain these variables, the concentration of reactants available at the CLs has to be estimated. In this chapter, a nonlinear distributed parameters observer[1] (NDPO) to estimate the concentration of gases along the gas channels of the PEM fuel cell is developed. The NDPO observation model presents the same spatial distribution characteristics as the simulation model, but considering the reactions and water transports as disturbances. These disturbances are estimated with a nonlinear disturbance observer

[1] In control theory, distributed parameters observers are formulated in terms of PDEs. In the scope of this work, the distributed parameter denomination comes from the discretisation of the PDEs that describe the plant presented in Chapter 4.

(NDOB) set in parallel with the NDPO. Finally, the NDPO uses a super-twisting algorithm (STA) approach to correct the observation error and to drive the estimates to the real value of the states.

In Chapter 5 the derivation of the output concentration values from the real measurements of the PEM fuel cell was explained. During the development of the NDPO studied in this chapter and the one presented in Chapter 7, these measurements are supposed to be available.

6.2 NDPO for the Estimation of the Gas Concentrations in the Gas Channels

6.2.1 Design Conditions

As introduced previously, the NDPO follows a model-based approach. In particular, the observer structure considers the discretised observation model presented in Equation (5.14).

For an n-order nonlinear system, the NDPO discretised structure is such that

$$\dot{\hat{\mathbf{c}}} = \mathbf{f}(t, \hat{\mathbf{c}}, \mathbf{u}) + \mathbf{g}(t, \hat{\mathbf{c}}, \hat{\mathbf{d}})\mathbf{u}_0, \tag{6.1a}$$

$$\hat{\mathbf{y}} = h(t, \hat{\mathbf{c}}), \tag{6.1b}$$

where $\hat{\mathbf{c}} \in \mathbb{R}^{5\times n_z}$ denotes the observed state vector and $\hat{\mathbf{y}} \in \mathbb{R}^5$ the output vector that was introduced in Section 5.5.1. Function $\mathbf{f}$ includes the nonlinear dynamics of the observation model presented in Equation (4.65), including the fuel cell molar inputs. Function $\mathbf{g}$ includes distributed reaction terms and water transports at both sides of the MEA which are considered in $\hat{\mathbf{d}} \triangleq \dot{\mathbf{n}} \in \mathbb{R}^{5\times n_z}$. Moreover, $\mathbf{u} \in \mathbb{R}^5$ is the input vector of the hydrogen and the water input terms at the anode and the oxygen, nitrogen and water input terms at the cathode. As shown in Equation (5.14), in the observation model the input vector $\mathbf{u}$ is different from zero for the first discretisation volume ($j = 1$). For the rest of the volumes this value is computed from gas concentration values of the previous volume. Finally, $\mathbf{u}_0 \in \mathbb{R}^5$ is the corrective input term for each one of the output concentrations species values.

The implementation of the observer in Equation (6.1) is only possible if the reactions and water transport terms which have been considered as disturbances ($\mathbf{d}$) are either measured

or estimated. Since measuring $\mathbf{d}$ is technologically impossible in fuel cells, in Section 6.4 an estimation procedure for the disturbances in all the discretisation volumes is presented.

Moreover, as it will be developed in Section 6.5, the corrective input term for each i-th gas species $u_{0,i}$ is a function of the output observation error $e_{y,i}$, which is defined as the difference between the estimated output $\hat{y}_i$ of the observer in Equation (6.1) and the measured vector y_i as expressed by

$$e_{y,i} = \hat{y}_i - y_i. \tag{6.2}$$

Regarding the state observation error for each i-th gas along the j-discretisation volumes, it can be expressed as follows:

$$\mathbf{e}_i = \hat{\mathbf{c}}_i - \mathbf{c}_i = \begin{bmatrix} \hat{c}_{i,1} - c_{i,1} \\ \hat{c}_{i,2} - c_{i,2} \\ \vdots \\ \hat{c}_{i,n_z} - c_{i,n_z} \end{bmatrix}. \tag{6.3}$$

In [125] it is demonstrated that the observer (6.1) is able to estimate the values of all the states along the j-discretisation volumes, driving the state observation error in Equation (6.3) to approximately zero in a finite amount of time given that a suitable corrective input term $\mathbf{u_0}$ is selected to drive the output error in Equation (6.2) to zero. The design conditions of the corrective input term are given in Section 6.5.

6.2.2 Implementation Aspects of the NDPO

It is possible to isolate the observation problem from Equation (6.1) into two subproblems, differentiating between the observation of the states of the anode ($\hat{\mathbf{c}}^A$) and cathode ($\hat{\mathbf{c}}^C$) gas channels

$$\dot{\hat{\mathbf{c}}} = \begin{Bmatrix} \mathbf{f}(t, \hat{\mathbf{c}}^A, \mathbf{u}^A) + \mathbf{g}^A(t, \hat{\mathbf{c}}^A, \hat{\mathbf{d}}^A)\mathbf{u}_0^A \\ \mathbf{f}(t, \hat{\mathbf{c}}^C, \mathbf{u}^C) + \mathbf{g}^C(t, \hat{\mathbf{c}}^C, \hat{\mathbf{d}}^C)\mathbf{u}_0^C \end{Bmatrix}, \tag{6.4a}$$

$$\hat{\mathbf{y}} = \begin{Bmatrix} h(t, \hat{\mathbf{c}}^A) \\ h(t, \hat{\mathbf{c}}^C) \end{Bmatrix}, \tag{6.4b}$$

There are two gas species at the anode, hence $\hat{\mathbf{c}}^A \in \mathbb{R}^{2\times n_z}$ and $\mathbf{u}^A \in \mathbb{R}^2$. Correspondingly, at the cathode, $\hat{\mathbf{c}}^C \in \mathbb{R}^{3\times n_z}$ and $\mathbf{u}^C \in \mathbb{R}^3$.

The decoupling vector $\mathbf{g}^k$ in Equation (6.4) is obtained from the observability matrix $\mathcal{O}^k$ presented in Chapter 5 by computing [125]

$$\mathbf{g}^k = (\mathcal{O}^k(\hat{\mathbf{c}}^k))^{-1} e_z^T, \tag{6.5}$$

for the anodic and cathodic sides of the fuel cell. The term e_z in Equation (6.5) is defined as follows:

$$e_z = [0, 0, \ldots, 1]. \tag{6.6}$$

This is to guarantee that the NDPO corrective input $\mathbf{u_0}$ only acts on the output concentration values in Equation (6.4).

In the observation strategy proposed in this chapter, the corrective input term $\mathbf{u_0}$ is based on a STA approach to correct the last discretisation volume concentrations. The rest of the volumes are estimated using the observation model in Equation (6.4) and a disturbance observer, which is introduced in Section 6.4. The design and implementation details of the corrective input term are presented in Section 6.5.

6.3 Observability Analysis

In this section, the observability condition for each one of the gas channels is studied. The observability condition in Equation (5.12) can be checked separately for the anode and the cathode sides as justified in Section 6.2.2.

6.3.1 Anode Gas Channel Observability

Considering the procedure described in section Section 5.5.1, the output concentrations $c^A_{H_2,n_z}$ and $c^A_{H_2O,n_z}$ are computed from indirect measurements. Developing Equation (5.14) for five

discretisation volumes ($n_z = 5$):

$$\mathcal{O}^A = \frac{\partial}{\partial \mathbf{x}} \begin{bmatrix} h_{H_2} \\ L_{\mathbf{f}(\mathbf{x})} h_{H_2} \\ L^2_{\mathbf{f}(\mathbf{x})} h_{H_2} \\ L^3_{\mathbf{f}(\mathbf{x})} h_{H_2} \\ L^4_{\mathbf{f}(\mathbf{x})} h_{H_2} \\ h_{H_2O} \\ L_{\mathbf{f}(\mathbf{x})} h_{H_2O} \\ L^2_{\mathbf{f}(\mathbf{x})} h_{H_2O} \\ L^3_{\mathbf{f}(\mathbf{x})} h_{H_2O} \\ L^4_{\mathbf{f}(\mathbf{x})} h_{H_2O} \end{bmatrix}, \tag{6.7}$$

with $\mathbf{x} \triangleq [c_{H_2,1}, \ldots, c_{H_2,n_z}; c_{H_2O,1}, \ldots, c_{H_2O,n_z}]$, $h_{H_2} \triangleq c_{H_2,n_z}$, $h_{H_2O} \triangleq c_{H_2O,z}$ and $\mathbf{f}$ being the nonlinear state terms of Equation (5.14).

Considering Equation (5.14) for $j \triangleq [1, \ldots, n_z]$, the following expressions are obtained:

$$f^A_{H_2,1} = -\zeta^A_1 c^A_{H_2,1} \left(c^A_{H_2,1} + c^A_{H_2O,1} - c^A_{H_2,2} - c^A_{H_2O,2}\right), \tag{6.8a}$$

$$f^A_{H_2O,1} = -\zeta^A_1 c^A_{H_2O,1} \left(c^A_{H_2,1} + c^A_{H_2O,1} - c^A_{H_2,2} - c^A_{H_2O,2}\right), \tag{6.8b}$$

$$f^A_{H_2,2} = -f^A_{H_2,1}(\mathbf{x}) - \zeta^A_1 c^A_{H_2,2} \left(c^A_{H_2,2} + c^A_{H_2O,2} - c^A_{H_2,3} - c^A_{H_2O,3}\right), \tag{6.8c}$$

$$f^A_{H_2O,2} = -f^A_{H_2O,1}(\mathbf{x}) - \zeta^A_1 c^A_{H_2O,2} \left(c^A_{H_2,2} + c^A_{H_2O,2} - c^A_{H_2,3} - c^A_{H_2O,3}\right), \tag{6.8d}$$

$$f^A_{H_2,3} = -f^A_{H_2,2}(\mathbf{x}) - \zeta^A_1 c^A_{H_2,3} \left(c^A_{H_2,3} + c^A_{H_2O,3} - c^A_{H_2,4} - c^A_{H_2O,4}\right), \tag{6.8e}$$

$$f^A_{H_2O,3} = -f^A_{H_2O,2}(\mathbf{x}) - \zeta^A_1 c^A_{H_2O,3} \left(c^A_{H_2,3} + c^A_{H_2O,3} - c^A_{H_2,4} - c^A_{H_2O,4}\right), \tag{6.8f}$$

$$f^A_{H_2,4} = -f^A_{H_2,3}(\mathbf{x}) - \zeta^A_1 c^A_{H_2,4} \left(c^A_{H_2,4} + c^A_{H_2O,4} - c^A_{H_2,5} - c^A_{H_2O,5}\right), \tag{6.8g}$$

$$f^A_{H_2O,4} = -f^A_{H_2O,3}(\mathbf{x}) - \zeta^A_1 c^A_{H_2O,4} \left(c^A_{H_2,4} + c^A_{H_2O,4} - c^A_{H_2,5} - c^A_{H_2O,5}\right), \tag{6.8h}$$

$$f^A_{H_2,5} = -f^A_{H_2,4}(\mathbf{x}) - \zeta^A_1 c_{H_2,5} \left(c_{H_2,5} + c_{H_2O,5}\right) + \zeta^A_2 c_{H_2,5}, \tag{6.8i}$$

$$f^A_{H_2O,5} = -f^A_{H_2O,4}(\mathbf{x}) - \zeta^A_1 c_{H_2O,5} \left(c_{H_2,5} + c_{H_2O,5}\right) + \zeta^A_2 c_{H_2O,5}. \tag{6.8j}$$

Developing Equation (6.7) taking into account the nonlinear terms in Equation (6.8):

$$\mathcal{O}^A = \begin{bmatrix} 0 & 0 & 0 & 0 & 0 & 0 & 0 & 0 & 1 & 0 \\ 0 & 0 & 0 & 0 & 0 & 0 & b_1 & b_2 & b_3 & b_4 \\ 0 & 0 & 0 & 0 & b_* & b_* & b_* & b_* & b_* & b_* \\ 0 & 0 & b_* & b_* & b_* & b_* & b_* & b_* & b_* & b_* \\ b_* & b_* & b_* & b_* & b_* & b_* & b_* & b_* & b_* & b_* \\ 0 & 0 & 0 & 0 & 0 & 0 & 0 & 0 & 0 & 1 \\ 0 & 0 & 0 & 0 & 0 & 0 & d_1 & d_2 & d_3 & d_4 \\ 0 & 0 & 0 & 0 & d_* & d_* & d_* & d_* & d_* & d_* \\ 0 & 0 & d_* & d_* & d_* & d_* & d_* & d_* & d_* & d_* \\ d_* & d_* & d_* & d_* & d_* & d_* & d_* & d_* & d_* & d_* \end{bmatrix}, \tag{6.9}$$

with the nonlinear expressions:

$$b_1 = \zeta_1^A \left(2c_{H_2,1} + c_{H_2O,1} - c_{H_2,2} - c_{H_2O,2}\right), \tag{6.10a}$$

$$b_2 = \zeta_1^A c_{H_2,1}, \tag{6.10b}$$

$$b_3 = -\zeta_1^A \left(c_{H_2,1} + (2c_{H_2,2} + c_{H_2O,2})\right) + \zeta_2^A, \tag{6.10c}$$

$$b_4 = -\zeta_1^A \left(c_{H_2,1} + c_{H_2,2}\right), \tag{6.10d}$$

$$d_1 = \zeta_1^A c_{H_2O,1}, \tag{6.10e}$$

$$d_2 = \zeta_1^A \left(c_{H_2,1} + 2c_{H_2O,1} - c_{H_2,2} - c_{H_2O,2}\right), \tag{6.10f}$$

$$d_3 = -\zeta_1^A \left(c_{H_2O,1} + c_{H_2O,2}\right), \tag{6.10g}$$

$$d_4 = -\zeta_1^A \left(c_{H_2O,1} + (c_{H_2,2} + 2c_{H_2O,2})\right) + \zeta_2^A. \tag{6.10h}$$

Generic functions b_* and d_* are also included in Equation (6.9). The derivation of these functions comes from applying the Lie algebra introduced in Section 5.2.1 to the higher order derivatives in Equation (6.7) and substituting the nonlinear terms in Equation (6.8). For practical reasons the actual values of b_* and d_* are not included in this document. The derivation has been performed with the symbolic computer software Maple.

The rank of Equation (6.9) has to be equal to the number of states in the nonlinear system. In the case of the anode channel, since there are five discretization volumes and two gas concentrations per volume this is equal to $2 \times 5 = 10$. However, the rank of Equation (6.7)

depends exclusively on the rank of a partial observability matrix $\mathcal{O}_p^A$ that can be expressed for the anode as follows:

$$\mathcal{O}_p^A = \begin{bmatrix} 0 & 0 & 0 & 0 & 0 & 0 & b_1 & b_2 \\ 0 & 0 & 0 & 0 & b_* & b_* & b_* & b_* \\ 0 & 0 & b_* & b_* & b_* & b_* & b_* & b_* \\ b_* & b_* & b_* & b_* & b_* & b_* & b_* & b_* \\ 0 & 0 & 0 & 0 & 0 & 0 & d_1 & d_2 \\ 0 & 0 & 0 & 0 & d_* & d_* & d_* & d_* \\ 0 & 0 & d_* & d_* & d_* & d_* & d_* & d_* \\ d_* & d_* & d_* & d_* & d_* & d_* & d_* & d_* \end{bmatrix}. \tag{6.11}$$

Equation (6.11) has to keep full rank to fulfil the observability condition. This condition will be met if and only if $\det(\mathcal{O}_p^A) \neq 0$. This is not proved symbolically in the present work and the implementation in this chapter and in Chapter 7 uses numerical methods to check the observability at certain periods of time of the simulation.

It is possible that at a given time, the previous condition does not hold, henceforth, the system becomes not observable during an indeterminate period of time. When this occurs the solution is to disconnect the observer while the determinant of matrix $\mathcal{O}_p^A$ is null and reconnect it when the observability matrix regains the full rank property.

6.3.2 Cathode Gas Channel Observability

When analysing the observability in the cathode gas channel, it has to be taken into account that a total of three output states are considered: c_{N_2,n_z}, c_{O_2,n_z} and c_{H_2O,n_z}. The

observability matrix is computed from Equation (5.12):

$$\mathcal{O}^C = \frac{\partial}{\partial \mathbf{x}} \begin{bmatrix} h_{N_2} \\ L_{\mathbf{f}(\mathbf{x})} h_{N_2} \\ L^2_{\mathbf{f}(\mathbf{x})} h_{N_2} \\ L^3_{\mathbf{f}(\mathbf{x})} h_{N_2} \\ L^4_{\mathbf{f}(\mathbf{x})} h_{N_2} \\ h_{O_2} \\ L_{\mathbf{f}(\mathbf{x})} h_{O_2} \\ L^2_{\mathbf{f}(\mathbf{x})} h_{O_2} \\ L^3_{\mathbf{f}(\mathbf{x})} h_{O_2} \\ L^4_{\mathbf{f}(\mathbf{x})} h_{O_2} \\ h_{H_2O} \\ L_{\mathbf{f}(\mathbf{x})} h_{H_2O} \\ L^2_{\mathbf{f}(\mathbf{x})} h_{H_2O} \\ L^3_{\mathbf{f}(\mathbf{x})} h_{H_2O} \\ L^4_{\mathbf{f}(\mathbf{x})} h_{H_2O} \end{bmatrix}, \tag{6.12}$$

with $\mathbf{x} \triangleq [c_{N_2,1}, \ldots, c_{N_2,n_z}; c_{O_2,1}, \ldots, c_{O_2,n_z}; c_{H_2O,1}, \ldots, c_{H_2O,n_z}]$, $h_{N_2} \triangleq c_{N_2,n_z}$, $h_{O_2} \triangleq c_{O_2,n_z}$, $h_{H_2O} \triangleq c_{H_2O,n_z}$ and $\mathbf{f}$ being the nonlinear state terms of Equation (5.14) for the cathode gas channel.

The procedure to arrive to the observability matrix is equivalent to the one employed in Section 6.3.1. The only difference in the cathode channel is that three gas species (nitrogen, oxygen and water) are present when developing Equation (6.8). However, the full development is not included in this document for practical reasons.

6.4 Disturbance Observer Design

Current sensor technology is not able to measure the real values of the hydrogen and oxygen reaction rates during the operation of a PEM fuel cell. Moreover, water flow rates, which are complex and greatly affect the performance of the system, can not be measured either. In Section 6.2.1 the design conditions for the NDPO were presented. In order to estimate

the reactions and water transport terms vector **d**, in this section an extension of the NDPO is presented in the form of a NDOB.

The observation-oriented model in Equation (5.14) can be expressed (following the main NDPO structure in Equation (6.1)) as a function of the dynamics of the plant, inputs and disturbances

$$\dot{\hat{c}}_{i,j} = f(t, \hat{c}_{i,j}) + g(t, \hat{c}_{i,j})u_{0,i} + z_{1,i}u_i + z_{2,i}\hat{d}_{i,j}, \tag{6.13a}$$

$$\hat{y}_i = h(t, \hat{c}_{i,n_z}), \tag{6.13b}$$

where the function f has been decoupled into $z_{1,i}$ for the inputs gains and g has been decoupled into $z_{2,i}$ for the disturbances gains. The gains vectors, following Equation (4.65), are expressed as

$$z_{1,i} = \frac{1}{\Delta z}\left[1, 0, \ldots, 0\right], \tag{6.14a}$$

$$z_{2,i} = -\frac{1}{\delta}\left[1, 1, \ldots, 1\right], \tag{6.14b}$$

for the n_z discretisation volumes along the z-direction.

To estimate the nonlinear disturbances $\hat{d}_{i,j}$ in (6.13), a NDOB strategy [126, 127, 128, 129, 130, 131] is introduced:

$$\hat{d}_{i,j} = p + m(\hat{c}_{i,j}), \tag{6.15}$$

where m is a function to be designed to minimise the estimation error and p is the internal state of the nonlinear observer defined as

$$\dot{p} = -l_{i,j}\left[z_{2,i}(p + m(\hat{c}_{i,j})) + f(t, \hat{c}_{i,j}) + z_{i,1}u_i\right], \tag{6.16}$$

being l the gain of the disturbance observer. The gain and the function m in Equation (6.15) are related through the following expression [127]:

$$l_{i,j}(\hat{c}_{i,j}) = \frac{\partial m(\hat{c}_{i,j})}{\partial \hat{c}_{i,j}}. \tag{6.17}$$

Assuming that the disturbances are slowly time varying, $\hat{d}_{i,j}$ approaches $d_{i,j}$ if m is chosen such that

$$\dot{\epsilon}_{i,j} + \frac{\partial m(\hat{c}_{i,j})}{\partial c_{i,j}} z_{2,i} \epsilon_{i,j}, \tag{6.18}$$

where the estimation error for the disturbances of each i-th gas species at each j-th discretisation volume is

$$\epsilon_{i,j} = d_{i,j} - \hat{d}_{i,j}. \tag{6.19}$$

The final topology of the NDPO with the NDOB extension is shown in Figure 6.1.

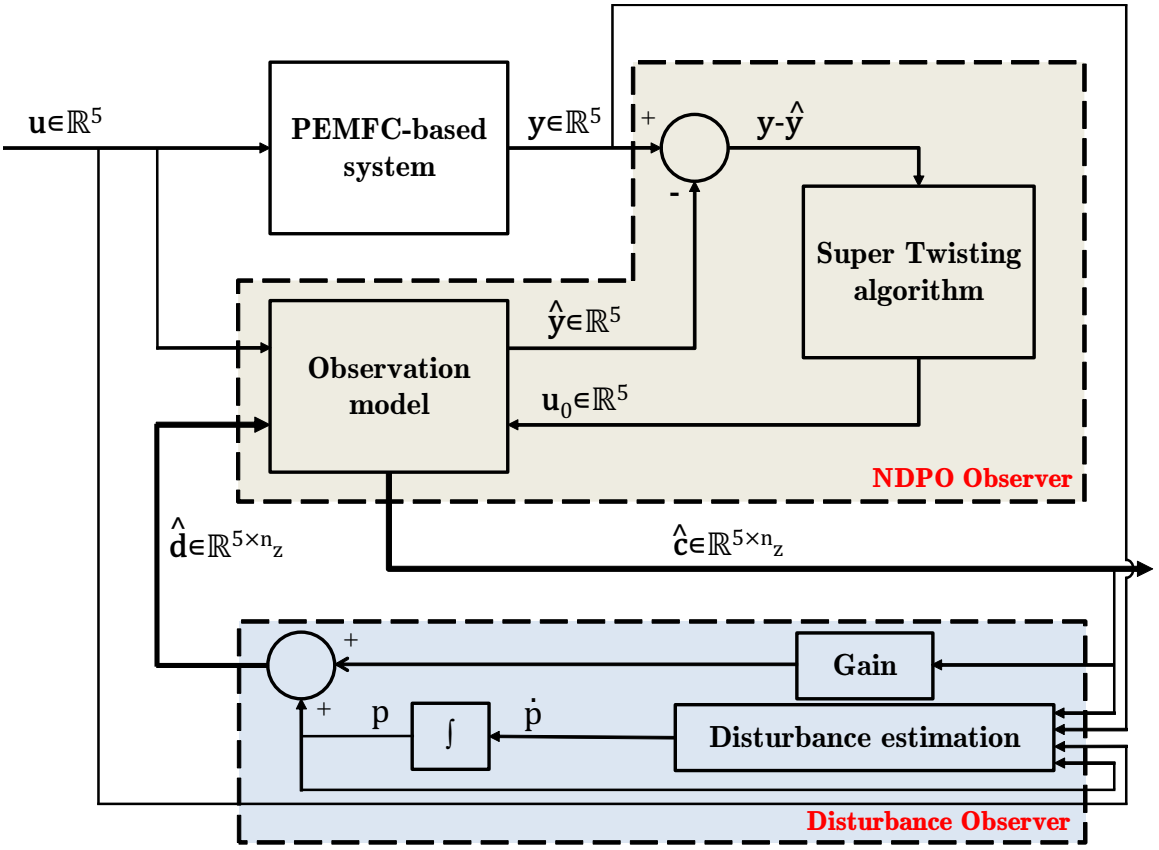

FIGURE 6.1: NDPO with NDOB extension

6.5 Corrective Input Term

Once the disturbances are estimated with the NDOB, it is possible to design the corrective input term for the NDPO in order to obtain the estimates of the concentration profiles along the gas channels.

In this work, $u_{0,i}$ is designed to achieve null output estimation error in order to drive the rest of the estimates to zero in a finite amount of time as explained in Section 6.2.1. In particular, a STA strategy, based in SMC principles [132] is implemented. Since the STA does not depend on the model as much as other solutions (i.e. MPC), the complexity of the observer, which already uses a nonlinear model, is not increased due to the design of the corrective action. Moreover, the STA approach provides robustness to the overall solution as it will be shown studying the robustness of the NDPO.

The general equation for the STA [132, 133] can be expressed as

$$u_{0,i} = u_{1,i} + \dot{u}_{2,i}, \tag{6.20a}$$

$$u_{1,i} = \begin{cases} -K_1|s_0|^{\rho} sign(s_i), & \text{if } |s_i| > |s_0|, \\ -K_1|s_i|^{\rho} sign(s_i), & \text{if } |s_i| \leq |s_0|, \end{cases} \tag{6.20b}$$

$$\dot{u}_{2,i} = -K_2 \frac{1}{2} sign(s_i), \tag{6.20c}$$

where K_1, K_2 and ρ are tuning constants of the correction algorithm. The sufficient conditions for the finite time convergence of Equation (6.20) to the observation error sliding surface are defined as [95, 132]

$$K_1^2 \geq \frac{4\Lambda}{\Gamma_m^2} \frac{\Gamma_M(K_2 + \Lambda)}{\Gamma_m(K_2 - \Lambda)}, \tag{6.21a}$$

$$K_2 > \frac{\Lambda}{\Gamma_m}, \tag{6.21b}$$

$$0 < \rho \leq 0.5, \tag{6.21c}$$

being Γ_M, Γ_m and Λ the upper and lower bounds for the sliding surface and the constant for the sliding region respectively [95]. The fine tuning of the STA parameters K_1, K_2 and ρ is out of the scope of this work. The fulfilling condition for the STA is that the relative degree between the sliding variable and the manipulable input is equal to one, as this is the case between the output concentrations and the corrective term of the STA. As explained beforehand, the sliding surface for each i-th gas species s_i is the output observation error in Equation (6.2). Therefore, the sliding surface can be expressed as follows:

$$s_i = e_{y,i}. \tag{6.22}$$

This guarantees that the observation is achieved in a finite amount of time [125] and the output error is reduced to zero.

6.6 Summary

In this chapter, a first NDPO strategy is presented. It is based on the discretised model of the PEM fuel cell to take advantage of the spatial derivatives that represent the internal behaviour of the system, which is critical to avoid starvation scenarios in control strategies.

Since the reaction rates and water transport terms can not be obtained from the measurements available in fuel cell systems, a NDOB extension has been designed to estimate them and feed this into the state observer to correct any possible deviation from the real states.

A second approach to solve the observation of the internal conditions of the PEM fuel cell is introduced in Chapter 7 along with a performance indicator to quantify the behaviour of both observation techniques. Simulations for a given case study are also presented in Chapter 7, comparing the two observation strategies proposed in this thesis work.

Chapter 7

High Order Sliding Mode Observer

7.1 Introduction

In Chapter 6, a model-based NDPO was presented. The strategy used a STA approach to minimise the state observation error and a disturbance observer extension in order to estimate the reactions and water transport terms along the discretised volumes of the PEM fuel cell. Nevertheless, the strategy presents some disadvantages, like the use of the STA, which only works in systems with relative degree equal to one, meaning that a disturbance estimation extension has to be implemented to estimate the states of all the discretisation volumes. The addition of the NDOB increases the computational burden of the observation strategy.

A novel observation strategy is developed and studied in this chapter. It is based on quasi-continuous control techniques [134] and makes use of a high order sliding mode (HOSM) approach to estimate the states and the reactions and water transport terms at the same time. As it will be shown in the present chapter, the approach is faster and more accurate than the NDPO with NDOB introduced in Chapter 6.

The structure of the HOSM observer is shown in Figure 7.1. From the value of the output concentrations, derived from the PEM fuel cell measurements as explained in Section 5.5.1, a back-stepping procedure is applied to recover the full state profile of all the gas species. The HOSM approach allows to implement the observer in systems with relative degrees greater

than one, which is the case of the discretised gas channels. In Chapter 6, this was solved by means of adding a NDOB to the main NDPO structure.

In a similar way than in the NDPO with NDOB extension, the HOSM observer for the gas concentrations makes use of the observation model presented in Section 5.4, obtaining the distributed estimation along the anode and cathode gas channels of the PEM fuel cell.

7.2 HOSM Hierarchical Control

In [134], a novel control scheme based on block control and quasi-continuous HOSM strategies is presented. The control objective is to track a desired signal y_d. In this section, a general introduction to [134] is presented.

Considering a state space model in block controllable structure:

$$\left.\begin{array}{rcl} \dot{x}_1 & = & f_1(x_1,t) + B_1(x_1,t)x_2 + g_1(x_1,t), \\ & \vdots & \\ \dot{x}_{n-1} & = & f_{n-1}(\overline{x}_{n-1},t) + B_{n-1}(\overline{x}_{n-1},t)x_{n-1} + g_{n-1}(\overline{x}_{n-1},t), \\ \dot{x}_n & = & f_n(\overline{x}_n,t) + B_n(\overline{x}_n,t)u_0 + g_n(\overline{x}_n,t), \end{array}\right\} \tag{7.1}$$

where $x \in \mathbb{R}^n$ is the state vector, $u_0 \in \mathbb{R}$ is the control vector and $\overline{x}_n = [x_1, x_2, \ldots, x_n]$. Moreover, f and B are smooth vector fields that relate the system states and g is a bounded unknown perturbation terms vector.

The control solution in [134] aims to design a controller such as the output $y = x_1$ tracks a reference y_d even in the presence of unknown bounded perturbations (represented by g). This is accomplished making use of a hierarchical quasi-continuous HOSM controller strategy and assuming that the full state vector x is known.

It is demonstrated in [134] that the HOSM control approach works properly since the system in Equation (7.1) is expressed in block controllable structure, relating each state with the rest of the states of the model in a way that virtual controls can be designed to obtain the final control action value through a back-stepping procedure. The discretised gas channel model in Equation (4.65) can be expressed in block controllable form, and thus, apply a similar approach as in [134] for control or observation purposes. Particularly, in this thesis work the

HOSM control strategy is rewritten to use it as a distributed parameters observer. As it will be explained in Section 7.3, the objective of the HOSM observation strategy is to estimate the full state vector of gas concentrations for each i-th gas species in the presence of bounded perturbation terms knowing the measurement of the output state in Equation (5.22).

After these concentration values have been obtained, applying the equations presented in Section 7.3 the concentrations in the CLs, the value of the ECSA and the liquid water content in the membrane can be computed for their use in the control strategies developed in Part IV.

7.3 HOSM Observer

To drive the state estimation error to zero in a finite amount of time, a novel observation algorithm is developed in this chapter. It is based on the control strategy introduced in Section 7.3 [134]. As mentioned, the design condition is that the system state space representation has to be written in block controllable form [135]. The control strategy will be rewritten into observer form to estimate the internal conditions of the fuel cell.

A special characteristic of the observation model of the gas species in Equation (4.65) is that the dynamic of the discretised volumes can be expressed in block controllable form as it will be presented in Section 7.3.1. This property arises from the fact that all the discretisation points are interconnected from the input to the output of the PEM fuel cells gas channels.

Taking the previous into account, it is possible to reformulate the control strategy in [134] for state estimation purposes. The required conditions are also applied in this work: the reference, perturbations, controls and states are supposed to be bounded. The novelty of the technique is that it is the first time that such HOSM algorithm is used for robust state estimation in distributed parameters nonlinear systems.

7.3.1 Block Controllable Structure

As introduced previously, the first step for the design of the HOSM observer [30] is to express the nonlinear system in Equation (4.65) in block controllable structure [134]

$$\left.\begin{array}{rcl} \dot{\hat{c}}_{i,1} & = & F_{i,1} + B_{i,1}u_{0,i} + G_{i,1}, \\ & \vdots & \\ \dot{\hat{c}}_{i,n-1} & = & F_{i,n-1} + B_{i,n-1}\hat{c}_{i,n-2} + G_{i,n-1}, \\ \dot{\hat{c}}_{i,n} & = & F_{i,n} + B_{i,n}\hat{c}_{i,n-1} + G_{i,n}, \end{array}\right\} \tag{7.2}$$

where $u_{0,i}$ is the correction input and $F_i : \{n_z\} \times \{1\} \in \mathbb{R}^{n_z}$ is the vector that includes the nonlinear dynamics that only depend for each element i of the vector on the j and $(j+1)$-discretisation volumes. Following the notation introduced in Equations. (4.65) and (4.66):

$$F_i = \begin{bmatrix} \frac{u_i}{\Delta z} - \zeta_1 \hat{c}_{i,1} \left(\sum_i \hat{c}_{i,1} - \sum_i \hat{c}_{i,2}\right) \\ -\zeta_1 \hat{c}_{i,2} \left(\sum_i \hat{c}_{i,2} - \sum_i \hat{c}_{i,3}\right) \\ \vdots \\ \hat{c}_{i,n} \left(\zeta_1 \sum_i \hat{c}_{i,n} + \zeta_2\right) \end{bmatrix}. \tag{7.3}$$

$B_i : \{n_z\} \times \{1\} \in \mathbb{R}^{n_z}$ is the vector that includes the nonlinear dynamics that depend on the $(j-1)$-discretisation volumes and the input molar flux

$$B_i = \begin{bmatrix} 1 \\ \zeta_1 \left(\sum_i \hat{c}_{i,1} - \sum_i \hat{c}_{i,2}\right) \\ \vdots \\ \zeta_1 \left(\sum_i \hat{c}_{i,n-1} - \sum_i \hat{c}_{i,n}\right) \end{bmatrix}. \tag{7.4}$$

And finally, $G_i : \{n\} \times \{1\} \in \mathbb{R}^{n_z}$ is the vector for the reaction terms $\dot{n}_{i,j}$ in Equation (4.65) which are considered as disturbances. These terms reflect the reactions perpendicular to the gas channels

$$G_i = -\frac{1}{\delta_C} \begin{bmatrix} \dot{n}_{i,1} \\ \dot{n}_{i,2} \\ \vdots \\ \dot{n}_{i,n_z} \end{bmatrix}. \tag{7.5}$$

7.3.2 HOSM Back-stepping Algorithm

To drive the state estimation to zero in a finite time, a novel back-stepping observation algorithm is presented in this work, rewriting the HOSM control strategy proposed in [134] for state estimation purposes. The HOSM relative degree is equal to n_z, which is the number of discretisation volumes for each one of the i-th gas species. The observation procedure follows an r-step algorithm, where $r \in [1, 2, \ldots, n_z]$, as shown in Algorithm 1.

for *Vi-th gas species* **do**
  for $r = n$ **to** 1 **do**
    if $r = n$ **then**
      $\hat{c}_{i,n} = \phi_{i,n}$;
      $\sigma_{i,n} = \bar{e}_{i,y} = \hat{c}_{i,n} - c_{i,n}$;
    else if $1 < r < n$ **then**
      $\hat{c}_{i,r} = \phi_{i,r}$;
      $\sigma_{i,r} = \hat{c}_{i,r} - \phi_{i,r-1}$;
    else
      $\sigma_{i,1} = \hat{c}_{i,1} - \phi_{i,r-1}$;
    end
  end
end

Algorithm 1: Back-stepping algorithm

The quasi-continuous term that has to drive the observation error to zero is included in the $\phi_{i,r}$ terms [134], which are defined as

$$\phi_{i,r} = D_{i,r}^{-1}\{-F_{i,r} + u_{r,i}\}, \tag{7.6}$$

where $u_{r,i}$ is the bounded virtual control at the r-step and $D_{i,r} : \{n_z\} \times \{n_z\} \in \mathbb{R}$ is a diagonal matrix computed as

$$D_{i,r} = \sum_{i}^{n_z} E_i B_{i,r} e_i, \tag{7.7}$$

being $E_i : \{n_z\} \times \{n_z\}$ a diagonal matrix with a 1 at each (i, i) position. Similarly $e : \{1\} \times \{n_z\}$ is a row vector with a 1 on every position.

The r-sliding homogeneous corrective action $u_{r,i}$ [136] that appears in Equation (7.6) has to be designed for $r < n_z$

$$u_{r,i} = -\alpha_r \Phi\left(\sigma, \dot{\sigma}, \ldots, \sigma^{r-1}\right), \tag{7.8}$$

with $\sigma_1 = \hat{c}_{i,1} - \phi(\hat{c}_{i,1})$. The computation of the derivatives σ, $\dot{\sigma}$, ..., σ^{r-1} in Equation (7.8) is made using robust differentiators with finite-time convergence [64]. The sign value of the derivatives defines the value of the sliding surface Φ [64].

Notice that in step $r = 1$, the real correction input $u_{0,i}$ is calculated as follows:

$$u_{0,i} = u_{r,i} = \alpha_r \Phi \left(\sigma, \dot{\sigma}, \ldots, \sigma^{r-1}\right) \text{ if } r = 1. \tag{7.9}$$

As is the case of the NDPO with disturbance observer, the back-stepping algorithm produces an accumulative estimation error since the full state profile is being estimated from the five output measurements. Nevertheless, as it will be analysed in Section 7.4, the robustness of the proposed method gives satisfactory results with almost negligible error.

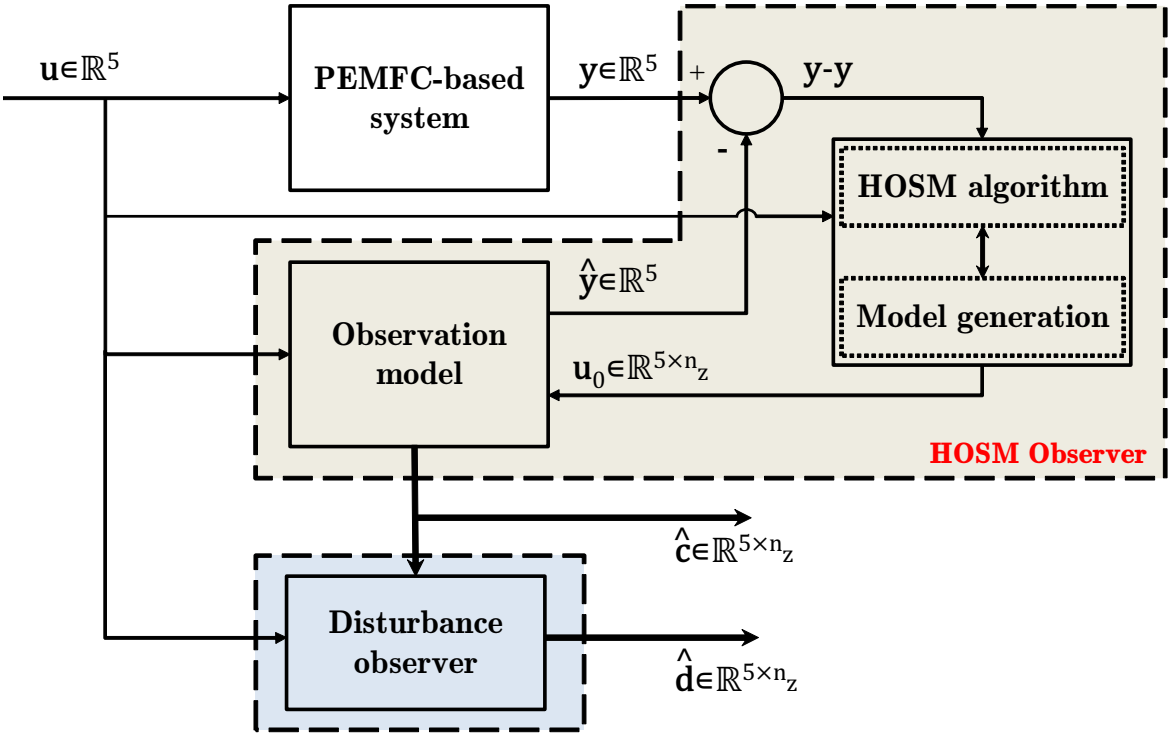

FIGURE 7.1: HOSM observer topology

7.4 Simulation Results

The two developed observers described in Chapters 6 and 7 are compared in the present section through a simulation analysis under the same operating conditions.

7.4.1 Performance Indicator

In Chapter 6 a first NDPO with disturbance estimation strategy was presented. In the present chapter, a HOSM approach has been developed with the same observation objectives. To compare the performance of both strategies, in this section a performance indicator is proposed.

Considering the state observation error of the i-th gas species through the n_z discretisation volumes in Equation (6.3), the Mean Absolute Error (MAE) is proposed:

$$MAE = \frac{1}{n_z} \sum_{i=1}^{5} \sum_{j=1}^{n_z} |e_{i,j}| = \frac{1}{n_z} \sum_{i=1}^{5} \sum_{j=1}^{n_z} |\hat{c}_{i,j} - c_{i,j}|. \tag{7.10}$$

Note that Equation (7.10) is defined for all the j-th discretisation volumes, which considers all the n_z volumes in the anode and cathode gas channels, not only the output volumes. It also considers all the i-th reactants.

To express the MAE in a quantitative way, the results are divided by the real value of the states and multiplied by 100 to obtain the MAE expressed in a percentage deviation from the real value of the state:

$$MAE(\%) = \frac{1}{n_z} \sum_{i=1}^{5} \sum_{j=1}^{n_z} 100 \, |\frac{e_{i,j}}{c_{i,j}}| = \frac{1}{n_z} \sum_{i=1}^{5} \sum_{j=1}^{n_z} 100 \, |\frac{\hat{c}_{i,j} - c_{i,j}}{c_{i,j}}|. \tag{7.11}$$

Moreover, the MAE is computed by comparing the state values at a given moment of the simulation with the observed ones. The total value is computed considering the simulation time t_{sim}:

$$MAE_T(\%) = \int_0^{t_{sim}} MAE(\%) \; dt. \tag{7.12}$$

7.4.2 Numerical Implementation

The vector $\mathbf{x_0} \in \mathbb{R}^{5 \times n_z}$ defines the initial state for all simulations and it has a dimension equal to five times the number of discretisation volumes, denoting the five gas species present in the gas channels for each one of the volumes. For the shown results, the mesh for the simulation model and the observer consists of 5 volume ($n_z = 5$) elements equally distributed. Both observers are initialised with the initial observer state vector $\hat{\mathbf{c}}_\mathbf{0} = \mathbf{0} \in \mathbb{R}^{5 \times n_z}$. Simulations

have been carried out using Simulink for MATLAB® R2011a (32 bits), running in a PC Intel® Core™ i7-3770 at 3.40 GHz with 8GB of RAM.

7.4.3 Simulation Scenario

To test the dynamic performance of the developed observers, the NEDC profile introduced in Chapter 4 is going to be applied to the PEM fuel cell. The observers do not have the NEDC current profile available in advance in order to test their performance on the event of unknown external disturbances such as drastic current changes which is the case of real driving scenarios. The PEM fuel cell is operated with anode and cathode stoichiometric rates of 1.3, a constant inlet pressure of 1.23 bar, a temperature of 353 K and a constant humidity of 50% for both gas channel inputs. Table 7.1 summarises the fuel cell operating conditions during the simulation.

Note that the cathode stoichiometry is low (1.3). In most of the driving applications of fuel cells, the cathode stoichiometry is set at 1.5 or more [3]. However, in order to study the behaviour of the observers when starvation conditions appear in the CLs, the cathode stoichiometry was set to 1.3. In Part IV of this thesis work, a closed-loop control strategy is presented. One of the control objectives is for the system to operate with the lowest possible stoichiometries to maximise the efficiency while guaranteeing that the fuel cell does not experience starvation in the catalyst sites.

TABLE 7.1: Initial operating conditions for the simulation

Condition	Unit	Value
Anode stoichiometry	-	1.3
Anode inlet humidity	%	50
Anode inlet pressure	bar	1.23
Cathode stoichiometry	-	1.3
Cathode inlet humidity	%	50
Cathode inlet pressure	bar	1.23
Fuel cell temperature	K	353

7.4.4 Results and Discussion

The total MAEs for the HOSM and the NDPO with NDOB extension strategies, expressed in percentage deviation from the real state value (see Equations (7.11) and (7.12)), are the following:

$$MAE_{T,HOSM} = 1.54\%, \tag{7.13}$$

$$MAE_{T,NDOB} = 1.79\%. \tag{7.14}$$

Both observers perform satisfactorily under the simulation conditions, nevertheless, the average MAE of the HOSM observer is lower and its performance is superior to the NDOB approach.

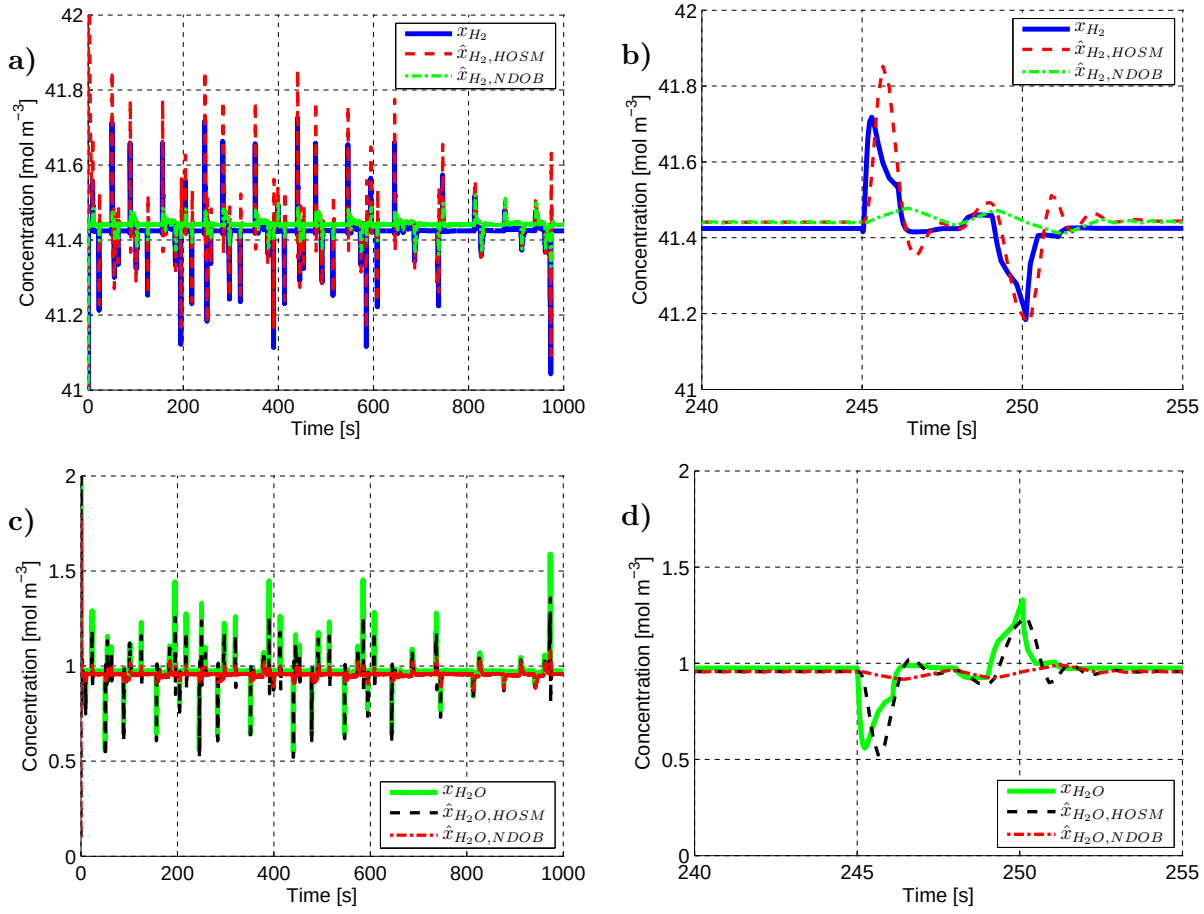

FIGURE 7.2: Observation of hydrogen (a and b) and water (c and d) concentrations in the middle point of the anode gas channel

The observation of the anode concentrations in the middle point of the gas channel are shown in Figure 7.2 and the cathode concentrations in the middle point of the gas channel are shown

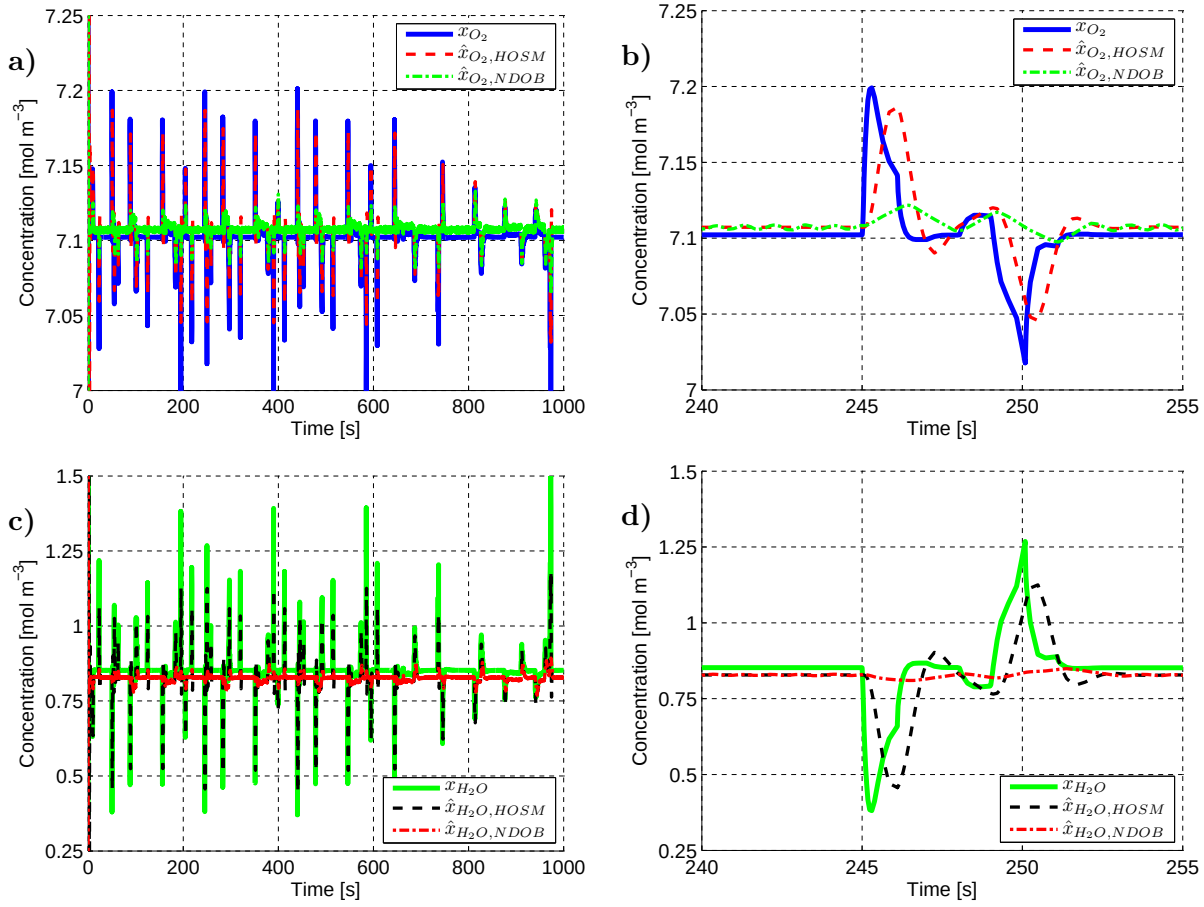

FIGURE 7.3: Observation of oxygen (a and b) and water (c and d) concentrations in the middle point of the cathode gas channel

in Figure 7.3. As explained, the observation of the gas concentration species is done for all the discretisation volumes, however Figures 7.2 and 7.3 only show the middle point of the anode and cathode gas channels. This point is of special interest because it is practically impossible to install sensors in this section of the fuel cell and commercial systems are not prepared to obtained measures inside the fuel cell. It can be seen that the HOSM observer detects possible local starvation points faster than the NDOB observer. This information will be used in Part IV of this work to design closed-loop control strategies in order to avoid possible degradation of the PEM fuel cell due to starvation scenarios.

As shown in Figures 7.2 and 7.3, the observation of the gas species (represented as dashed lines) is performed properly in a simulation environment, even in the presence of steep changes in the current profile. These current variations create a fast change in the concentration values than can result in local fuel and oxidant starvation points. Without the use of state observation techniques it is not possible to detect these starvation points and therefore, it is

not possible to apply actions that can improve or avoid the situation. For the present chapter study, the operating conditions (input molar flows) have remained constant as presented in Section 7.4.3, since the focus of the study is on the development of the observation techniques.

Figures 7.2b and d and Figures 7.3b and d show a detail of the observation. At the time instant 245 s, the decrease of the demanded current acts on the hydrogen and oxygen concentration values, increasing them. Since there is a volumetric relation between the gas species in the gas channels, the water concentrations are diminished opposite to the reactants. The reverse effect occurs around the time instant 250 s, when the current demand increases and the reactant concentration values are diminished.

7.4.5 Robustness Analysis

To test the robustness of the observers proposed in this work, three simulations in the presence of unknown inputs and model uncertainties are carried out. First, the NDOB with NDOB extension robustness is studied under delays and model uncertainties. Then, the HOSM strategy is also analysed to test its behaviour under model uncertainties.

7.4.5.1 NDPO with NDOB Robustness Analysis

To begin with, a simulation that considers the delays associated with the measurement of the input molar flows and output concentrations has been used to test the observer behaviour in front of these measurement delays. A pure delay of 15 seconds has been considered for the measured outputs of the system (a common value for commercial humidity sensors). For the input measurements, a delay of 1 second has been considered since mass flow meters operate with delays around 1 second. In Figure 7.4, the effect of these measurement delays on the estimation is shown when the input molar fluxes change their value abruptly according to Table 7.2. It can be seen that the convergence to the real value, which depends on the input measurements, is practically achieved within few seconds, obtaining appropriate state estimation even in the presence of the output measurement delay of 15 seconds. An oscillation before stabilisation appears (shown in the detail), which is produced by the output measurements delay, however, it has a small overshoot. Therefore, the observer performs correctly with the measurement delays and it does not introduce important estimation delays that could hinder closed-loop stability.

TABLE 7.2: Step values for the dynamical analysis

Input molar flow	Time [s]	Initial ⇒ Final [mol m^{-2} s^{-1}]
O_2	125	60 ⇒ 30
H_2	250	16 ⇒ 14
H_2O (anode)	375	4 ⇒ 3

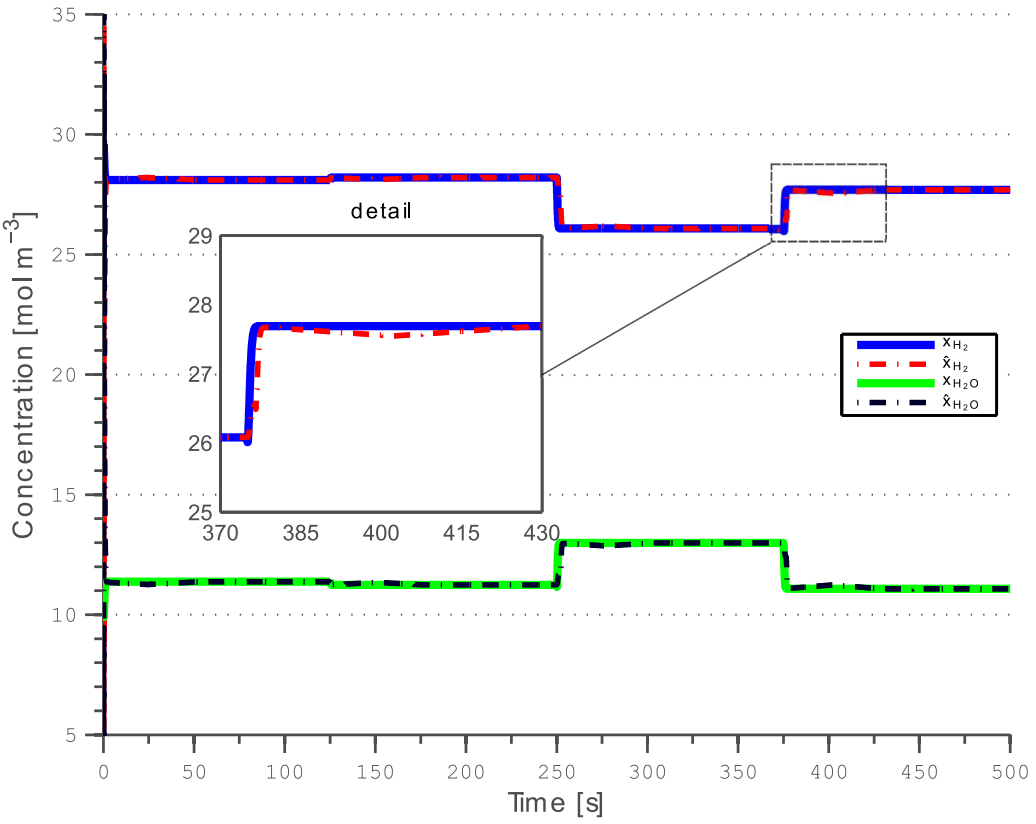

FIGURE 7.4: NDPO with NDOB state estimation in the anode gas channel in the presence of time delays

The second simulation to test the robustness of the NDPO with NDOB extension considers that the PEM fuel cell-based system is under the effect of a model uncertainty. Specifically, the temperature of the system is considered to be under the effect of band-limited white noise with a ±15% band limit from the original temperature value. As it is shown in Figure 7.5, the observer is able to track perfectly the states under the presence of this uncertainty in the plant.

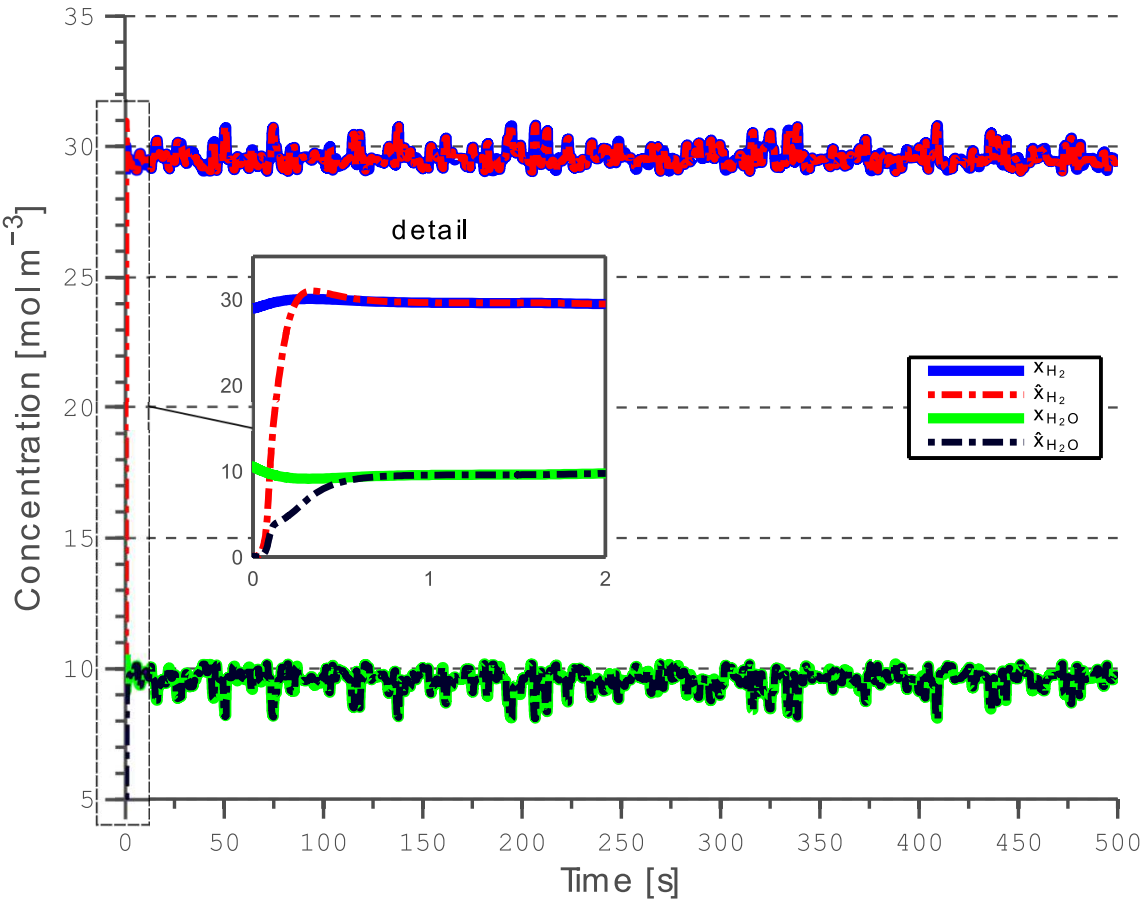

FIGURE 7.5: NDPO with NDOB state estimation in the anode gas channel in the presence of ±15% temperature changes perturbation

7.4.5.2 HOSM Observer Robustness Analysis

A third simulation case to study the behaviour of the HOSM observer against model uncertainties includes a temperature gradient from 0 to 10 K between the cathode gas channel and the cathode catalyst layer. This is a common situation in PEM fuel cells, where the internal layers are usually at higher temperatures than the exterior parts of the fuel cell. To test this scenario, it was assumed that the cathode catalyst layer has a ΔT temperature gradient with respect to the cathode gas channel. During the simulation, different values of ΔT where given at different times. As it is shown in Figure 7.6, the observer is able to track the states under the presence of this particular model uncertainty.

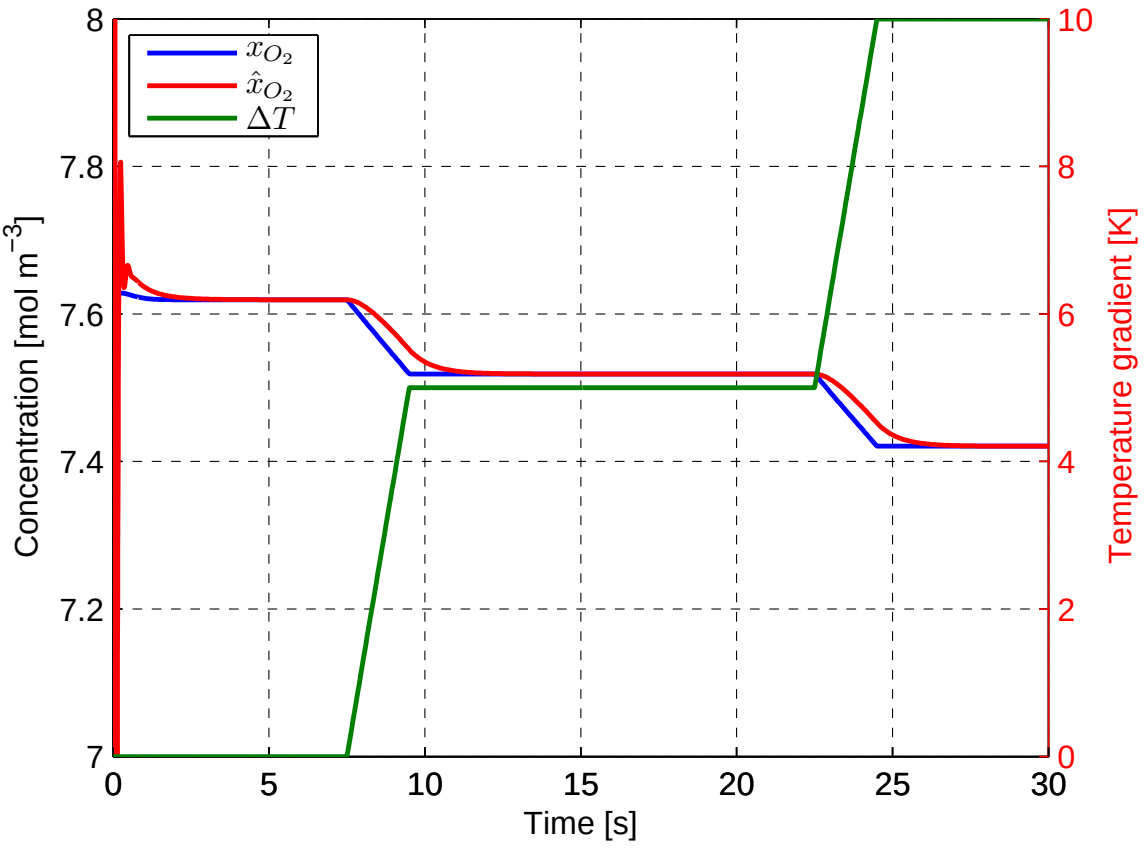

FIGURE 7.6: HOSM observer oxygen estimation in the cathode gas channel in the presence of temperature gradients between the cathode gas channel and catalyst layers

7.4.6 Observation of the Disturbances

An inherent characteristic of the NDPO and HOSM observers is the estimation of the reaction and water transport terms (flow rates from the membrane to the channels) in parallel with the state estimation. These values can be used to map the current density distribution along the PEM fuel cell without the need to use segmented cells or internal sensors. Based on the performance results obtained in Section 7.4.4, in this section the estimation of the disturbances are only studied for the HOSM case.

Considering the same simulation scenario of the previous section, the reaction and water terms are obtained using the HOSM approach to the observation problem. In Figure 7.7, the estimated hydrogen, oxygen and water transport terms for the case study in the middle of the fuel cell are presented for the first 80 seconds of the simulation. At each side of the membrane, positive values mean that the transport occurs from the gas channels towards the membrane in the y-direction. When the sign of the molar transport term is negative it

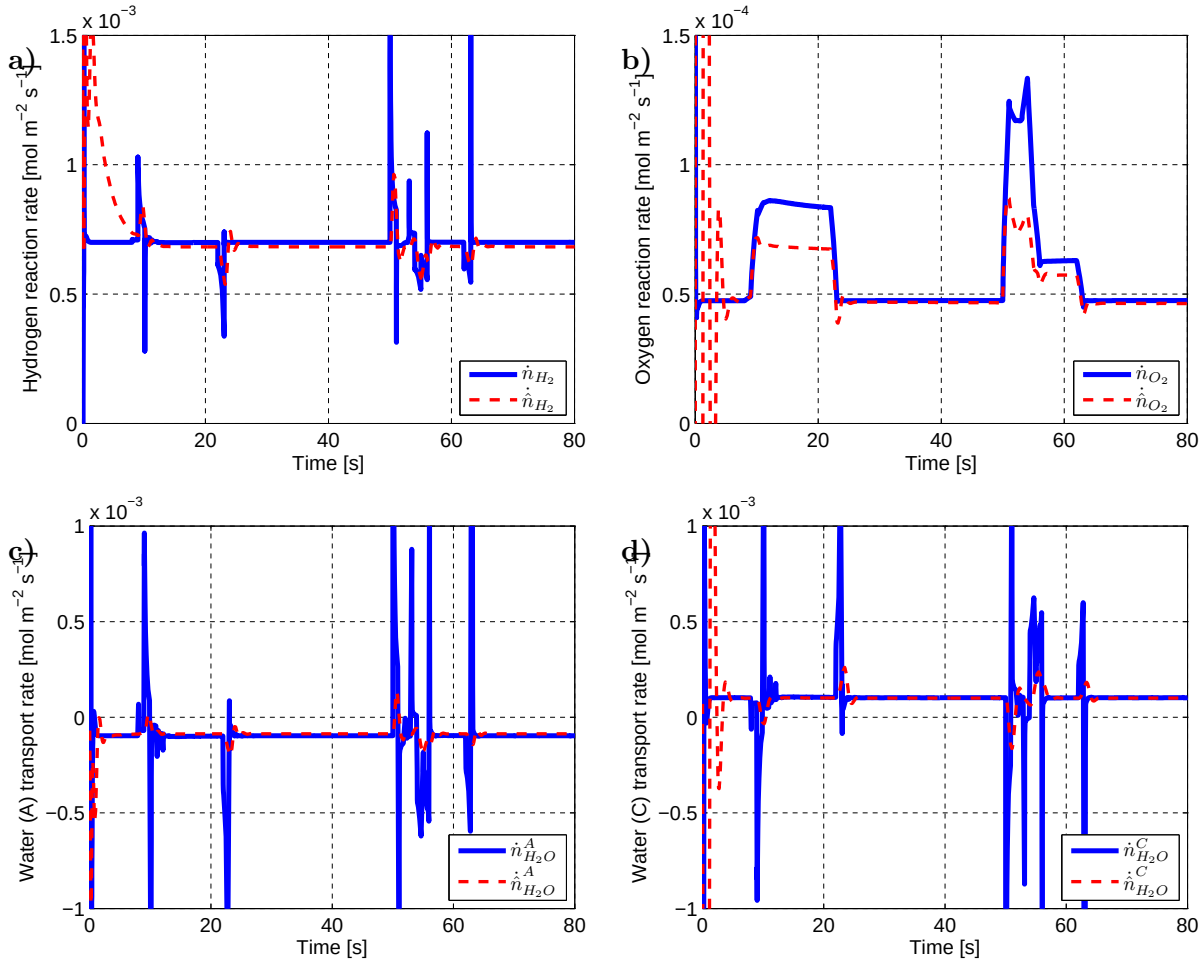

FIGURE 7.7: Hydrogen (a), oxygen (b) and water (c for the anode and d for the cathode) transport terms in the middle point of the anode and cathode gas channels

means that the flow travels towards the gas channels, as is the case of the water transport terms during some parts of the simulation. The sign criteria for the transport terms was showed in Figure 4.5.

The oxygen reaction rate in the middle volume of the cathode gas channel is shown in Figure 7.7b. As expected, it follows the current profile demand and given its positive value, it is a flow from the channel towards the membrane in the y-direction of the PEM fuel cell.

Water transports behave similarly, as depicted in Figures 7.7c and d. The negative sign in Figure 7.7c indicates that water is travelling from the membrane towards the anode gas channel. The positive values in Figure 7.7d display that the water is flowing from the cathode gas channel towards the membrane. The water transport dynamics are driven by the membrane model presented in Section 4.3.1.6.

7.5 Summary

In this chapter, the proposed nonlinear estimation strategies are compared to observe the full state, made of the gas concentration profiles in a PEM fuel cell anode and cathode gas channels. One approach is the NDPO with NDOB extension that was presented in Chapter 6 and the other is the HOSM observer introduced in this chapter. The two strategies have been compared and their performance evaluated, obtaining satisfactory observation results for a particular simulation framework. As explained in Section 7.4.4, the MAE along the anode and cathode gas channels shows the better performance of the HOSM strategy over the NDPO with NDOB. Besides, the estimation of the reaction and water transport terms for a distributed parameter PEM fuel cell model was presented for the HOSM case.

A total of five discretisation volumes for the distributed parameter model have been considered to carry on the simulations. From the point of view of the observers the increase of the number of discretisation volumes introduces mathematical complexity when synthesising the aforesaid observers. It is necessary to achieve a trade-off between the required level of detail of the recovered state information and the mathematical complexity of the observers. With the five discretisation configuration, the information that can be extracted from the simulations is quite satisfactory. Nevertheless, future research will be aimed at generalising the approach to higher numbers of discretisation points in order to increase the detail of the solution.

As it was explained, the HOSM approach performs slightly better than the NDPO with NDOB extension. In the following chapters, the HOSM strategy is included in a closed-loop control strategy to implement output-feedback techniques that take advantage of the full nonlinear estimation of the internal states. Furthermore, the observer could also be integrated with diagnosis tools to display the current PEM fuel cell health status.

Part IV

Control

The contents of this part have been published in the following articles:

- *J. Luna, C. Ocampo-Martinez and M. Serra.* Nonlinear predictive control for the concentrations profile regulation under unknown reaction disturbances in a fuel cell anode gas channel, Journal of Power Sources, 282: 129-139, 2015
- *J. Luna, S. Jemei, N. Yousfi-Steiner, A. Husar, M. Serra and D. Hissel.* Nonlinear Predictive Control for Durability Enhancement and Efficiency Improvement in a Fuel Cell Power System, Journal of Power Sources, 328: 250–261 2016
- *J. Luna, E. Usai, A. Husar and M. Serra.* Enhancing the Lifetime of a Proton Exchange Membrane Fuel Cell using Nonlinear Model Predictive Control with Nonlinear Observation (submitted to IEEE TIE, under revision)

Chapter 8

Control Problem

8.1 Introduction

The fuel cell stack in Figure 4.2 delivers power under the perturbation of the NEDC current profile shown in Figure 4.12. The control strategies proposed in this work aim to guarantee that this is done under the proper operating conditions to prevent the accelerated degradation of the system. Moreover, it is expected that the system, composed by the fuel cell and BoP ancillaries (see Figure 4.2), operates with the maximum electrical efficiency possible at each time instant, meaning that the cost of delivering the demanded current is the minimum possible without entering into starvation scenarios.

The control objectives and other technical aspects of the control problem are presented in this chapter.

8.2 Control Objectives

In Chapter 4 it was pointed out that degradation of the fuel cell CLs derives into a reduction of the ECSA [18] and therefore, less area is available for the chemical reaction to take place. The reduction of the active area may also be caused by a miss-distribution of liquid water. Active procedures can aid to maintain the ECSA value at a maximum value given the amount of liquid water in the CLs and the temperature of the fuel cell. Finding the optimal operating

point that guarantees that the reaction surface is the maximum is the first control objective proposed.

Moreover, the fuel cell has to operate with the highest possible efficiency. In the literature, most of the authors only consider the efficiency of the fuel cell disregarding the effect of the ancillaries. This approach is a simplification of the energy management problem and in this doctoral work the efficiency of the fuel cell system is defined as

$$\eta = \frac{P_{net}}{P_{tot}}, \tag{8.1}$$

where the net electrical power P_{net} is the expressed as follows:

$$P_{net} = P_{fc,elec} - P_{cmp} - P_{aux}, \tag{8.2}$$

as it was introduced in Section 4.2. The total energy given to the system can be expressed as a function of the total hydrogen used to feed the system ($H_{2,used}$) and the hydrogen higher heating value (HHV)

$$P_{tot} = H_{2,used}\Delta H, \tag{8.3}$$

with ΔH being the HHV. In Chapter 9 hydrogen recirculation is not taken into account when calculating the total power.

Taking into consideration Equations (8.2 and 8.3), the global efficiency of the system can be expressed as follows:

$$\eta = \frac{P_{fc,elec} - P_{cmp} - P_{aux}}{H_{2,used}\Delta H}. \tag{8.4}$$

The second control objective is to maximise the global system efficiency in Equation (8.4). To achieve this, the controller has to minimise the consumption of $H_{2,used}$. The third objective is to avoid starvation, the control strategies have to take into account local and global starvation constraints for both the fuel and the oxidant, which can accelerate the degradation of the fuel cell.

The presented control objectives implicitly include a specific water distribution. Indeed, an important parameter that affects the fuel cell voltage and thus, the total electrical power generated $P_{fc,elec}$ is the humidification of the membrane. In this doctoral dissertation this is characterised with the total amount of liquid water in the membrane, namely Λ. In order

to maximise efficiency, the control strategy has to maintain an optimal humidification of the membrane that guarantees that the membrane resistance is the minimum possible (it decreases with the increase of Λ) without flooding the GDLs and CLs, which could block the normal flow of fuel and oxidant with the result of accelerated degradation of the fuel cell.

Regarding degradation, always that a fuel cell is operated there is a baseline degradation that can not be avoided. Henceforth, in this work the focus is set on the mitigation of cycling and incident-induced degradation. An important characteristic of the NMPC strategies presented in Chapter 9 is the availability of setting the state constraints. The use of state constraints and a distributed parameters control model guarantees the avoidance of local and global starvation points at the anode and cathode sides of the PEM fuel cell, thus preventing cycling starvation effects as well as incident-induced degradation and not compromising the durability of the system. Regarding the cycling effects on degradation, it is also possible to reduce them by means of a battery or super-capacitors, although this is out of the scope of this doctoral dissertation. To test the capacities of the proposed control strategies, the PEM fuel cell is assumed to facilitate all the power to the load and the ancillaries, being this the worst-case scenario to study the possible improvements.

Another characteristic of the control strategies in Chapter 9 is the possibility of setting the slew-rate values of the inputs, which limit the degree of variation that the system actuators can apply at each time step of the control horizon. Slew-rate values also influence the system degradation. However, slew-rate values are difficult to set since some trade-offs may appear.

For example, a low slew-rate of the compressor current limits the reactants concentrations recovery but also avoids high air pressure transients at the cathode that can damage the membrane when the system is operating under highly cycling conditions, such as is the case of the NEDC. Moreover, in PEM fuel cells for mobile applications (the focus of the results in Chapter 9) the slew-rate can affect the drivability, which is a function of the power demanded by the user (throttle) and the power that the fuel cell can deliver. A low compressor current slew-rate will avoid pressure transients but at the same time, the user will not get the demanded power in time.

As explained beforehand, the control objectives proposed in this doctoral dissertation aim to maximise the total ECSA while maintaining the most efficient operation condition in the PEM fuel cell and a suitable membrane humidification. This has to be accomplished

avoiding possible local and global starvation scenarios to enhance the lifetime of the system. To implement these control objectives, the internal conditions of the fuel cell have to be known. Since it is not possible to install sensors inside a PEM fuel cell due to its enclosed geometry, using the NDPOs presented in Chapter 6 and Chapter 7, these internal conditions will be estimated and included in the NMPC cost function.

8.3 Prediction Model

In order to implement the NMPC strategy that will be presented in Chapter 9 (or any model-based control method), a mathematical model that represents the dynamic behaviour of the system is needed beforehand. In this section, a control-oriented prediction model of the system, partially based on the simulation model in Chapter 4, is presented. The differences between the simulation model and the prediction model are covered by the intrinsic robustness of the NMPC and its reconfigurability capabilities [6, 137]. Moreover, the unmeasurable variables of the prediction model are estimated using the HOSM observation strategy presented in Part III of this document.

The first control objective established in Section 8.2, was that the control strategy has to maximise the total ECSA of the fuel cell. The prediction model for the ECSA is derived from the discretised Equation (5.17)

$$\widehat{ECSA}_j(k) = \frac{\hat{i}_{0,j} A_{geo}(i_{0,ref}^{-1})}{e^{\left(-\Delta G^* \left(1-\frac{T_{cell}(k)}{T_{ref}}\right) R^{-1} T_{cell}(k)^{-1}\right)}} \left(\frac{\hat{p}_{O_2,j}(k)}{p_{O_2}^{ref}}\right)^{-0.5}, \tag{8.5}$$

where the discrete-time variable is denoted by $k \in \mathbb{Z}$. Note that the prediction model makes use of estimated variables, denoting them with the caret symbol. Moreover, as introduced in Chapter 4, the simulation model is spatially discretised over n_z volumes, giving the prediction model further information about the internal dynamics of the system.

To predict the value of the system efficiency, the NMPC has to include a discretised model of the fuel cell power. Transforming Equation (4.60) into discrete-time:

$$V_{fc,cell,j}(k) = E_r - \frac{RT_{cell}(k)}{\alpha 2F}\left[ln\left(\frac{i(k)}{\hat{i}_{0,j}(k)}\right) - ln\left(\frac{\hat{p}_{O_2,j}(k)}{p_{O_2}^{ref}}\right)\right] - i(k)R_{ohm,j}. \tag{8.6}$$

Regarding the prediction of the internal conditions of the fuel cell, the discrete-time model for the gas channels of the PEM fuel cell, derived from Equation (4.65) is the following:

$$c_{i,j}(k+1) = c_{i,j}(k) + \dot{c}_{i,j}(k)\Delta t, \tag{8.7}$$

where the state variables are $c_{H_2,j}$ the hydrogen concentrations, $c_{O_2,j}$ the oxygen concentrations, $c_{N_2,j}$ the nitrogen concentrations and $c_{H_2O,j}$ the vapour water concentrations (at both sides of the PEM fuel cell), all along the j discretised volumes of the gas channels.

From Equation (4.50), the following discrete-time dynamic model of the compressor is obtained:

$$p_{O_2}(k+1) = p_{O_2}(k) + \dot{p}_{O_2}(k)\Delta t, \tag{8.8a}$$

$$p_{N_2}(k+1) = p_{N_2}(k) + \dot{p}_{N_2}(k)\Delta t, \tag{8.8b}$$

$$\omega_{cmp}(k+1) = \omega_{cmp}(k) + \dot{\omega}_{cmp}(k)\Delta t, \tag{8.8c}$$

$$p_{sm}(k+1) = p_{sm}(k) + \dot{p}_{sm}(k)\Delta t. \tag{8.8d}$$

8.4 Summary

To summarise, the control objectives that are proposed in this doctoral dissertation to extend the lifetime of the fuel cell based system while maximising the global efficiency of the system are the following:

1. Maximise the ECSA
2. Maximise the global efficiency η
3. Guarantee suitable membrane humidification
4. Avoid fuel and oxidant starvation at the CLs
5. Operate under smooth control actions, avoiding cycling conditions that can further degrade the stack

The prediction model in Section 8.3 is used to forecast the evolution of the optimised variables over a prediction horizon. The predicted ECSA and fuel cell voltage are calculated using

algebraic relations of the PEM fuel cell model and the gas concentrations HOSM observer from Chapter 7, which is found to be more precise than the NDPO with NDOB extension.

In Chapter 9, the control objectives stated beforehand are transformed into cost functions that are minimised over k time discretised steps, using the prediction model presented in Section 8.3.

Chapter 9

Nonlinear Model Predictive Control for PEM Fuel Cell Systems

9.1 Introduction

As any real system, PEM fuel cells have plenty of dynamical processes and variables bounded by physical limits that should be considered when designing a control law (e.g., voltages, currents, flows, etc.). Moreover, the interaction of the diverse compositional subsystems determines several operational constraints that, in the same way as the state bounds, should be taken into account when formulating a closed-loop control scheme. In this sense, MPC has been recognised as a powerful methodology since it has the intrinsic ability to deal with system constraints in a systematic and straightforward manner [6]. Added to this fact, there exists other strong reasons for utilising this control technique such as the capability of considering several variables (multi-variable systems) and control objectives (multi-objective control) as well as the inclusion of system disturbances handling in on-line mode.

MPC is sensitive to the model accuracy since the control computation is precisely based on a mathematical model of the plant (in this case, the fuel cell). Moreover, the MPC controller design depends on the nature of the PEM fuel cell model: from the purely NMPC [138], to linear approaches [92, 139], piece-wise affine (PWA) models [140, 141] and hybrid systems forms [142].

The NMPC approach has several advantages due to the consideration of the nonlinear dynamics of the system, key aspect when studying automotive applications as is the case of this thesis work. In automotive applications the fuel cell operating range is very large and a unique linear model can not represent the whole dynamic behaviour. On the other hand, one of the main problems that can be encountered when using this control strategy is the high computational burden. In this chapter a NMPC strategy based on a nonlinear distributed parameters model of a PEM fuel cell is proposed.

In this chapter, the NMPC strategy under three different solutions are proposed and studied in a simulation environment when the system is operating under a NEDC driving cycle.

9.2 NMPC Controller Design

9.2.1 Control Architecture

The architecture of the control solution proposed in this doctoral dissertation is presented in Figure 9.1. Four manipulated control variables manage the fuel cell based system: the compressor current I_{cmp}, the reference cathode relative humidity RH^C_{ref}, the coolant mass flow $\dot{m}_{cool}$ and the hydrogen molar input $\dot{n}_{H_2,in}$. The control actions can be summarised in vector form as follows:

$$u = \begin{pmatrix} I_{cmp} \\ RH^C_{ref} \\ \dot{m}_{cool} \\ \dot{n}_{H_2,in} \end{pmatrix}. \tag{9.1}$$

Regarding the output variable y, it is a vector that contains the measured outputs that were introduced in Chapter 5, namely the relative humidity at the end of both gas channels RH_{out}, the pressures at the output of the anode and cathode gas channels p_{out}, the input molar fluxes for all the gas species $\dot{n}_{i,in}$, the temperature of the fuel cell T_{fc}. The demanded current I_{fc} is a measured input added to the list of measured outputs. Summarising, the

output y can be expressed as

$$y = \begin{pmatrix} RH^A_{out} \\ RH^C_{out} \\ p^A_{out} \\ p^C_{out} \\ \dot{n}_{H_2,in} \\ \dot{n}_{O_2,in} \\ \dot{n}_{N_2,in} \\ \dot{n}_{H_2O,in} \\ T_{fc} \\ I_{fc} \end{pmatrix}. \tag{9.2}$$

The internal conditions of the fuel cell change with the variation of the demanded fuel cell current I_{fc}. The controller has to manage the four manipulated variables to minimise the cost function stated in Section 9.4 that prioritises the objectives of the control strategy.

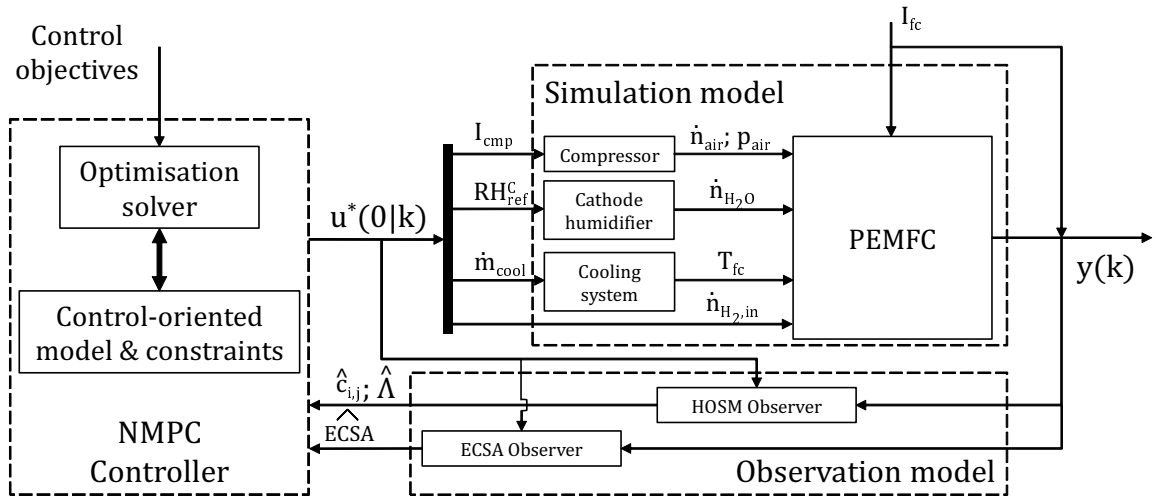

FIGURE 9.1: Closed-loop control scheme including input and output variables

9.2.2 System Constraints

The system studied in this doctoral dissertation has physical constraints that have to be taken into account. While fuel cells are able to operate under highly variable operating conditions, these conditions can accelerate the degradation that occurs in the system. Moreover, the slow dynamic response of some ancillary subsystems, such as the compressor, have to be

taken into account when describing the constraints of the system. There are two types of system constraints considered in the NMPC strategy: input and state constraints.

Regarding the input constraints, they depend on the limitations of the equipment employed, which for this doctoral dissertation are the compressor [98], the refrigeration system [99] and the hydrogen mass flow controller [124]. These constraints can be written as

$$1.2 \leq I_{cmp} \leq 3.5\ A, \tag{9.3a}$$

$$0 \leq RH^{C}_{ref} \leq 1, \tag{9.3b}$$

$$0 \leq \dot{m}_{cool} \leq 7\ kg\ s^{-1}, \tag{9.3c}$$

$$0 \leq \dot{n}_{H_2,in} \leq 40\ mol\ m^{-2}\ s^{-1}. \tag{9.3d}$$

Apart from the input constraints, the control strategy allows to set-up state constraints values. In this doctoral work, these state constraints are put on the hydrogen, oxygen and water concentrations at the CLs at each one of the j discretisation volumes $c_{i,j,CL}$. These constraints can be writen as

$$0 < c_{H_2,j,CL} \leq 70\ mol\ m^{-3}, \forall j, \tag{9.4a}$$

$$0 < c_{O_2,j,CL} \leq 70\ mol\ m^{-3}, \forall j, \tag{9.4b}$$

$$0 \leq c_{H_2O,j,CL} \leq 20\ mol\ m^{-3}, \forall j. \tag{9.4c}$$

Equation (9.4a) is related to the hydrogen concentrations and (9.4b) to the oxygen concentrations along the j discretisation volumes. Since all the discretisation volumes are constrained to have non-zero and positive concentration values, there will always be enough hydrogen in the anode and oxygen in the cathode CLs to satisfy the power demanded by the load and thus, avoiding local (condition guaranteed in all j discretisation volumes) and global starvation in the system. Regarding the upper value for Equations (9.4a) and (9.4b), it has been selected to guarantee that the partial pressure at the anode and cathode CLs is bounded by a value of two times the ambient pressure, minimising the possibility of pressure-induced failures that can accelerate the degradation of the fuel cell.

Regarding the set of constraints for the water concentrations in Equation (9.4c), the upper limit has been numerically obtained to avoid flooding the fuel cell. As depicted by

Equation (4.44), the conductivity increases with the amount of liquid water present in the membrane. Nevertheless, water content values of $\Lambda > 16$ have been demonstrated to be problematic due to the generation of flooding issues in the stack [71]. In this work a mapping of the relation between the amount of water concentration at the anode and cathode boundaries of the membrane and Λ has been studied as shown in Figure 9.2. This relation is obtained from the water model presented in Section 4.3.1.6. To guarantee that the water content remains below the flooding limit ($\Lambda \leq 16$), the set of upper constraints has been defined 20 $mol\ m^{-3}$.

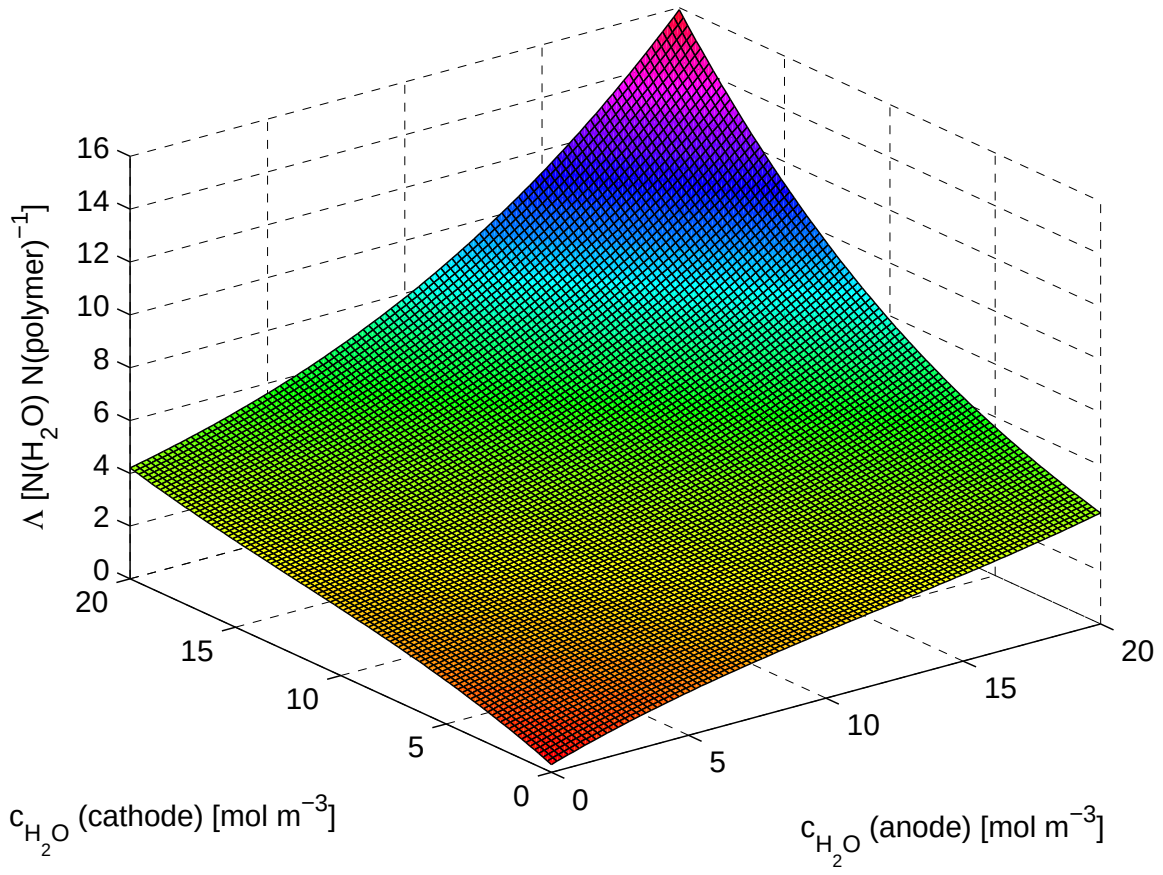

FIGURE 9.2: Water content variation with $c_{H_2O,CL}$ at 80°C at the cathode and anode sides of the fuel cell

9.3 From Control Objectives to Cost Function

In this section the control objectives presented in Section 8.2 are translated into mathematical expressions to build the multi-objective cost function of the NMPC strategy.

9.3.1 Maximise the ECSA

The ECSA performance indicator for all the n_z discretisation volumes is defined at instant k as

$$\ell_k^e \triangleq \left|\left| \sum_{j=1}^{n_z} \frac{1}{ECSA_j} \right|\right|. \tag{9.5}$$

Note that the ECSA term in Equation (9.5) is inverted. This is due to the minimisation problem described in Section 8, ℓ_k^e has to be an inverse function to maximise the ECSA value during the optimisation procedure. Notation $||\cdot||$ indicates the euclidean norm. Note than in Equation (9.5) the norm is applied to each j-th discretisation volume. Therefore, it can be denoted as follows:

$$\ell_k^e \triangleq \left|\left| \sum_{j=1}^{n_z} \frac{1}{ECSA_j} \right|\right| = \sqrt{\sum_{j=1}^{n_z} \left(\frac{1}{ECSA_j} \right)^2}. \tag{9.6}$$

9.3.2 Maximise the Global Efficiency η

Regarding the maximisation of the global efficiency objective, denoted by η in Equation (8.4), the cost can be expressed at instant k as

$$\ell_k^\eta \triangleq \left| \frac{1}{\eta} \right|. \tag{9.7}$$

Following the same argument as in Section 9.3.1, ℓ_k^η is an inverse function in order to maximise the global efficiency of the system.

9.3.3 Guarantee Suitable Membrane Humidification

As mentioned beforehand, increasing the humidification of the membrane increases its conductivity, reducing the total ohmic resistance losses. Nevertheless, if the membrane water content is too high, the gas channels can be flooded, blocking the diffusion of the fuel and oxidant gas flows towards the CLs. This means that the fuel cell can enter fuel and oxidant starvation scenarios if the water content of the membrane is too high.

The set of constraints defined in Equation (9.4c) guarantees that the water content of the membrane is between admissible values proposed in the literature [71].

9.3.4 Avoid Fuel and Oxidant Starvation at the CLs

With respect to the objective of avoiding fuel and oxidant starvation scenarios at the anode and cathode CLs, this is guaranteed by the set of constraints defined in Equations (9.4a) and (9.4b). The NMPC strategy will maintain these values during the case study to avoid situations that can damage the life expectancy of the fuel cell.

9.3.5 Operate Under Smooth Control Actions

Regarding the control objective to operate under smooth control actions, a cost function regarding the slew-rate is introduced. It can be mathematically expressed at each discrete time instant k as follows:

$$\ell_k^{\Delta u} \triangleq ||\Delta u_i||_{W_u}, \tag{9.8}$$

being $\Delta u_i(k) \triangleq u_i(k) - u_i(k-1)$ the penalisation for the slew-rate of each i-th control signal in Equation (9.1). Moreover, notation $||\cdot||_{W_u}$ indicates the quadratic weighted norm for each slew-rate term. The weighting matrices are defined as $W_u = diag(\gamma_{u_i})\mathbb{I}$, with $\gamma_{u_i} \in \mathbb{R}$ and $\mathbb{I}$ being an identity matrix of suitable dimensions.

9.4 Cost Function

Given the control objectives stated in Section 9.3, the resultant cost function that has to be minimised can be expressed as the summation of each cost in Equations (9.5), (9.7) and (9.8):

$$\mathcal{J}_k = \lambda_1 \ell_k^e + \lambda_2 \ell_k^\eta + \lambda_3 \ell_k^{\Delta u}, \tag{9.9}$$

being λ_1, λ_2 and λ_3 weights to prioritise between the control objectives. Notice that Equation (9.9) is a multi-objective minimisation function. The control optimiser will try to satisfy all the objectives in a weighted manner. Depending on the strategy, the λ weights can be chosen to prioritise one of the objectives. A trial an error procedure can be followed until

the behaviour of the controller is the desired for a given case study. In Section 9.7 different strategies and weight values are studied during the simulations.

9.5 NMPC Formulation

Adopting the approach proposed in [137], the NMPC algorithm is formulated as written in Problem 1:

Problem 1 (NMPC formulation). Let[1]

$$\mathbf{u}(k) \triangleq (u(0|k), \ldots, u(H_p - 1|k)) \tag{9.10}$$

be the sequence of control inputs over a fixed-time prediction horizon H_p at each discrete time instant k. Hence, the NMPC design is based on the solution of the finite-time open-loop optimization problem (FTOOP), depending also on the initial condition $x(0|k) \triangleq x_0$:

$$\min_{\mathbf{u}(k) \in \mathbb{R}^{m \times H_p}} \mathcal{J}(x_0, \mathbf{u}(k)), \tag{9.11}$$

subject to

- prediction model in (8.5, 8.6, 8.7 and 8.8) over H_p,
- input constraints in (9.3) over H_p,
- state constraints in (9.4) over H_p,
- slew rate input constraints in (9.8) over H_p,

where $\mathcal{J}(\cdot) : \mathbb{U}^{m \times H_p} \times \mathbb{R}^{H_p} \mapsto \mathbb{R}$ in (9.9) is the cost function, with $m = 4$ and H_u being the control horizon. It has been assumed that the control and prediction horizons have the same value ($H_p = H_c$). This is to guarantee the maximum possible degrees of freedom for the optimisation even when considering a short prediction horizon in order to improve the computational cost.

[1]Here, $f(k+i|k)$ denotes the prediction of the variable f at time $k+i$ performed at k. For instance, $x(k+i|k)$ denotes the prediction of the system state, starting from its initial condition $x(0|k) = x(k)$.

Assuming that the FTOOP in Equation (9.11) is feasible, there will be an optimal solution for the sequence of control inputs

$$\mathbf{u}^*(k) \triangleq (u^*(0|k), u^*(1|k), \ldots, u^*(H_p - 1|k)) \tag{9.12}$$

and then, according to the receding horizon philosophy, $u_i^*(0|k)$ is applied to the system, while the process is repeated for the next time instant $k \in \mathbb{Z}$.

9.6 Implementation of the NMPC

The mesh for the simulation model consists of 5 elements equally distributed along the z-direction, 5 elements for the cathode GDL in y-direction and 5 elements for the CCL along the y-direction. The mesh of the observation model for the full concentrations profile consists of 5 elements along the z-direction and the initial state for the i-th gas concentrations values are $\hat{\mathbf{c}}_i(t = 0) = \mathbf{0} \in \mathbb{R}^{5 \times n_z}$. Simulations have been carried out using MATLAB R2011a (32 bits), running in a PC Intel Core i7-3770 at 3.40 GHz with 8 GB of RAM.

9.7 Simulation Scenarios

In this section the simulation results of the closed-loop strategy are presented. Three NMPCs are going to be simulated and analysed to study the performance of the strategy:

- NMPC 1: Maximise the ECSA
- NMPC 2: Maximise the global efficiency η
- NMPC 3: Maximise the ECSA and the global efficiency η

One of the main capabilities of the proposed NMPC strategy is the vast reconfigurability of the controller via the tuning of its parameters, including prediction and control horizons, penalisation terms, norms, etc. The NMPC is going to be configured for each case in order to guarantee that the control objectives introduced in Chapter 8.

9.7.1 Initial Conditions

For the each one of the three NMPCs analysed in this chapter, the initial conditions of the simulation are defined by a given operating point described in Table 9.1. Initially the PEM fuel cell is working with anode stoichiometry of 1.3 and cathode stoichiometry of 2.0. Both the anode and cathode sides operate with 50% relative humidity in the inlet channels.

The NEDC demanded current profile described in Chapter 4 is going to be applied to the system in order to test the dynamic performance of the developed control strategy. As it will be shown in the following sections, the cycle has been extended to 2000 seconds in order to study the full dynamic response of the fuel cell when it achieves steady state conditions.

TABLE 9.1: Initial operating conditions for the simulation

Condition	Unit	Value
Anode stoichiometry	–	1.3
Anode inlet humidity	%	50
Anode inlet pressure	bar	1.23
Cathode stroichiometry	–	2.0
Cathode inlet humidity	%	50
Cathode inlet pressure	bar	1.23
Fuel cell temperature	K	353

9.7.2 NMPC 1: Maximise the ECSA

9.7.2.1 Controller Setup

Table 9.2 shows the controller setup parameters and the sampling and simulation times used for the NMPC 1 simulation scenario.

In all the control strategies the prediction horizon is $H_p = 2$. Considering the sampling time Δt of 1 second, this gives a total prediction horizon of 2 seconds at each control step. The low value of the prediction horizon is to reduce the computational burden of the controller at each discretisation step. For each controller, the total computation time and the computational burden for each iteration is studied.

TABLE 9.2: NMPC setup parameters for the NMPC 1

Parameter	Description	Value
γ_{u_1}	I_{cmp} slew-rate penalisation	1
γ_{u_2}	T_{ref} slew-rate penalisation	1
γ_{u_3}	$\dot{n}_{H_2,in}$ slew-rate penalisation	1
γ_{u_4}	RH^C_{ref} slew-rate penalisation	1
λ_1	ECSA maximisation penalisation	10
λ_2	Efficiency maximisation penalisation	0
λ_3	Slew-rate penalisation	1
H_p	Prediction horizon	2
H_c	Control horizon	2
Δt	Sampling time	1 s
T_{sim}	Simulation time	2000 s

9.7.2.2 Simulation Results

The behaviour of the modelled ECSA and the observed variable $\widehat{ECSA}$ is presented in Figure 9.3. At the beginning of the simulation, the liquid to vapour water ratio s has a low value, which is depicted by the low available active area. This is due to the initial conditions of the fuel cell when the simulation starts. The controller, through the use of the cooling circuit, reduces T_{fc} (see Figure 9.4) until the ECSA starts increasing. As shown in Figure 9.4, the temperature achieves an optimal temperature around the 1000 s simulation mark. The ECSA continues increasing until the end of the simulation. As expected, the response of the ECSA is slow due to its dependency to slow dynamic effects such the evaporation of water. Regarding the observation of the ECSA, it is shown in Figure 9.3 that the observer tracks the real value properly throughout the NEDC cycle with some spikes that appear when the demand of the current suddenly changes. Nevertheless, the ECSA observer corrects the observation error and converges to the real value.

Regarding the efficiency, as shown in Figure 9.5, only increasing the ECSA does not guarantee a high global efficiency of the system. In fact, the strategy is clearly less efficient than a classic constant stoichiometry approach as depicted by the comparison presented in Figure 9.5. This is because the NMPC control algorithm finds an optimum with higher values of compressor current (see Figures 9.6a), decreasing the global efficiency defined in Equation (8.4).

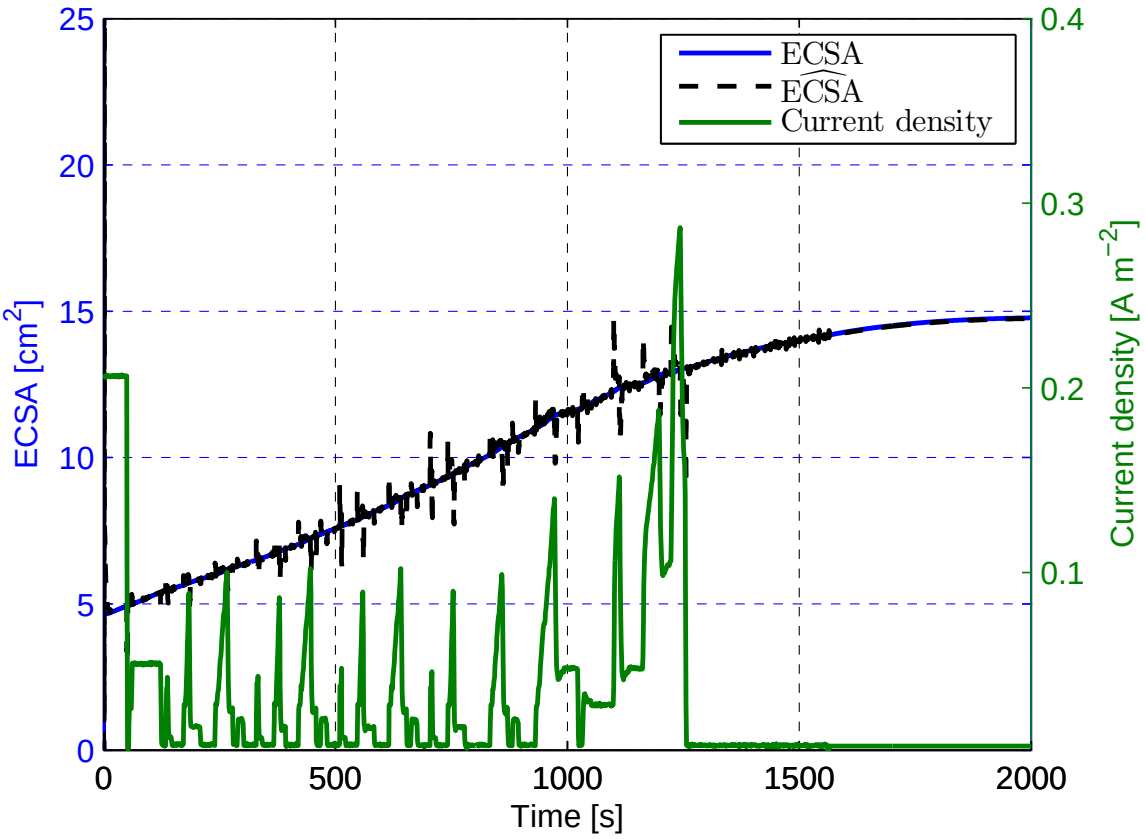

FIGURE 9.3: Evolution of modelled and observed ECSA and NEDC stack current density demand [3] for the NMPC 1

In the following sections, two more NMPC tunings that have the efficiency as a control objective will be studied.

Regarding the controller, the dynamic behaviour of the manipulable inputs applied to the system during the simulation time are shown in Figure 9.6. These optimal control inputs maximise the ECSA while maintaining suitable operating conditions for the PEM fuel cell, such as avoiding starvation situations, which would accelerate the degradation of the fuel cell. It is important to remark the performance of the coolant mass flow in Figure 9.6b, which shows how the controller reduces the fuel cell temperature until an optimal value for the ECSA maximisation is found, which in this case is around 66°C as shown in Figure 9.4. The current and relative humidity follow a similar pattern, as presented in Figures 9.6a and c. When the current increases, the liquid water in the CCL evaporates, justifying the increase of the relative humidity to maintain an optimal ECSA value. Regarding the input hydrogen molar flow, Figure 9.6 depicts how the controller follows the current demand and injects the

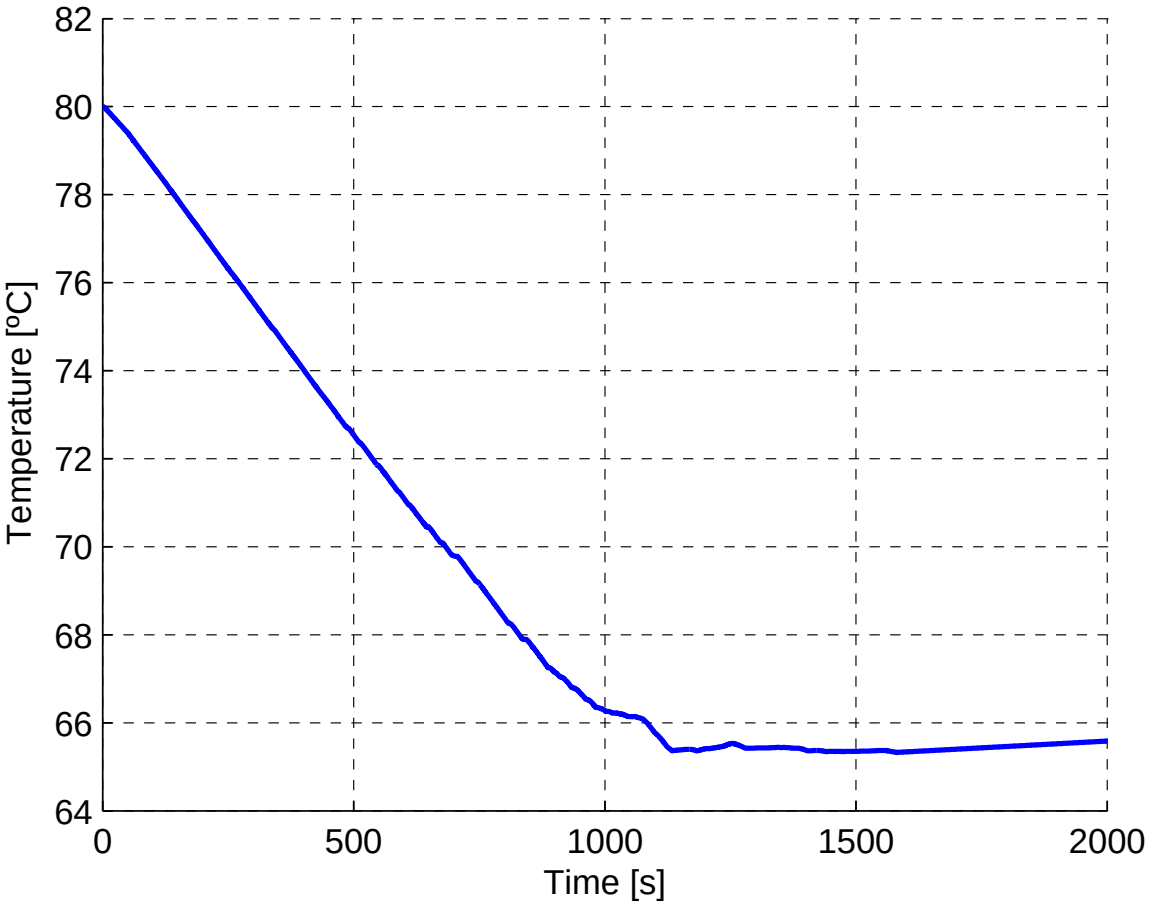

FIGURE 9.4: Temperature of the fuel cell stack for the NMPC 1

required hydrogen without taking into account efficiency or hydrogen economy conditions (this will be studied in the cases NMPC 2 and 3).

As pointed out previously, the implementation of the NMPC using a nonlinear distributed parameters prediction model introduces a high computational effort. Nevertheless, as shown in Figure 9.7, the total accumulated computation time remains below the total simulation time, making it feasible for implementation in a real PEM fuel cell-based system. Nevertheless, during some optimisation steps, the iteration computation time is higher than the sampling time (1 second). This problem can be solved using a higher end computer when implementing the solution.

In the next cases this implementation time will also be studied.

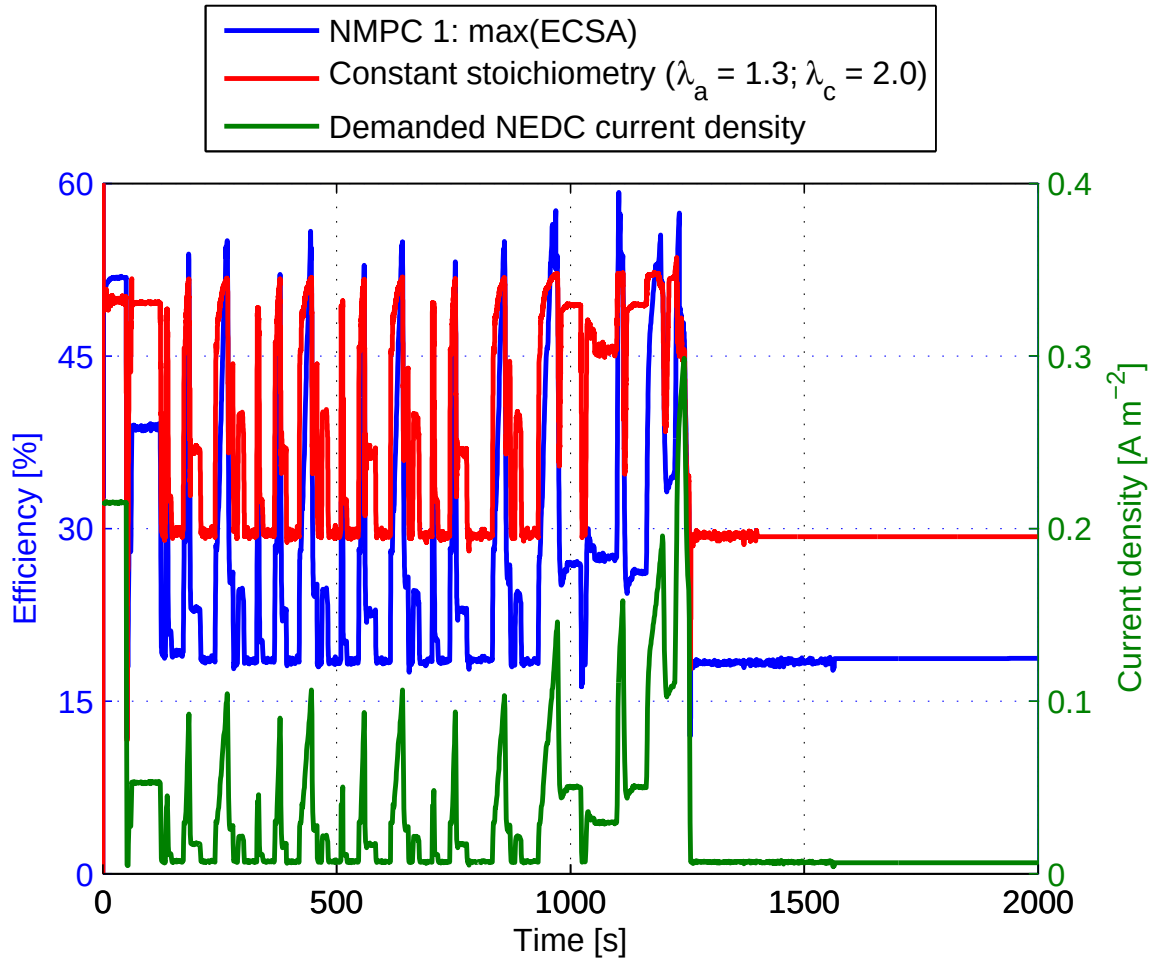

FIGURE 9.5: Efficiency of the system with the NMPC strategy (NMPC 1) and with constant operating conditions under a NEDC current demand

9.7.2.3 Observer Performance

The HOSM observer feeds the NMPC controller with the estimated state vector for the gas concentrations and the ECSA as depicted in Figure 9.1. This information is used by the controller to avoid local starvation in the fuel cell by guaranteeing that these values are between the desired restrictions (see Equation (9.3)). Figure 9.8 shows the behaviour of the observed variables during the simulation time. Although in Figure 9.8 only the observation of the concentrations in the middle point of the gas channels is presented, the observation is performed in all of the discretisation volumes. This is done to facilitate the reading of the results. The same decision will be applied for NMPCs 2 and 3.

Figures 9.8a and b, refer to the concentration estimation at the anode side. On the other hand, Figure 9.8c and d, refer to the cathode gas channel concentrations estimation. The

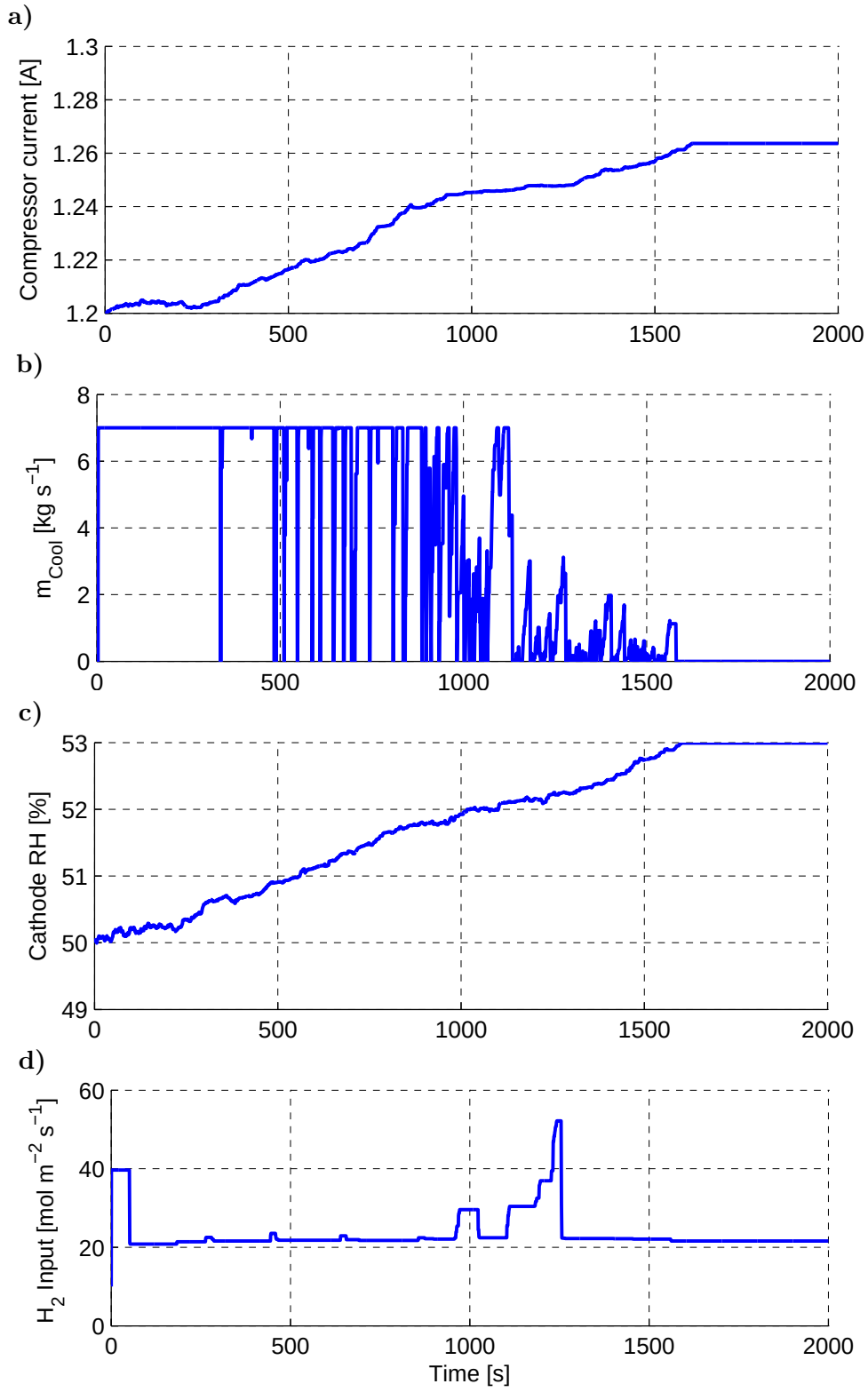

FIGURE 9.6: Compressor current (a), coolant mass flow (b), relative humidity (c) and H_2 input molar flux (d) control actions supplied by the NMPC for the NMPC 1

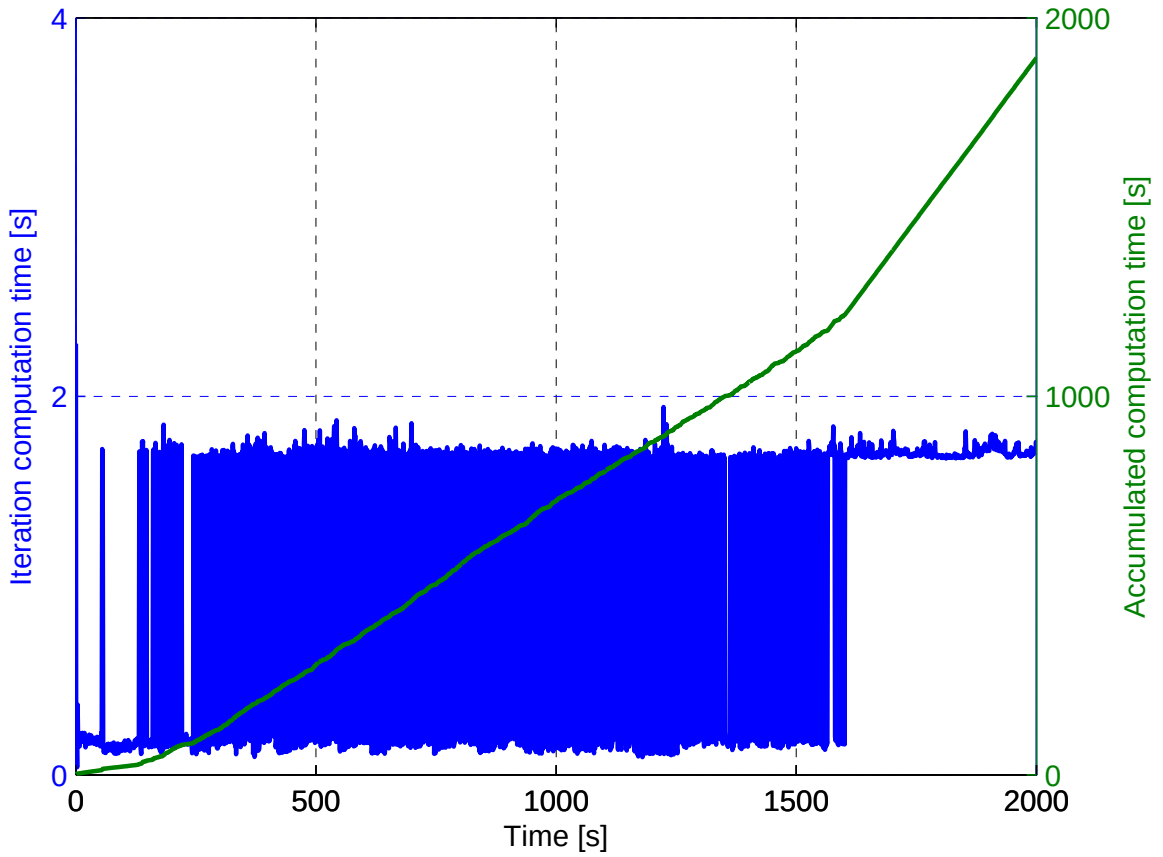

FIGURE 9.7: NMPC computation time for the NMPC 1

estimation is robust during all the simulation as shown in Figure 9.8. Without the observer these internal variables would not be available to use in the control loop due to the impossibility of measuring inside the gas channels of the fuel cell.

In the case of Figures 9.8a and c, denoting the hydrogen and oxygen concentrations, the controller maintains these values between certain boundaries with the objective of avoiding local starvation. For the water concentrations in the anode and cathode sides of the PEM fuel cell, depicted in Figures 9.8b and d, the controller guarantees that the humidification of the fuel cell is adequate without flooding the membrane.

9.7.3 NMPC 2: Maximise the Global Efficiency η

9.7.3.1 Controller Setup

In NMPC 1 the objective prioritisation variable λ_1 was set to 10 and λ_2 to 0. In this section, these values are reversed and as shown in Table 9.3, the control priority is set to the

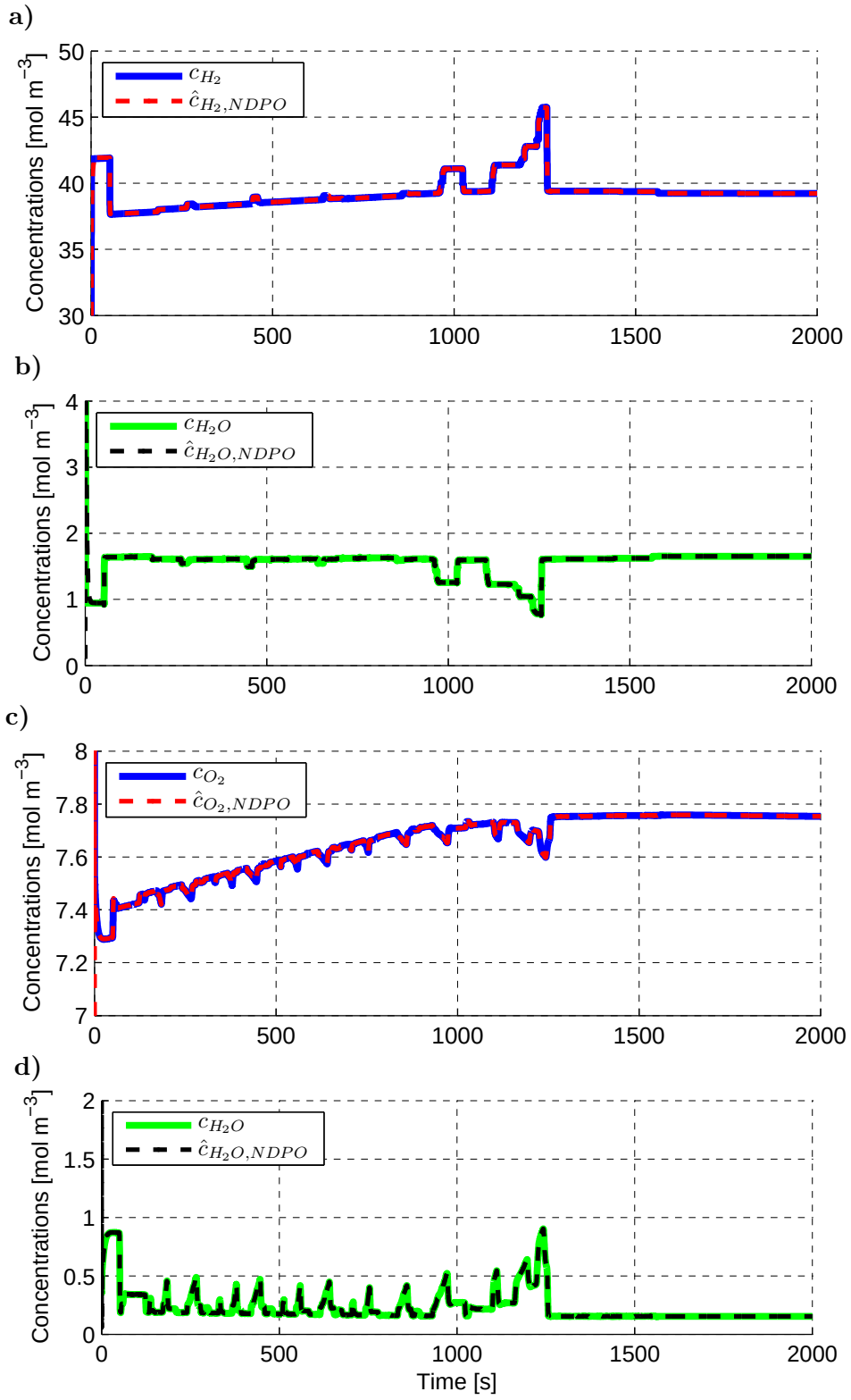

FIGURE 9.8: Behaviour of the NDPO versus the plant states in the middle discretisation volume of the anode (a and b) and the cathode (c and d) for the NMPC 1

maximisation of the efficiency, with λ_1 set to 0 and λ_2 to 10.

TABLE 9.3: NMPC setup parameters for the NMPC 2

Parameter	Description	Value
γ_{u_1}	I_{cmp} slew-rate penalisation	1
γ_{u_2}	T_{ref} slew-rate penalisation	1
γ_{u_3}	$\dot{n}_{H_2,in}$ slew-rate penalisation	1
γ_{u_4}	RH^C_{ref} slew-rate penalisation	1
λ_1	ECSA maximisation penalisation	0
λ_2	Efficiency maximisation penalisation	10
λ_3	Slew-rate penalisation	1
H_p	Prediction horizon	2
H_c	Control horizon	2
Δt	Sampling time	1 s
T_{sim}	Simulation time	2000 s

9.7.3.2 Simulation Results

The dynamic behaviour of the efficiency defined in Equation (8.1) is represented in Figure 9.11. As it can be seen in the figure, the NMPC 2 is clearly superior compared with the constant stoichiometry operation of the system. The controller makes the fuel cell to operate at lower hydrogen and oxygen stoichiometries with higher efficiency while guaranteeing that the PEM fuel cell does not endure local starvation scenarios. Regarding the ECSA, as it was expected, the results are not as good as the ones obtained for the NMPC 1 since it is not an optimisation variable in NMPC 2. While the ECSA increases during the first half of the simulation (see Figure 9.9), when higher current densities are demanded to the PEM fuel cell, the liquid water in the CCL evaporates thus reducing the available active area. This is not reflected on the global efficiency of the system but it could induce accelerated degradation on the fuel cell. Therefore, on NMPC 3, the combination of NMPCs 1 and 2 is going to be analysed.

Regarding the temperature of the fuel cell for the NMPC 2, as shown in Figure 9.10, it fluctuates during the simulation time around the initial temperature value of 80°C. The NMPC controller finds an optimum value at each step to guarantee that the electrical efficiency is maximum.

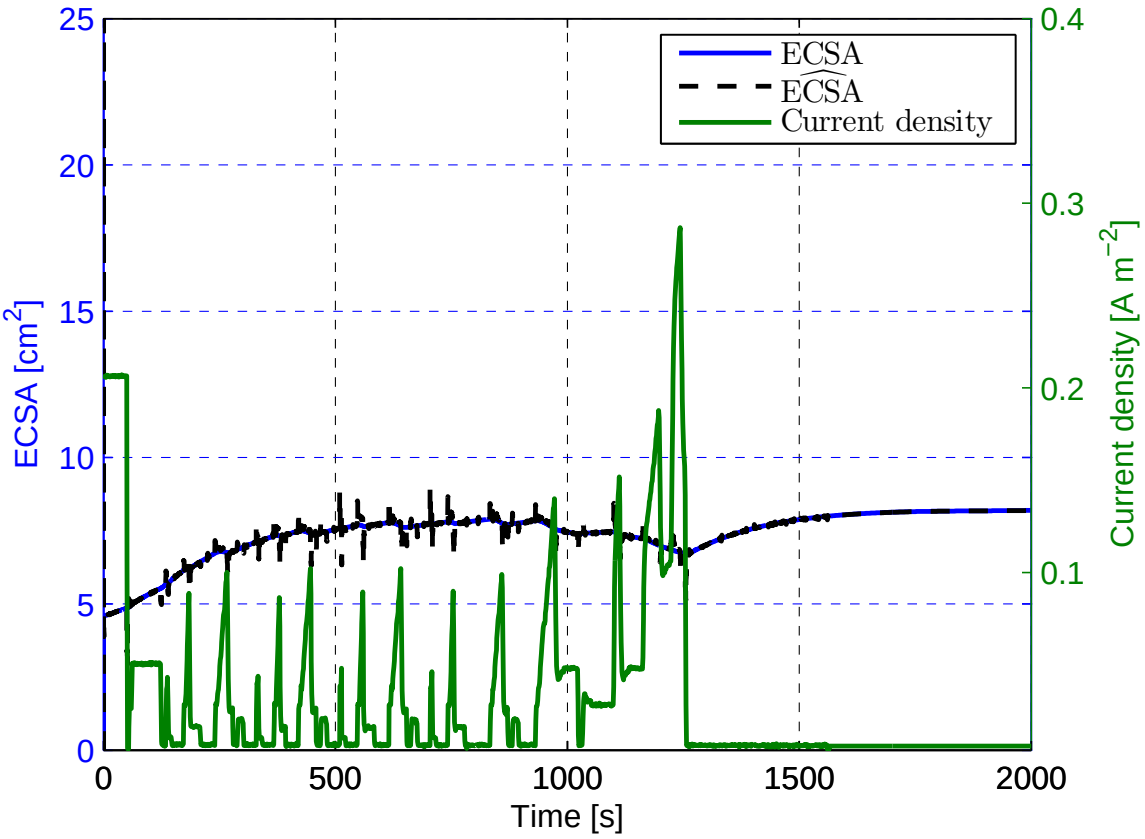

FIGURE 9.9: Evolution of modelled and observed ECSA and NEDC stack current density demand [3] for the NMPC 2

The control actions for NMPC 2 are shown in Figure 9.12. These values are the optimal set for each simulation step as computed by the NMPC strategy. Moreover, as it can be seen in the figure, the values remain between the boundaries determined in Equation (9.3). Notice how the compressor current (Figure 9.12a) and hydrogen molar input (Figure 9.12d) have lower values than in NMPC 1. This is translated into lower hydrogen and oxygen stoichiometry values which produces higher efficiency values while maintaining the fuel cell between the safety constraints that guarantee that starvation does not occur on all the surface of the catalyst layers.

As shown in Figure 9.13, the computation time of the NMPC 2 is much lower than in NMPC 1. Apart of some few points than remain higher than the sampling time, implementation is possible since the total accumulated simulation time is lower than the simulation horizon of 2000 s.

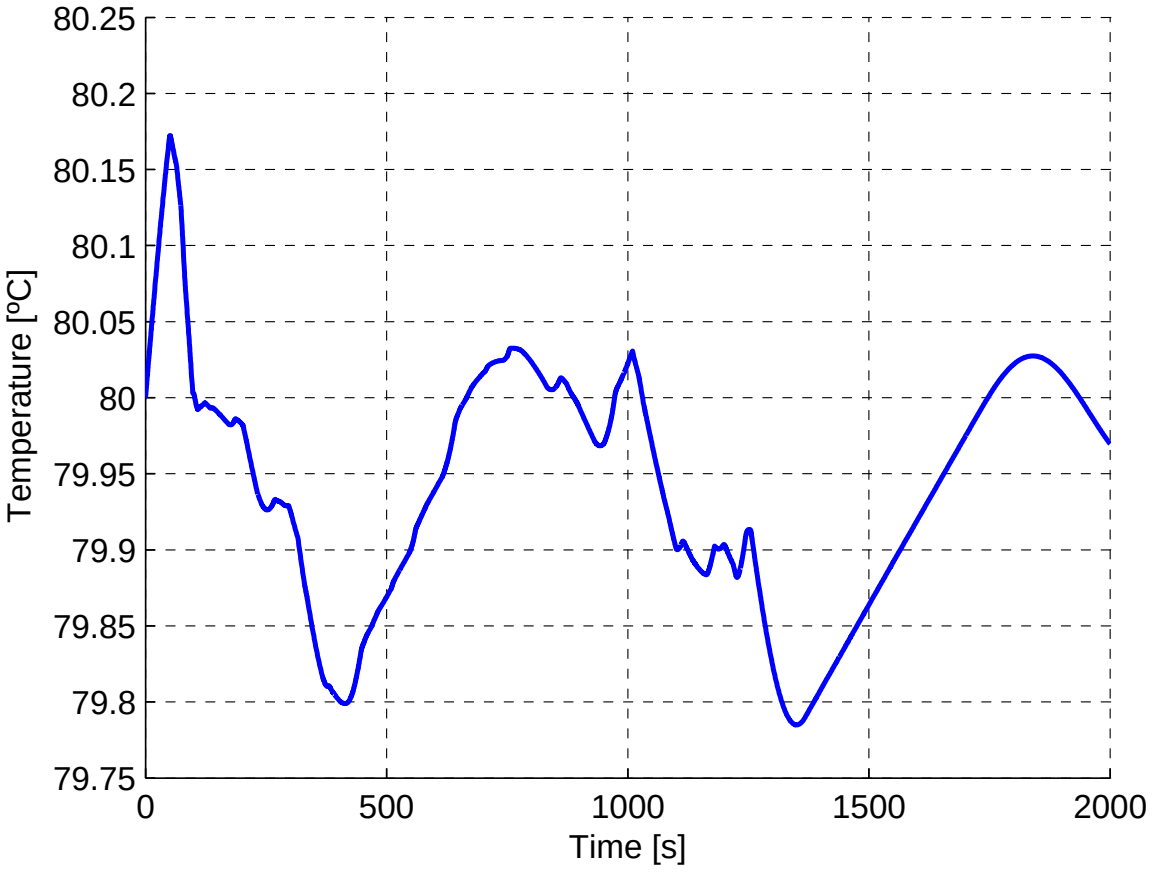

FIGURE 9.10: Temperature of the fuel cell stack for the NMPC 2

9.7.3.3 Observer Performance

In a similar format as in Section 9.7.2.3, Figures 9.14a and b, represent the concentration estimation at the middle point of the anode side. On the other hand, Figure 9.14c and d, depict the middle point cathode gas channel concentrations estimation. The gas concentrations HOSM observer performs robustly even in the presence of sudden changes of the current density demand.

9.7.4 NMPC 3: Maximise the ECSA and the Global Efficiency η

9.7.4.1 Controller Setup

Table 9.4 shows the controller setup parameters and the sampling and simulation times used for the NMPC 3 simulation scenario. In this case, the two control objectives of maximising

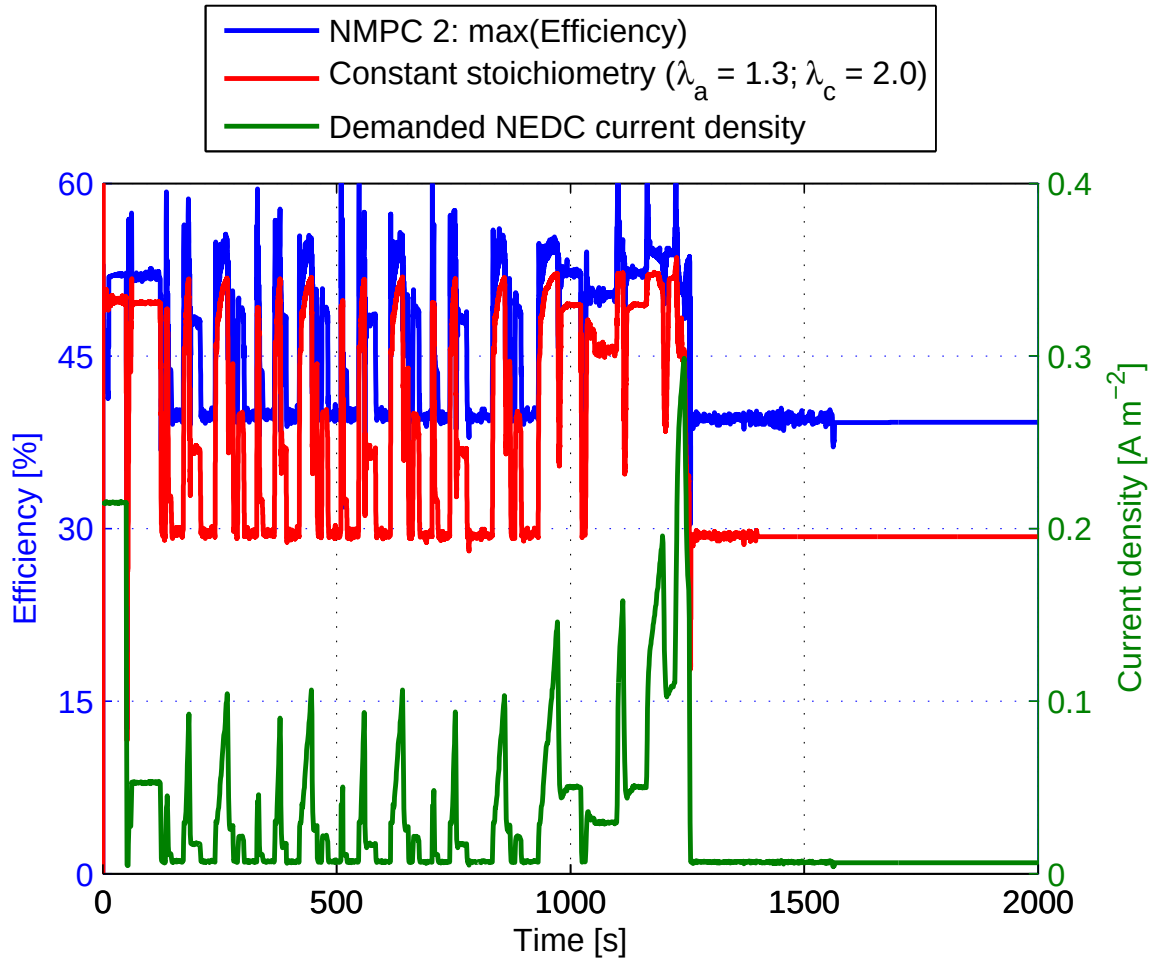

FIGURE 9.11: Efficiency of the system with the NMPC strategy (NMPC 2) and with constant operating conditions under a NEDC current demand

the ECSA and the global efficiency are included in the cost function, denoted by λ_1 set to 10 and λ_2 equal to 10 as well.

9.7.4.2 Simulation Results

In Sections 9.7.2 and 9.7.3 two separate control objectives have been considered in order to maximise the ECSA and the global efficiency respectively. In the present section, these two conditions are combined to find an optimal performance of the system and at the same time increase the ECSA to enhance the lifetime of the fuel cell.

The ECSA behaviour for the NMPC 3 is presented in Figure 9.15. It can be concluded from the figure that, while the ECSA final value is not as high as in the NMPC 1 (Figure 9.3), the obtained results are much better than in the NMPC 2 (see Figure 9.9). At the same

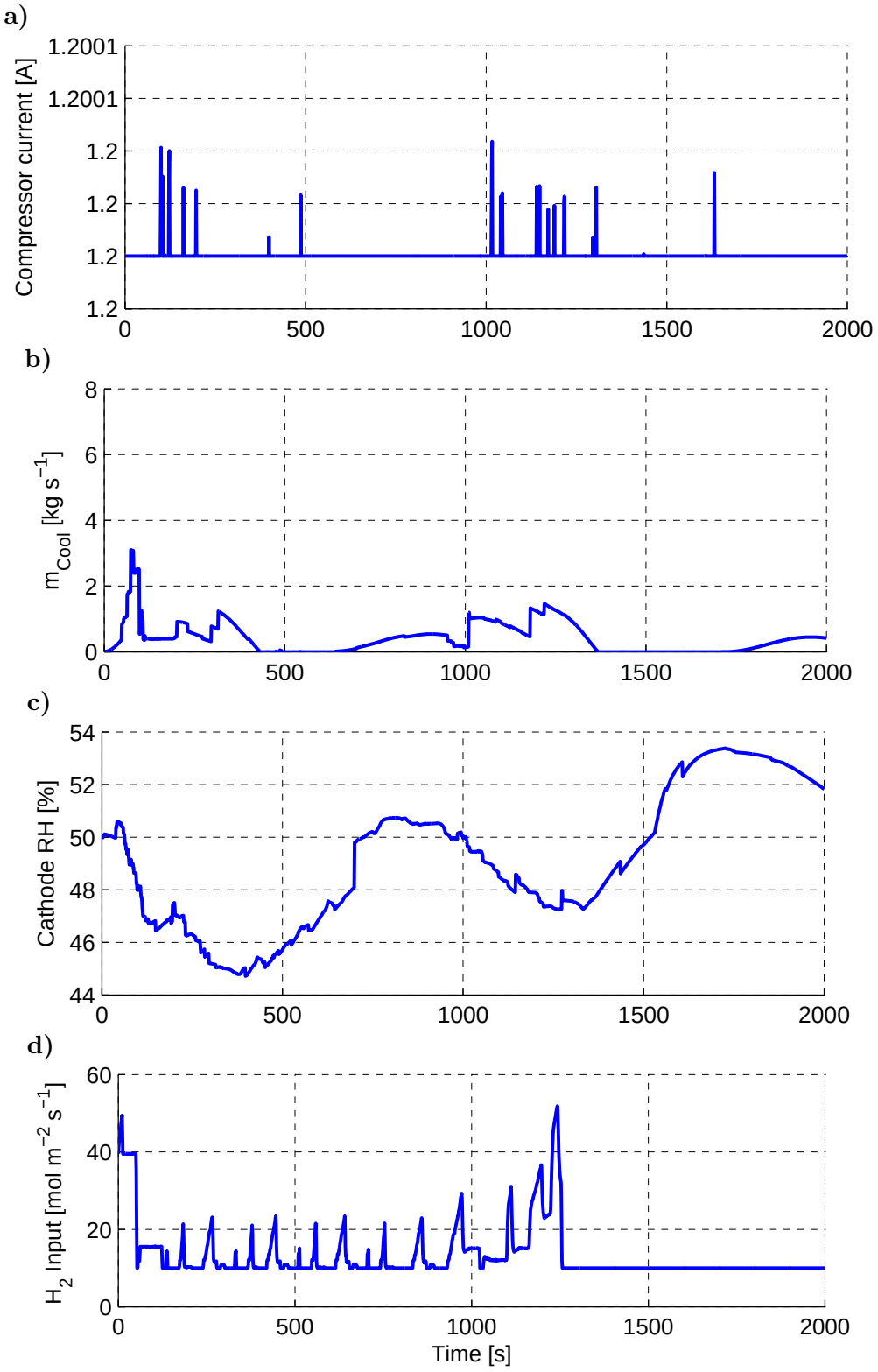

FIGURE 9.12: Compressor current (a), coolant mass flow (b), relative humidity (c) and H_2 input molar flux (d) control actions supplied by the NMPC for the NMPC 2

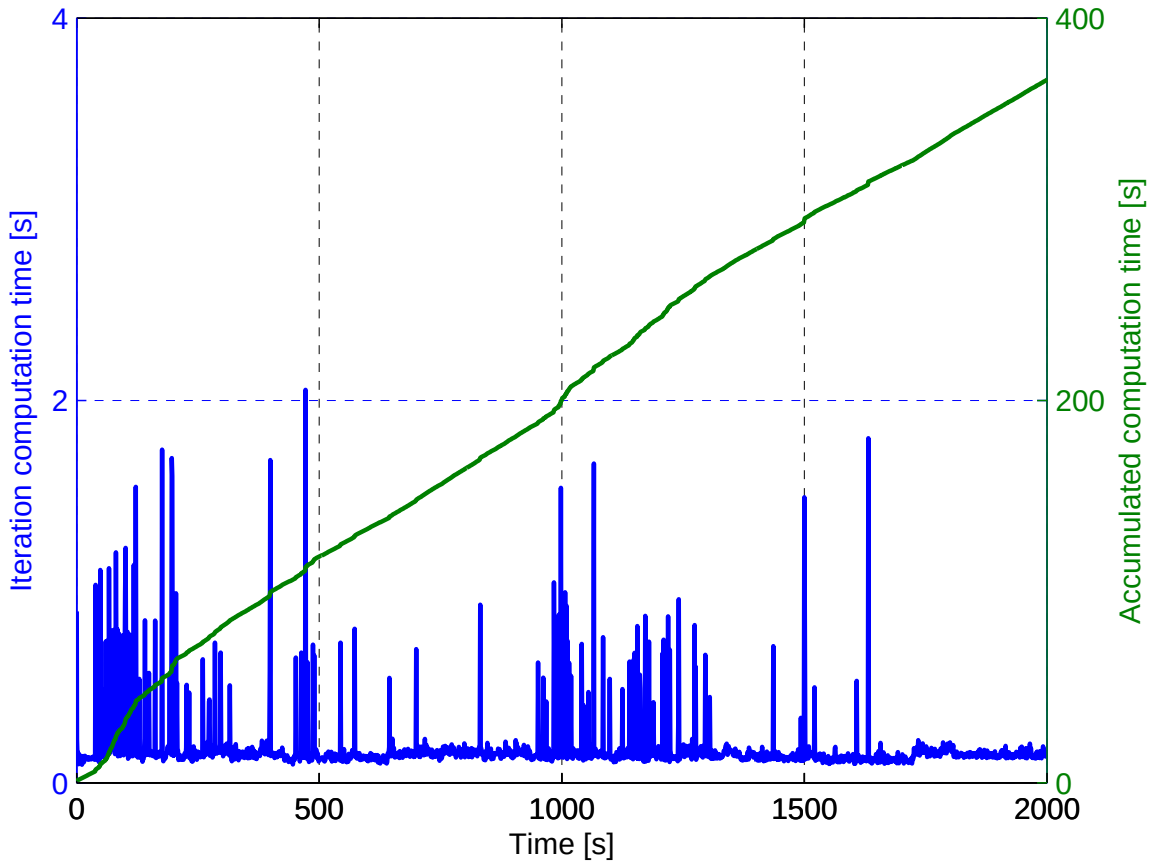

FIGURE 9.13: NMPC computation time for the NMPC 2

TABLE 9.4: NMPC setup parameters for the NMPC 3

Parameter	Description	Value
γ_{u_1}	I_{cmp} slew-rate penalisation	1
γ_{u_2}	T_{ref} slew-rate penalisation	1
γ_{u_3}	$\dot{n}_{H_2,in}$ slew-rate penalisation	1
γ_{u_4}	RH^C_{ref} slew-rate penalisation	1
λ_1	ECSA maximisation penalisation	10
λ_2	Efficiency maximisation penalisation	10
λ_3	Slew-rate penalisation	1
H_p	Prediction horizon	2
H_c	Control horizon	2
Δt	Sampling time	1 s
T_{sim}	Simulation time	2000 s

time, the global efficiency is similar as in NMPC 2 as depicted in Figure 9.17 (in fact, as it will be analysed in Section 9.8, it is slightly lower). The combination of efficiency and

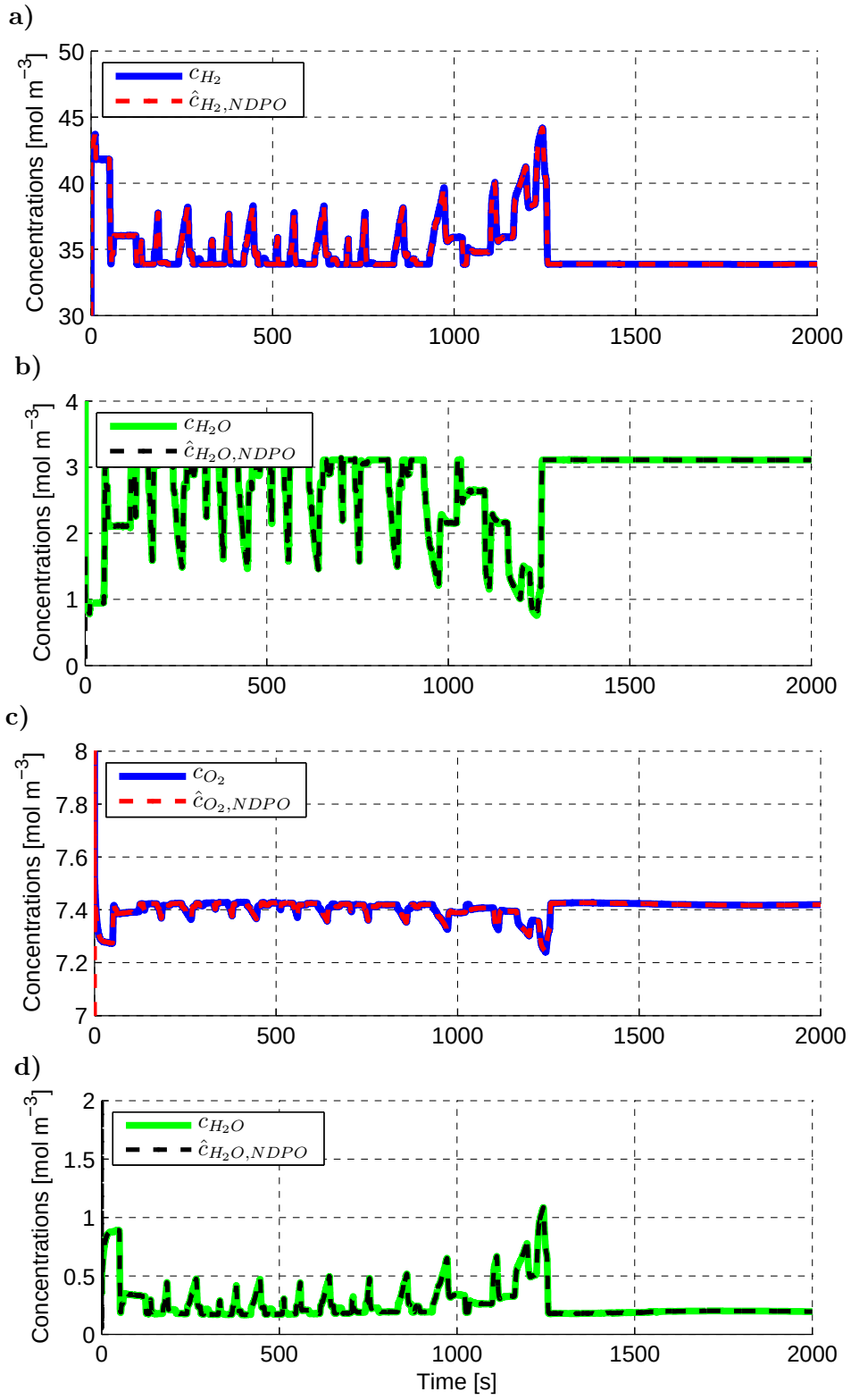

FIGURE 9.14: Behaviour of the NDPO versus the plant states in the middle discretisation volume of the anode (a and b) and the cathode (c and d) for the NMPC 2

ECSA maximisation improves efficiency on the transient periods in which the current density demand changes abruptly.

Regarding the temperature of the fuel cell for the NMPC 3, as shown in Figure 9.16, it follows a similar pattern as in the NMPC 1 (the optimal value is found in the neighbourhood around 73°C). In this case, the temperature behaviour is affected by the trade-off of the two control objectives defined for this case.

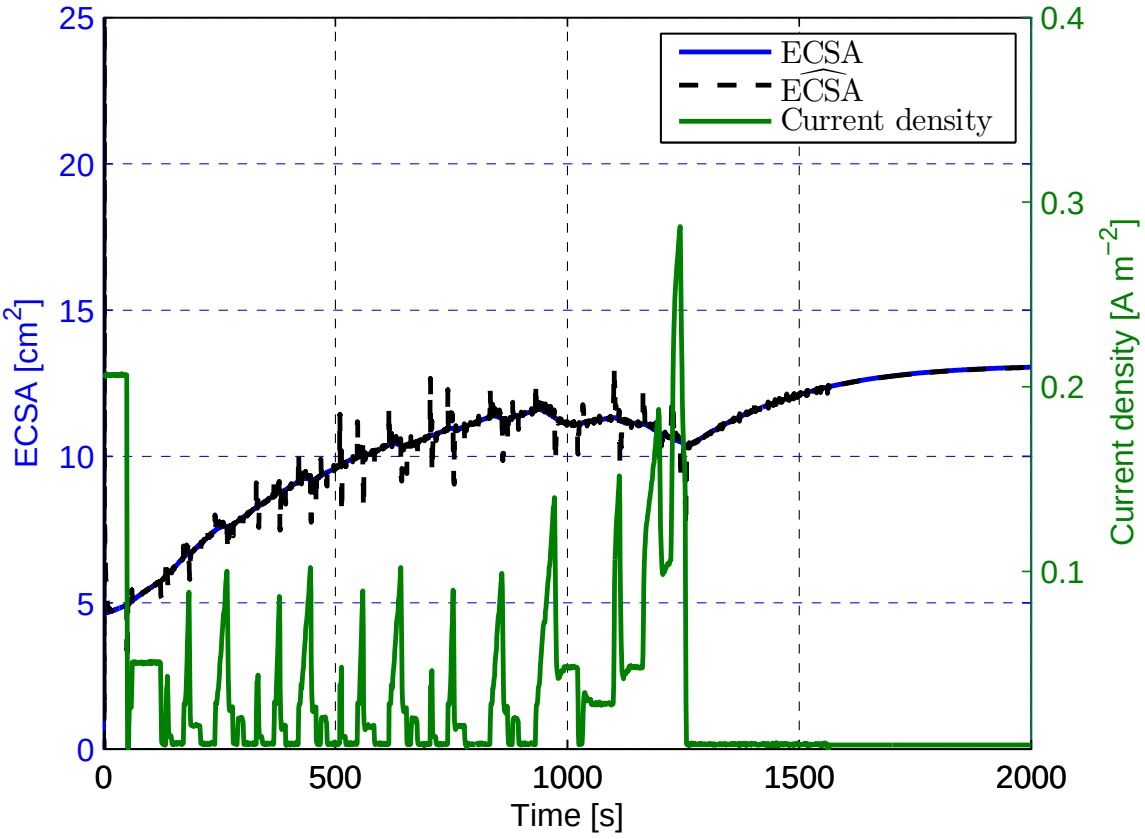

FIGURE 9.15: Evolution of modelled and observed ECSA and NEDC stack current density demand [3] for the NMPC 3

With respect to the control actions, Figure 9.18 presents the dynamic behaviour of the manipulated inputs for the NMPC 3. The compressor current and hydrogen molar input depicted in Figures 9.18a and d follow a similar behaviour as in the NMPC 2. This was expected since the maximisation of the global efficiency objective forces the system to operate under lower stoichiometries than in the constant stoichiometry case. At the same time, the NMPC strategy guarantees that the system does not enter in local starvation scenarios. The coolant mass flow input in Figure 9.18b achieves higher values than the ones presented in Figure 9.12 for the NMPC 2. This is due to the lower temperatures than the fuel cell has

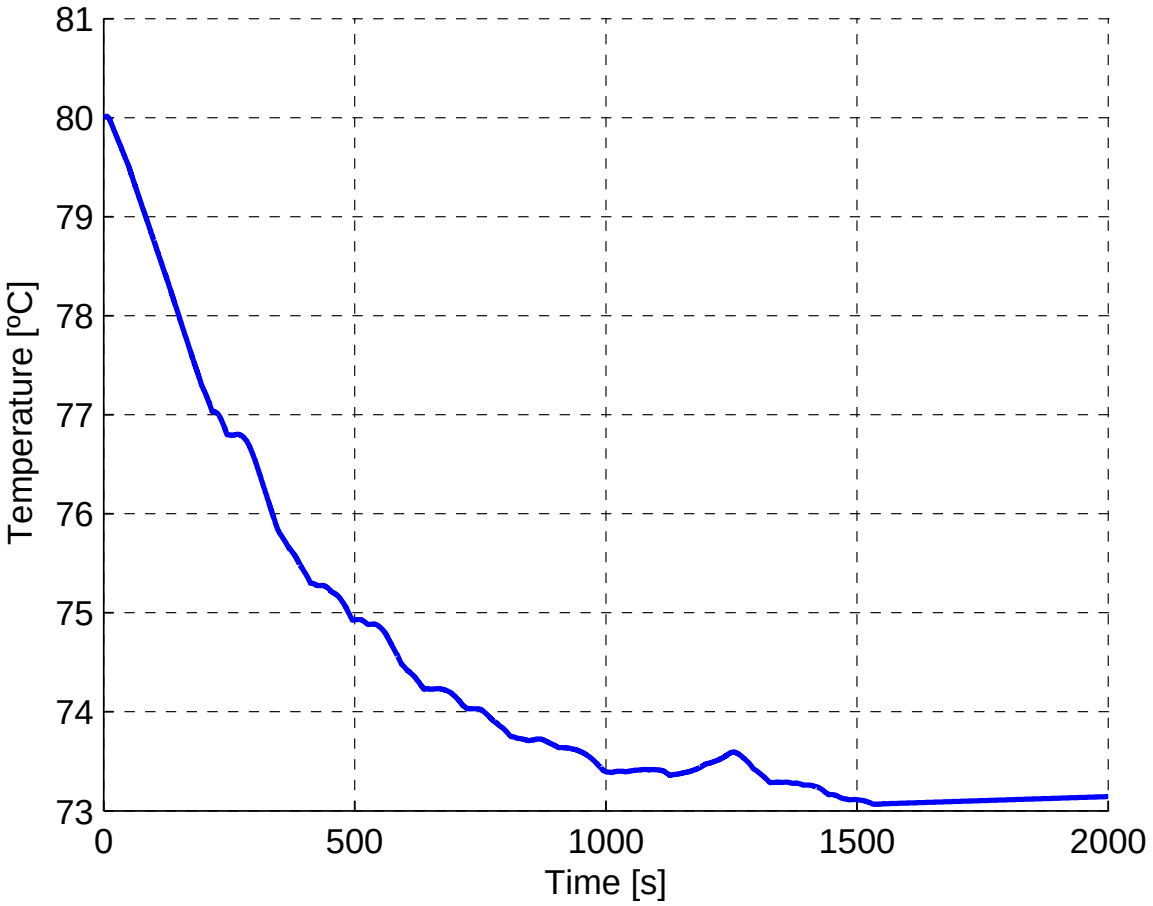

FIGURE 9.16: Temperature of the fuel cell stack for the NMPC 3

to attain as a result of the maximise the ECSA condition set on the control objectives. The relative humidity range does not fluctuate greatly during the simulation time as presented in Figure 9.18c.

As Figure 9.19 shows, the computation time for the combined control objectives is considerably higher than in the two previous cases. This is an expected result since the addition of multiple objectives adds computational burden. Nevertheless, the computation time is close to the simulation time. Better tuning of the controller or the use of a faster machine for the simulations could help reducing this accumulated value. Regarding the computation time of each individual iteration, during most of the simulation this value is higher than the sampling time of 1 second. Again, to study a possible implementation the iteration computation time has to be lower than the sampling time. This can be achieved with a faster machine and/or a more efficient optimisation solver.

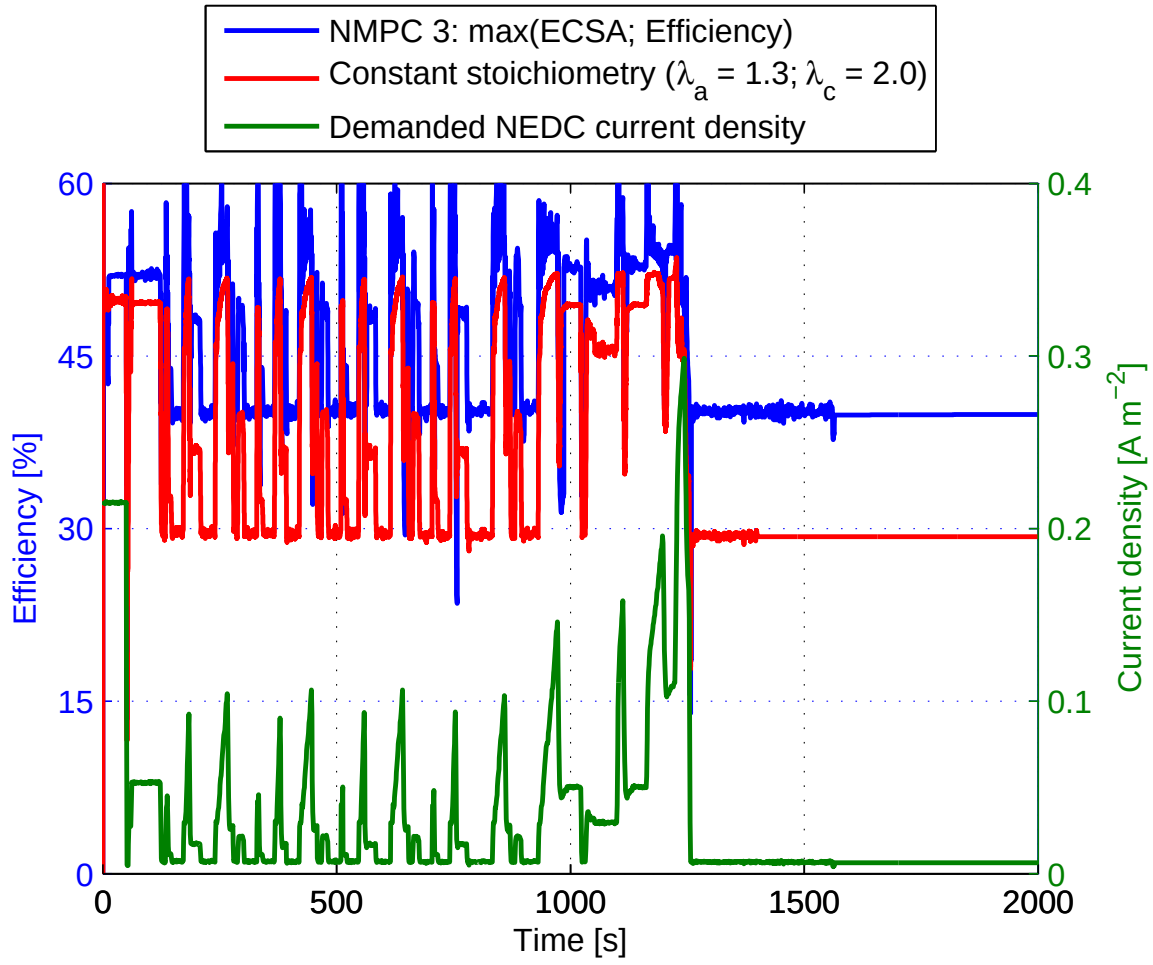

FIGURE 9.17: Efficiency of the system with the NMPC strategy (NMPC 3) and with constant operating conditions under a NEDC current demand

9.7.4.3 Observer Performance

As in the two previous cases, the HOSM observer performs robustly during all the simulation time as presented in Figure 9.20. Moreover, the ECSA also follows the real value and corrects the possible observation errors in a negligible amount of time (see Figure 9.15.

9.8 Summary

In Section 9.7 three cases for the NMPC strategy are presented and studied under a simulation scenario. The obtained results for each one of the cases are discussed and the behaviour of the control strategy analysed.

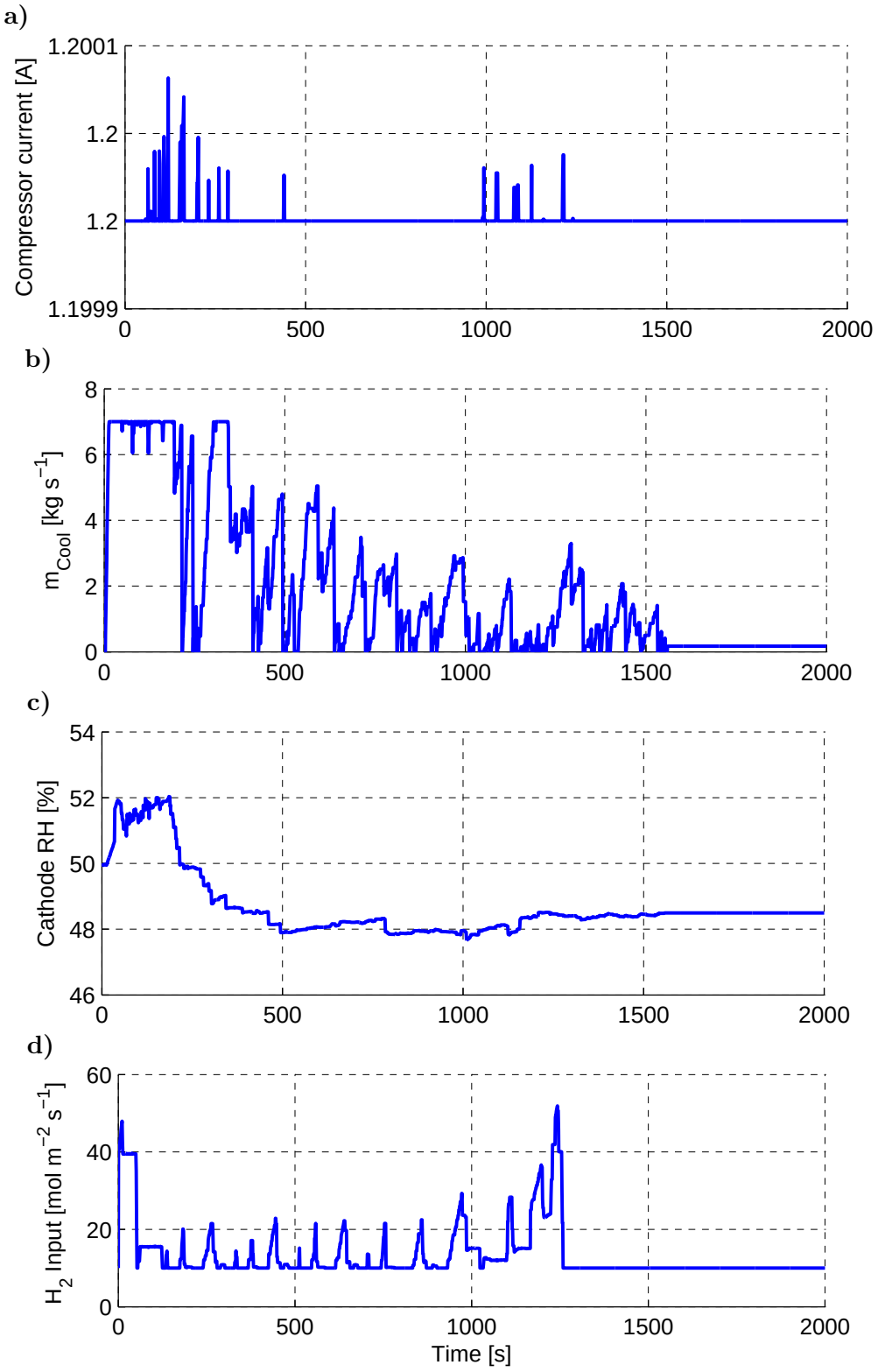

FIGURE 9.18: Compressor current (a), coolant mass flow (b), relative humidity (c) and H_2 input molar flux (d) control actions supplied by the NMPC for the NMPC 3

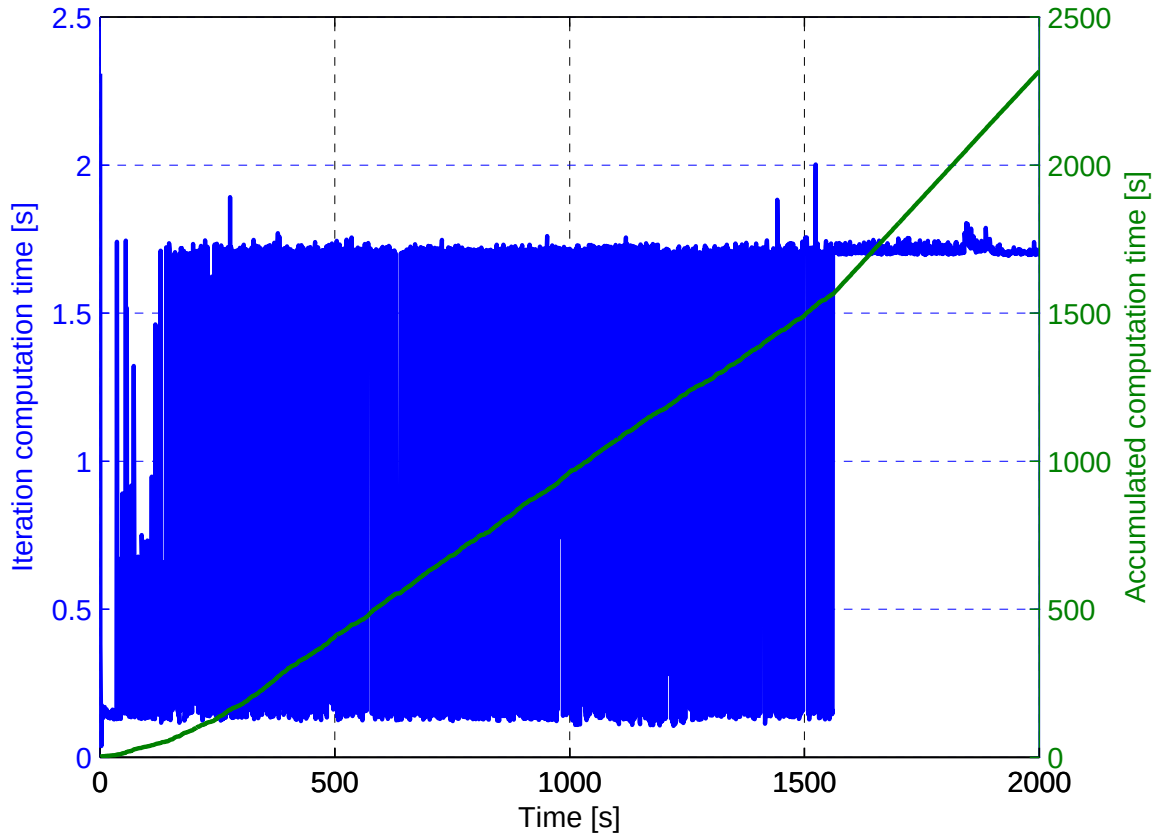

FIGURE 9.19: NMPC computation time for the NMPC 3

It has been concluded in Sections 9.7.3 and 9.7.4 that the global efficiency of the system can be improved with the use of the proposed controllers. The results have been compared with a constant stoichiometry approach, which considers only the fuel cell operation and it does not take into account the compressor efficiency or hydrogen economy.

The average efficiency over all the simulation scenario ($\overline{\eta}$) is computed as follows:

$$\overline{\eta} = \frac{\int_0^{t_{sim}} \eta \; dt}{t_{sim}}. \tag{9.13}$$

And for each one of the controllers the results are:

- $\overline{\eta}_{NMPC_1} = 25.11\%$
- $\overline{\eta}_{NMPC_2} = 44.63\%$
- $\overline{\eta}_{NMPC_3} = 44.27\%$

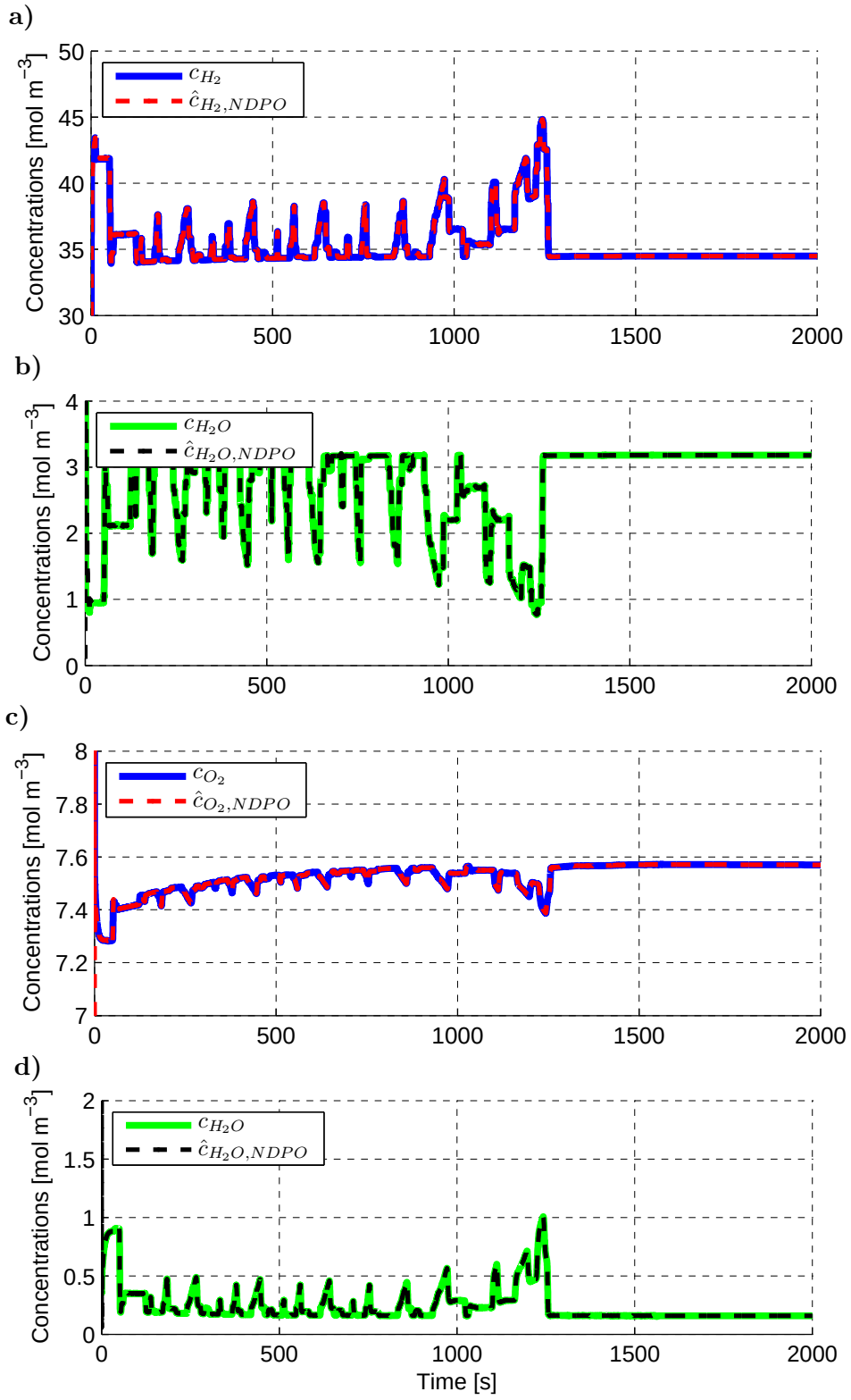

FIGURE 9.20: Behaviour of the NDPO versus the plant states in the middle discretisation volume of the anode (a and b) and the cathode (c and d) for the NMPC 3

Showing that the NMPC 2 controller, which focus on the improvement of the global efficiency, achieves a higher value as it was expected. Nevertheless, the results are very similar to the ones obtained with the NMPC 3 controller.

The characterisation of the effective active area of the fuel cell has been done with the ECSA variable. This variable can be increased during the operation of the fuel cell, improving the available area for the oxygen to react as explained in Sections 9.7.2 and 9.7.4. Furthermore, as presented in Section 9.7.4, the maximisation of the ECSA combined with the reduction of the stoichiometry can achieve high efficiency values with an improved active area, which avoids conditions that can damage the catalyst layer.

With the considered model, the ECSA value only depends on the humidification conditions of the fuel cell and the construction parameters of the membrane (see Section 4.4.5). A degradation function can be implemented in the ECSA that takes into account how the membrane losses Pt with time. Using the appropriate controllers, this Pt loss effect can be minimised finding a new optimal operating point in order to maximise the active area. As mentioned, this is accomplished in NMPCs 1 and 3 without taking into account the Pt loss aspect of the problem.

The implementation of the controller has not been treated in this thesis. However, information about the computation time has been facilitated in Figures 9.7, 9.13 and 9.19. Clearly, the total computation time is below the total simulation time in the first two cases (and near the simulation time in NMPC 3), allowing the future implementation in a real system.

To conclude, the combination of the control strategies presented in this chapter has improved greatly the performance of the system. The proposed controller can be easily tuned to give priority to certain objectives and it can be expanded to include more measurements and new control objectives that can be implemented easily. Chapter 10 summarises these and further conclusions extracted from this thesis.

Part V

Concluding Remarks

Chapter 10

Conclusions and Future Work

10.1 Conclusions

In this work, nonlinear observation and control strategies have been proposed and applied to a PEM fuel cell stack system with its BoP ancillaries. The proposed observers and controllers are based on a distributed parameters model of a PEM fuel cell.

Regarding the observers, two nonlinear distributed parameters estimation solutions are proposed to observe the full state gas concentration profiles along the gas channels in a PEM fuel cell. These estimates are used to infer indicators of the effective catalytic area. One approach is the NDPO with NDOB extension and the other is the HOSM observer. The two strategies have been compared and their performance evaluated, obtaining satisfactory observation results for a particular simulation framework (NEDC automotive application) in both cases. The MAE along the anode and cathode gas channels shows the better performance of the HOSM over the NDPO with NDOB approach.

In relation to the controllers, an NMPC control strategy has been designed, developed and tested in simulation to operate a PEM fuel cell-based system. This approach allows to handle the nonlinear dynamics of the plant when a highly dynamic power profile is being demanded. In this way, it has been shown that the efficiency can be improved with respect to a constant stoichiometry strategy while avoiding degradation of the systems by means of ensuring some minimum local concentrations of reactants in the catalyst layers. Moreover, the controller includes an specific control objective to maximise the active catalytic area defined by the

variable ECSA which is directly related to the liquid water ratio in the CCL pores. The performance of three different controllers designed to optimise different objective functions has been evaluated, obtaining satisfactory results for a given simulation scenario and proving the flexibility of the NMPC strategy.

The main contributions of this doctoral thesis can be summarised as follows:

- Modelling principles of PEM fuel cells were introduced and a control and estimation-oriented model of a PEM fuel cell was built. The model fulfils the requirements stated in Chapter 3:
  - Representation of the nonlinear phenomena of the PEM fuel cell
  - Spatial derivatives along the gas channels
  - Water distribution
- By means of spatial discretisation and reformulation, the model has been proven to be easily adaptable for the formulation of model-based estimation and control strategies.
- Two nonlinear state estimation strategies for distributed parameters systems have been developed and proven to converge to the real value of the variables in suitable times.
- A closed-loop control strategy using a nonlinear distributed parameters model as virtual reality has been developed to evaluate the performance of the PEM fuel cell-based system.
- Results of the closed-loop simulation according to different control objectives have been shown to improve the performance of the fuel cell with respect to a constant stoichiometry strategy while avoiding local and global starvation scenarios. These control objectives are: (i) maximise the ECSA at the cathode side of the fuel cell, (ii) maximise the global efficiency of the system and (iii) maximise the ECSA and the efficiency at the same time.

10.2 Future Work

During the course of this doctoral work, a wide set of control and observation methodologies applied to PEM fuel cell systems has been studied. However, several research lines can be explored in the future. This includes:

Experimental validation of the control and observation strategies

The observation and control strategies presented in Parts III and IV respectively have been evaluated in a simulation environment employing the nonlinear distributed model of the PEM fuel cell and the ancillaries of the BoP. The issue of the validation of these strategies has not been studied in this thesis. Nevertheless, it is a compelling continuation of the research.

The main issue to design a validation study for the distributed parameters strategies developed in this work is to have available a PEM fuel cell that allows the measurement of the internal variables of the system. Commercial fuel cells do not have these measurements available, which was one of the reasons behind the design and development of the distributed parameters estimators. In order to perform the validation, the fuel cell has to have internal sensors. Another alternative is to build a multi-fuel cell scheme to emulate the discretisation procedure followed in this work without the need of a specific fuel cell with internal measurements.

New uses for the observers

Since the observation strategies developed in this thesis are based on a distributed parameters model, they can be applied in numerous fields that use systems in which the spatial derivatives greatly affect the performance.

With respect to PEM fuel cells, the observers can also be integrated with diagnosis tools to display the fuel cell health status and design distributed parameters fault detection strategies that aim to avoid possible faults that occur in fuel cells.

Incorporate parametric uncertainty

The prediction model and the simulation model studied in this work have the same values for the physical parameters. In a situation where the simulation model is substituted with a real PEM fuel cell, the addition of parametric uncertainty is a key issue.

Diagnostics of the fuel cell could help to parametrise these uncertainties and feed them into the prediction model in the NMPC strategy.

Control strategy with fewer measurements

A certain set of measurements has been assumed to implement the observation and control strategies studied in this work. Nevertheless, it could be that in a real application, the fuel cell

(or the rest of the elements of the system) do not have available some of the aforementioned measurements.

The study and design of NMPC strategies that cope with these reduced sets of measurements is an interesting future research line.

Fine tuning of the controller

One of the main characteristics of the NMPC strategy proposed in Part IV is its high flexibility due to different adjustable setup parameters combinations. The fine tuning of the NMPC parameters was not studied in this work. A continuation of the approach proposed is to find methods to tune these parameters in an optimal way.

Another way to improve the NMPC performance is to test new solvers that aid to find the optimal point in less computational time.

Appendix A

Air Supply System

A.1 Equations for the Air Supply Model in Equation (4.50)

$$
\begin{aligned}
d_1 &= \tfrac{RT_{fc}k_{ca,in}}{V_{ca}M_{O_2}}\tfrac{x_{O_2}}{(1+\omega_{atm})}; & d_2 &= p_{sat};\\
d_3 &= \tfrac{RT_{fc}}{V_{ca}}; & d_4 &= M_{O_2};\\
d_5 &= M_{N_2}; & d_6 &= M_v p_{sat};\\
d_7 &= \tfrac{RT_{fc}n_c}{V_{ca}4F}; & d_8 &= \tfrac{RT_{fc}k_{ca,in}}{V_{ca}M_{N_2}}\tfrac{1-x_{O_2}}{(1+\omega_{atm})};\\
d_9 &= \tfrac{f}{J_{cmp}}; & d_{10} &= \tfrac{c_pT_{amb}}{J_{cmp}\eta_{cmp}};\\
d_{11} &= p_{atm}; & d_{12} &= \tfrac{\gamma-1}{\gamma};\\
d_{13} &= \tfrac{\eta_{cmp}k_t}{J_{cmp}}; & d_{14} &= \tfrac{RT_{atm}}{M_aV_{sm}};\\
d_{15} &= \tfrac{1}{\eta_{cm}}; & d_{16} &= k_{ca,in};\\
d_{17} &= k_{ca,out}; & d_{18} &= k_{ca,in}\tfrac{x_{O_2}}{(1+\omega_{atm})};
\end{aligned}
$$

Appendix B

Model Implementation

B.1 MATLAB Parameters

B.1.1 Physical Constants

Table B.1: Physical constants present in the PEM fuel cell system model

Constant	Description	Value	Unit
C_{P,H_2}	Hydrogen heat capacity	28.82	J mol^{-1} K^{-1}
C_{P,N_2}	Nitrogen heat capacity	29.38	J mol^{-1} K^{-1}
C_{P,O_2}	Oxygen heat capacity	29.12	J mol^{-1} K^{-1}
C^g_{P,H_2O}	Vapour water heat capacity	37.47	J mol^{-1} K^{-1}
C^l_{P,H_2O}	Liquid water heat capacity	75.33	J mol^{-1} K^{-1}
F	Faraday constant	96485.34	C mol^{-1}
h_{f,H_2}	Hydrogen standard enthalpy of formation @ 298 K	0	J mol^{-1}
h_{f,O_2}	Oxygen standard enthalpy of formation @ 298 K	0	J mol^{-1}
h_{f,N_2}	Nitrogen standard enthalpy of formation @ 298 K	0	J mol^{-1}
h^g_{f,H_2O}	Vapour water standard enthalpy of formation @ 298 K	-241818	J mol^{-1}
h^l_{f,H_2O}	Liquid water standard enthalpy of formation @ 298 K	-285800	J mol^{-1}
M_{air}	Air molar mass	28.96	g mol^{-1}
M_{H_2}	Hydrogen molar mass	2.02	g mol^{-1}
M_{N_2}	Nitrogen molar mass	28.00	g mol^{-1}

TABLE B.1: Physical constants present in the PEM fuel cell system model

Constant	Description	Value	Unit
M_{O_2}	Oxygen molar mass	32.00	g mol^{-1}
M_{water}	Water molar mass	18.02	g mol^{-1}
p^{amb}	Ambient pressure	101325	Pa
R	Gas constant	8.31	J mol^{-1} K^{-1}
$\mu^{l}_{H_2O}$	Liquid water viscosity	3.52×10^{-4}	Pa s
ρ_A	Air density	1.23	kg m^{-3}
ρ_{N_2}	Nitrogen density	1.165	kg m^{-3}
ρ_{O_2}	Oxygen density	1.331	kg m^{-3}
$\rho^{l}_{H_2O}$	Liquid water density	970	kg m^{-3}
$\sigma^{l}_{H_2O}$	Liquid water surface tension	0.0625	N m^{-3}

B.1.2 PEM Fuel Cell Model Parameters

TABLE B.2: Values of the coefficients in the PEM fuel cell simulation model

Parameter	Description	Value	Unit
C^A	Anode volumetric capacitance	8.25×10^6	F m^{-3}
C^C	Cathode volumetric capacitance	8.25×10^6	F m^{-3}
E_r	Theoretical fuel cell potential	1.23	V
K^A	Anode Darcy's coefficient	1×10^{-5}	m^2 s^{-1} Pa^{-1}
K^C	Cathode Darcy's coefficient	1×10^{-4}	m^2 s^{-1} Pa^{-1}
K^{evap}	Liquid water evaporation rate	5000	s^{-1}
K^{sorp}_{CDL}	Adsorption rate at the CCL	500	s^{-1}
K^{sorp}_{CCL}	Adsorption rate at the cathode GDL	50	s^{-1}
L	Fuel cell length	0.4	m
L_x	Gas channel width	1×10^{-3}	m
n_{Pt}	Number of platinum particles per pore at the CCL	[1, 24]	—
X_{dry}	Membrane molar capacity	0.909	mol kg(dry)$^{-1}$
α	Cathode charge transfer coefficient	0.5	—
ΔG^*	Gibbs activation energy	73	kJ mol^{-1}
δ^A	Anode gas channel thickness	0.7×10^{-3}	m
δ^{AG}	Anode gas diffusion layer thickness	0.34×10^{-3}	m
δ^{ACL}	Anode catalyst layer thickness	4×10^{-5}	m
δ^M	Membrane thickness	1.75×10^{-4}	m
δ^{CCL}	Cathode catalyst layer thickness	1.1×10^{-4}	m
δ^{CG}	Cathode gas diffusion layer thickness	0.34×10^{-3}	m
δ^C	Cathode gas channel thickness	0.7×10^{-3}	m
τ_{Pt}	Platinum pore radius	[10, 30]	nm
θ_{GDL}	GDL contact angle	100	—
θ_{CCL}	CCL contact angle	89	—
ε_{CCL}	CCL porosity	[0.497, 0.491]	—
ε_{GDL}	GDL porosity	0.5	—

B.1.3 Compressor Parameters

TABLE B.3: Compressor parameters

Parameter	Description	Value	Unit
$k_{ca,in}$	Cathode inlet orifice constant	0.3629×10^{-5}	kg Pa^{-1} s^{-1}
$k_{ca,out}$	Cathode outlet orifice constant	0.76×10^{-4}	kg Pa^{-1} s^{-1}
k_t	Motor constant	0.31	N m^{-1} A^{-1}
f	Motor friction constant	0.00136	V rad^{-1} s^{-1}
J_{cmp}	Compressor inertia	671.9×10^{-5}	kg m^{-2}
V_{ca}	Cathode volume	$V_{ca,fc} \times n_c$	m^3
V_{sm}	Supply manifold volume	$V_{ca} \times 2$	m^3
η_{cm}	Motor mechanical efficiency	0.98	%
η_{cmp}	Compressor efficiency	0.8	%
γ	Specific heat ratio of air	1.4	—

B.1.4 Thermal Model Parameters

TABLE B.4: Thermal model parameters

Parameter	Description	Value	Unit
$C_{P,cool}$	Water-ethylene glycol heat capacity	3.56	kJ kg^{-1} K^{-1}
k_{conv}	Thermal conductivity coefficient	15	W m^{-2} K^{-1}
$T_{cool,out} - T_{cool,in}$	Heat exchange temperature gradient	5	K

Bibliography

[1] Fuel cell stack from pragma industries, http://www.fuelcellmarkets.com/Pragma_Industries_Fuel_Cell_Stacks_Testing/forming_relationships/3,1,28270,18,28921.html.

[2] J. Larminie, A. Dicks, M. S. McDonald, Fuel cell systems explained, Vol. 2, Wiley New York, 2003.

[3] M. Mayur, S. Strahl, A. Husar, W. G. Bessler, A multi-timescale modeling methodology for PEMFC performance and durability in a virtual fuel cell car, International Journal of Hydrogen Energy 40 (46) (2015) pp. 16466–16476.

[4] F. Barbir, PEM fuel cells: theory and practice, Elsevier Academic Press, 2013.

[5] F. Barbir, Transition to renewable energy systems with hydrogen as an energy carrier, Energy 34 (3) (2009) pp. 308–312.

[6] J. M. Maciejowski, Predictive control with constraints, Pearson education, 2002.

[7] T. B. Johansson, Renewable energy: sources for fuels and electricity, Island Press, 1993.

[8] B. J. De Vries, D. P. Van Vuuren, M. M. Hoogwijk, Renewable energy sources: Their global potential for the first-half of the 21st century at a global level: An integrated approach, Energy Policy 35 (4) (2007) pp. 2590–2610.

[9] G. Resch, A. Held, T. Faber, C. Panzer, F. Toro, R. Haas, Potentials and prospects for renewable energies at global scale, Energy Policy 36 (11) (2008) pp. 4048–4056.

[10] B. E. Logan, Peer reviewed: extracting hydrogen and electricity from renewable resources, Environmental Science & Technology 38 (9) (2004) pp. 160A–167A.

[11] S. H. Jensen, P. H. Larsen, M. Mogensen, Hydrogen and synthetic fuel production from renewable energy sources, International Journal of Hydrogen Energy 32 (15) (2007) pp. 3253–3257.

[12] O. Z. Sharaf, M. F. Orhan, An overview of fuel cell technology: Fundamentals and applications, Renewable and Sustainable Energy Reviews 32 (2014) pp. 810–853.

[13] D. E. Curtin, R. D. Lousenberg, T. J. Henry, P. C. Tangeman, M. E. Tisack, Advanced materials for improved PEMFC performance and life, Journal of Power Sources 131 (1) (2004) pp. 41–48.

[14] R. Methekar, V. Prasad, R. Gudi, Dynamic analysis and linear control strategies for proton exchange membrane fuel cell using a distributed parameter model, Journal of Power Sources 165 (1) (2007) pp. 152–170.

[15] M. Mangold, A. Bück, R. Hanke-Rauschenbach, Passivity based control of a distributed PEM fuel cell model, Journal of Process Control 20 (3) (2010) pp. 292–313.

[16] Y. Shao, G. Yin, Y. Gao, Understanding and approaches for the durability issues of pt-based catalysts for PEM fuel cell, Journal of Power Sources 171 (2) (2007) pp. 558–566.

[17] X. Yu, S. Ye, Recent advances in activity and durability enhancement of pt/c catalytic cathode in PEMFC: Part II: Degradation mechanism and durability enhancement of carbon supported platinum catalyst, Journal of Power Sources 172 (1) (2007) pp. 145–154.

[18] J. Wang, G. Yin, Y. Shao, S. Zhang, Z. Wang, Y. Gao, Effect of carbon black support corrosion on the durability of pt/c catalyst, Journal of Power sources 171 (2) (2007) pp. 331–339.

[19] N. Yousfi-Steiner, P. Moçotéguy, D. Candusso, D. Hissel, A review on polymer electrolyte membrane fuel cell catalyst degradation and starvation issues: Causes, consequences and diagnostic for mitigation, Journal of Power Sources 194 (1) (2009) pp. 130–145.

[20] W. He, G. Lin, T. Van Nguyen, Diagnostic tool to detect electrode flooding in proton-exchange-membrane fuel cells, AIChE Journal 49 (12) (2003) pp. 3221–3228.

[21] J. Luna, C. Ocampo-Martinez, M. Serra, Nonlinear predictive control for the concentrations profile regulation under unknown reaction disturbances in a fuel cell anode gas channel, Journal of Power Sources 282 (2015) pp. 129–139.

[22] J. Luna, A. Husar, M. Serra, Nonlinear distributed parameter observer design for fuel cell systems, International Journal of Hydrogen Energy 40 (34) (2015) pp. 11322–11332.

[23] J. Luna, E. Usai, A. Husar, M. Serra, Nonlinear observation in fuel cell systems: A comparison between disturbance estimation and high-order sliding-mode techniques, International Journal of Hydrogen Energy 41 (43) (2016) pp. 19737–19748.

[24] J. Luna, S. Jemei, N. Yousfi-Steiner, A. Husar, M. Serra, D. Hissel, Nonlinear predictive control for durability enhancement and efficiency improvement in a fuel cell power system, Journal of Power Sources 328 (2016) pp. 250–261.

[25] J. Luna, E. Usai, Attila, M. Serra, Enhancing the efficiency and lifetime of a proton exchange membrane fuel cell using nonlinear model predictive control with nonlinear observation (2016, submitted to IEEE TIE).

[26] J. Luna, C. Batlle, C. Kunusch, J. Riera, M. Sarmiento-Carnevali, M. Serra, Observation of the internal states of a PEMFC anode gas channel, in: XXXIV Jornadas de Automática, Terrassa, Spain, 2013.

[27] J. Luna, A. Husar, M. Serra, State observers design for PEMFC systems, in: Ibero-American Conference on Hydrogen and Fuel Cells, Bellaterra, Spain, 2014.

[28] J. Luna, C. Ocampo-Martinez, M. Serra, Nonlinear predictive control for the concentrations profile regulation in a PEM fuel cell anode gas channel, in: European Control Conference, Strasbourg, France, 2014, pp. pp. 1807–1812.

[29] J. Luna, E. Usai, A. Husar, M. Serra, Distributed parameter nonlinear state observer with unmatched disturbance estimation for PEMFC systems, in: 6th International Conference on Fundamentals and Development of Fuel Cells, Toulouse, France, 2015.

[30] J. Luna, E. Usai, A. Husar, M. Serra, State estimation in fuel cell systems: A sliding mode approach, in: V Iberian Symposium on Hydrogen, Fuel Cells and Advanced Batteries (Hyceltec), Tenerife, Spain, 2015.

[31] J. Luna, N. Yousfi-Steiner, S. Jemei, A. Husar, M. Serra, Nonlinear model predictive control methodology for efficiency and durability improvement in a fuel cell power system, in: World Hydrogen Energy Conference (WHEC), Zaragoza, Spain, 2016.

[32] J. Luna, E. Usai, A. Husar, M. Serra, Observation of the electrochemically active surface area in a proton exchange membrane fuel cell, in: 42nd Annual Conference of IEEE Industrial Electronics Society, Firenze, Italy, 2016.

[33] R. O'Hayre, S.-W. Cha, W. Colella, F. Prinz, Fuel cell fundamentals, John Wiley & Sons New York, 2006.

[34] N. Sammes, R. Boersma, Small-scale fuel cells for residential applications, Journal of Power sources 86 (1) (2000) pp. 98–110.

[35] L. Barelli, G. Bidini, F. Gallorini, A. Ottaviano, Dynamic analysis of PEMFC-based CHP systems for domestic application, Applied Energy 91 (1) (2012) pp. 13–28.

[36] J. Sinha, S. Lasher, Y. Yang, P. Kopf, Direct hydrogen PEMFC manufacturing cost estimation for automotive applications, 2010 DOE Annual Merit Review, Washington, DC.

[37] J. Owejan, J. Gagliardo, J. Sergi, S. Kandlikar, T. Trabold, Water management studies in PEM fuel cells, part i: Fuel cell design and in situ water distributions, International Journal of Hydrogen Energy 34 (8) (2009) pp. 3436–3444.

[38] Z. Lu, S. Kandlikar, C. Rath, M. Grimm, W. Domigan, A. White, M. Hardbarger, J. Owejan, T. Trabold, Water management studies in PEM fuel cells, part II: Ex situ investigation of flow maldistribution, pressure drop and two-phase flow pattern in gas channels, International Journal of Hydrogen Energy 34 (8) (2009) pp. 3445–3456.

[39] S. Kim, S. Shimpalee, J. Van Zee, The effect of stoichiometry on dynamic behavior of a proton exchange membrane fuel cell (PEMFC) during load change, Journal of Power Sources 135 (1) (2004) pp. 110–121.

[40] Q. Yan, H. Toghiani, H. Causey, Steady state and dynamic performance of proton exchange membrane fuel cells (PEMFCs) under various operating conditions and load changes, Journal of Power Sources 161 (1) (2006) pp. 492–502.

[41] M. Wöhr, K. Bolwin, W. Schnurnberger, M. Fischer, W. Neubrand, G. Eigenberger, Dynamic modelling and simulation of a polymer membrane fuel cell including mass transport limitation, International Journal of Hydrogen Energy 23 (3) (1998) pp. 213–218.

[42] S. Strahl, A. Husar, A. A. Franco, Electrode structure effects on the performance of open-cathode proton exchange membrane fuel cells: A multiscale modeling approach, International Journal of Hydrogen Energy 39 (18) (2014) pp. 9752–9767.

[43] T. Nguyen, R. White, A water and heat management model for proton-exchange-membrane fuel cells, Journal of the Electrochemical Society 140 (8) (1993) pp. 2178–2186.

[44] A. Rowe, X. Li, Mathematical modeling of proton exchange membrane fuel cells, Journal of power sources 102 (1) (2001) pp. 82–96.

[45] S. Um, C. Wang, K. Chen, Computational fluid dynamics modeling of proton exchange membrane fuel cells, Journal of the Electrochemical Society 147 (12) (2000) pp. 4485–4493.

[46] S. Um, C. Wang, Three-dimensional analysis of transport and electrochemical reactions in polymer electrolyte fuel cells, Journal of Power Sources 125 (1) (2004) pp. 40–51.

[47] W. Tao, C. Min, X. Liu, Y. He, B. Yin, W. Jiang, Parameter sensitivity examination and discussion of PEM fuel cell simulation model validation: Part i. current status of modeling research and model development, Journal of Power Sources 160 (1) (2006) pp. 359–373.

[48] C. Min, Y. He, X. Liu, B. Yin, W. Jiang, W. Tao, Parameter sensitivity examination and discussion of pem fuel cell simulation model validation: Part ii: Results of sensitivity analysis and validation of the model, Journal of Power Sources 160 (1) (2006) pp. 374–385.

[49] J. Pukrushpan, A. Stefanopoulou, H. Peng, Control of fuel cell power systems: principles, modeling, analysis and feedback design, Springer Science & Business Media, 2004.

[50] M. M. Mench, E. C. Kumbur, T. N. Veziroglu, Polymer electrolyte fuel cell degradation, Academic Press, 2011.

[51] S. Zhang, X. Yuan, H. Wang, W. Mérida, H. Zhu, J. Shen, S. Wu, J. Zhang, A review of accelerated stress tests of MEA durability in PEM fuel cells, International Journal of Hydrogen Energy 34 (1) (2009) pp. 388–404.

[52] Y. Li, T. Zhao, Understanding the performance degradation of anion-exchange membrane direct ethanol fuel cells, International Journal of Hydrogen Energy 37 (5) (2012) pp. 4413–4421.

[53] D. Feroldi, M. Serra, J. Riera, Energy management strategies based on efficiency map for fuel cell hybrid vehicles, Journal of Power Sources 190 (2) (2009) pp. 387–401.

[54] N. Sulaiman, M. Hannan, A. Mohamed, E. Majlan, W. W. Daud, A review on energy management system for fuel cell hybrid electric vehicle: Issues and challenges, Renewable and Sustainable Energy Reviews 52 (2015) pp. 802–814.

[55] P. Garcia, L. M. Fernandez, C. A. Garcia, F. Jurado, Energy management system of fuel-cell-battery hybrid tramway, IEEE Transactions on Industrial Electronics 57 (12) (2010) pp. 4013–4023.

[56] M. Zandi, A. Payman, J.-P. Martin, S. Pierfederici, B. Davat, F. Meibody-Tabar, Energy management of a fuel cell/supercapacitor/battery power source for electric vehicular applications, IEEE transactions on vehicular technology 60 (2) (2011) pp. 433–443.

[57] M. Uzunoglu, O. Onar, M. Alam, Dynamic behavior of pem fcpps under various load conditions and voltage stability analysis for stand-alone residential applications, Journal of Power Sources 168 (1) (2007) pp. 240–250.

[58] H. Nijmeijer, T. Fossen, New directions in nonlinear observer design, Vol. 244, Springer, 1999.

[59] D. Luenberger, Observing the state of a linear system, IEEE Transactions on Military Electronics 8 (2) (1964) pp. 74–80.

[60] C.-H. Lien, Robust observer-based control of systems with state perturbations via LMI approach, IEEE Transactions on Automatic Control 49 (8) (2004) pp. 1365–1370.

[61] H. H. Choi, M. J. Chung, Robust observer-based $\mathcal{H}_\infty$ controller design for linear uncertain time-delay systems, Automatica 33 (9) (1997) pp. 1749–1752.

[62] W. Perruquetti, J.-P. Barbot, Sliding mode control in engineering, CRC Press, 2002.

[63] G. Bartolini, A. Pisano, E. Punta, E. Usai, A survey of applications of second-order sliding mode control to mechanical systems, International Journal of Control 76 (9-10) (2003) pp. 875–892.

[64] A. Levant, Higher-order sliding modes, differentiation and output-feedback control, International Journal of Control 76 (9-10) (2003) pp. 924–941.

[65] İ. Eker, Second-order sliding mode control with experimental application, ISA transactions 49 (3) (2010) pp. 394–405.

[66] J. Davila, L. Fridman, A. Levant, Second-order sliding-mode observer for mechanical systems, IEEE Transactions on Automatic Control 50 (11) (2005) pp. 1785–1789.

[67] C. Kunusch, J. Moreno, M. Angulo, Identification and observation in the anode line of PEM fuel cell stacks, in: 52nd Annual Conference on Decision and Control (CDC), IEEE, 2013, pp. pp. 1665–1670.

[68] R. Carroll, D. Lindorff, An adaptive observer for single-input single-output linear systems, IEEE Transactions on Automatic Control 18 (5) (1973) pp. 428–435.

[69] V. Alcaraz-González, A. Genovesi, J. Harmand, A. González, A. Rapaport, J. Steyer, Robust exponential nonlinear interval observer for a class of lumped models useful in chemical and biochemical engineering. application to a wastewater treatment process, in: Proc. MISC'99 Workshop on Applications of Interval Analysis to Systems and Control, 1999, pp. pp. 225–235.

[70] M. Bitzer, M. Zeitz, Design of a nonlinear distributed parameter observer for a pressure swing adsorption plant, Journal of Process Control 12 (4) (2002) pp. 533–543.

[71] H. Görgün, M. Arcak, F. Barbir, An algorithm for estimation of membrane water content in PEM fuel cells, Journal of power sources 157 (1) (2006) pp. 389–394.

[72] I. Kazmi, A. Bhatti, S. Iqbal, A nonlinear observer for PEM fuel cell system, in: 13th International Multitopic Conference, 2009, IEEE, 2009, pp. pp. 1–6.

[73] E.-S. Kim, C.-J. Kim, K.-S. Eom, Nonlinear observer design for PEM fuel cell systems, in: International Conference on Electrical Machines and Systems, IEEE, 2007, pp. pp. 1835–1839.

[74] M. Arcak, H. Gorgun, L. Pedersen, S. Varigonda, A nonlinear observer design for fuel cell hydrogen estimation, Transactions on Control Systems Technology, 12 (1) (2004) pp. 101–110.

[75] A. Pilloni, A. Pisano, E. Usai, Observer based air excess ratio control of a PEM fuel cell system via high order sliding mode, IEEE Transactions on Industrial Electronics.

[76] P. Rodatz, Dynamics of the polymer electrolyte fuel cell: experiments and model-based analysis, Ph.D. thesis, Swiss Federal Institute of Technology (2003).

[77] F. Grasser, A. Rufer, A fully analytical PEM fuel cell system model for control applications, IEEE Transactions on Industry Applications 43 (6) (2007) pp. 1499–1506.

[78] C. Kunusch, A. Husar, P. Puleston, M. Mayosky, J. Moré, Linear identification and model adjustment of a PEM fuel cell stack, International Journal of Hydrogen Energy 33 (13) (2008) pp. 3581–3587.

[79] F. Bianchi, C. Ocampo-Martinez, C. Kunusch, R. Sanchez-Pena, Fault-tolerant unfalsified control for PEM fuel cell systems, IEEE Transactions on Energy ConversionIn press.

[80] M. Bavarian, M. Soroush, I. Kevrekidis, J. Benziger, Mathematical modeling, steady-state and dynamic behavior, and control of fuel cells: A review, Industrial & Engineering Chemistry Research 49 (17) (2010) pp. 7922–7950.

[81] K. Thanapalan, G. Liu, J. Williams, B. Wang, Review and analysis of fuel cell system modelling and control, International Journal of Computer Aided Engineering and Technology 1 (2) (2009) pp. 145–157.

[82] Q. Li, W. Chen, Z. Liu, J. Huang, L. Ma, Net power control based on linear matrix inequality for proton exchange membrane fuel cell system, IEEE Transactions on Energy Conversion 29 (1) (2014) pp. 1–8.

[83] C. Damour, M. Benne, C. Lebreton, J. Deseure, B. Grondin-Perez, Real-time implementation of a neural model-based self-tuning PID strategy for oxygen stoichiometry control in PEM fuel cell, International Journal of Hydrogen Energy 39 (24) (2014) pp. 12819–12825.

[84] C. Restrepo, T. Konjedic, C. Guarnizo, O. Avino-Salvado, J. Calvente, A. Romero, R. Giral, Simplified mathematical model for calculating the oxygen excess ratio of a PEM fuel cell system in real-time applications, IEEE Transactions on Industrial Electronics 61 (6) (2014) pp. 2816–2825.

[85] S. Strahl, A. Husar, J. Riera, Experimental study of hydrogen purge effects on performance and efficiency of an open-cathode proton exchange membrane fuel cell system, Journal of Power Sources 248 (2014) pp. 474–482.

[86] Y. Hou, C. Shen, D. Hao, Y. Liu, H. Wang, A dynamic model for hydrogen consumption of fuel cell stacks considering the effects of hydrogen purge operation, Renewable Energy 62 (2014) pp. 672–678.

[87] C. Ramos-Paja, C. Bordons, A. Romero, R. Giral, L. Martinez-Salamero, Minimum fuel consumption strategy for PEM fuel cells, IEEE Transactions on Industrial Electronics 56 (3) (2009) pp. 685–696.

[88] D. Friedman, R. Moore, PEM fuel cell system optimization, Proceedings Electrochemical Society 27 (1998) pp. 407–423.

[89] I. Matraji, S. Laghrouche, M. Wack, Pressure control in a PEM fuel cell via second order sliding mode, International Journal of Hydrogen Energy 37 (21) (2012) pp. 16104–16116.

[90] M. Grujicic, K. Chittajallu, E. Law, J. Pukrushpan, Model-based control strategies in the dynamic interaction of air supply and fuel cell, Proceedings of the Institution of Mechanical Engineers 218 (7) (2004) pp. 487–499.

[91] J.-W. Ahn, S.-Y. Choe, Coolant controls of a PEM fuel cell system, Journal of Power Sources 179 (1) (2008) pp. 252–264.

[92] C. Bordons, A. Arce, A. Del Real, Constrained predictive control strategies for PEM fuel cells, in: American Control Conference, IEEE, 2006, pp. pp. 6–pp.

[93] M. Serra, A. Husar, D. Feroldi, J. Riera, Performance of diagonal control structures at different operating conditions for polymer electrolyte membrane fuel cells, Journal of Power Sources 158 (2) (2006) pp. 1317–1323.

[94] C. Kunusch, P. Puleston, M. Mayosky, A. Husar, Control-oriented modeling and experimental validation of a PEMFC generation system, IEEE Transactions on Energy Conversion 26 (3) (2011) pp. 851–861.

[95] C. Kunusch, P. Puleston, M. Mayosky, J. Riera, Sliding mode strategy for PEM fuel cells stacks breathing control using a super-twisting algorithm, IEEE Transactions on Control Systems Technology 17 (1) (2009) pp. 167–174.

[96] F. Bianchi, C. Kunusch, C. Ocampo-Martinez, R. Sánchez-Peña, A gain-scheduled LPV control for oxygen stoichiometry regulation in PEM fuel cell systems, IEEE Transactions on Control Systems Technology 22 (5) (2014) pp. 1837–1844.

[97] C. Kunusch, P. Puleston, M. Mayosky, A. Dávila, Efficiency optimisation of an experimental PEM fuel cell system via super twisting control, in: 11th International Workshop on Variable Structure Systems (VSS), IEEE, 2010, pp. pp. 319–324.

[98] S. Laghrouche, I. Matraji, F. S. Ahmed, S. Jemei, M. Wack, Load governor based on constrained extremum seeking for pem fuel cell oxygen starvation and compressor surge protection, International Journal of Hydrogen Energy 38 (33) (2013) pp. 14314–14322.

[99] V. Liso, M. P. Nielsen, S. K. Kær, H. H. Mortensen, Thermal modeling and temperature control of a pem fuel cell system for forklift applications, International Journal of Hydrogen Energy 39 (16) (2014) pp. 8410–8420.

[100] B. Blunier, A. Miraoui, Air management in pem fuel cells: State-of-the-art and prospectives, in: Electrical Machines and Power Electronics, 2007. ACEMP'07. International Aegean Conference on, IEEE, 2007, pp. pp. 245–254.

[101] R. Taylor, R. Krishna, Multicomponent mass transfer, Vol. 2, John Wiley & Sons, 1993.

[102] H. Wu, X. Li, P. Berg, On the modeling of water transport in polymer electrolyte membrane fuel cells, Electrochimica Acta 54 (27) (2009) pp. 6913–6927.

[103] A. Buck, New equations for computing vapor pressure and enhancement factor, Journal of Applied Meteorology 20 (12) (1981) pp. 1527–1532.

[104] W. Neubrand, Modellbildung und Simulation von Elektromembranverfahren, Logos-Verlag, 1999.

[105] J. T. Pukrushpan, H. Peng, A. G. Stefanopoulou, Simulation and analysis of transient fuel cell system performance based on a dynamic reactant flow model, in: ASME 2002 International Mechanical Engineering Congress and Exposition, American Society of Mechanical Engineers, 2002, pp. pp. 637–648.

[106] Y. Shan, S.-Y. Choe, A high dynamic PEM fuel cell model with temperature effects, Journal of Power Sources 145 (1) (2005) pp. 30–39.

[107] H. Ju, H. Meng, C.-Y. Wang, A single-phase, non-isothermal model for PEM fuel cells, International Journal of Heat and Mass Transfer 48 (7) (2005) pp. 1303–1315.

[108] Y. Shan, S.-Y. Choe, Modeling and simulation of a PEM fuel cell stack considering temperature effects, Journal of Power Sources 158 (1) (2006) pp. 274–286.

[109] Bahia Bench V2.1-A1, `http://www.areva.com/EN/operations-4576/bahia-bench-overview.html`.

[110] P. Wilmott, S. Howison, J. Dewynne, The mathematics of financial derivatives: a student introduction, Cambridge University Press, 1995.

[111] P. J. Olver, Introduction to partial differential equations, Springer, 2014.

[112] MATLAB, `http://mathworks.com/products/matlab/`.

[113] Toyota mirai, `http://www.toyota.com/mirai/fcv.html`.

[114] S. Samuel, L. Austin, D. Morrey, Automotive test drive cycles for emission measurement and real-world emission levels-a review, Proceedings of the Institution of Mechanical Engineers, Part D: Journal of Automobile Engineering 216 (7) (2002) pp. 555–564.

[115] L. Pelkmans, P. Debal, Comparison of on-road emissions with emissions measured on chassis dynamometer test cycles, Transportation Research Part D: Transport and Environment 11 (4) (2006) pp. 233–241.

[116] UN, E/ECE/TRANS/505/Rev.2/Add.100/Rev.3/Amend.1 agreement concerning the adoption of uniform technical prescriptions for wheeled vehicles, equipment and parts which can be fitted and/or be used on wheeled vehicles and the conditions for reciprocal recognition of approvals granted on the basis of these prescriptions (2013).

[117] J.-J. E. Slotine, W. Li, et al., Applied nonlinear control, Vol. 199, Prentice-Hall Englewood Cliffs, NJ, 1991.

[118] J. Hedrick, A. Girard, Control of nonlinear dynamic systems: Theory and applications, Controllability and Observability of Nonlinear Systems.

[119] J. L. Casti, Nonlinear system theory, Vol. 175, Academic Press, 1985.

[120] H. K. Khalil, J. Grizzle, Nonlinear systems, Vol. 3, Prentice hall New Jersey, 1996.

[121] W. Merida, D. Harrington, J. Le Canut, G. McLean, Characterisation of proton exchange membrane fuel cell (PEMFC) failures via electrochemical impedance spectroscopy, Journal of Power Sources 161 (1) (2006) pp. 264–274.

[122] P. A. Tipler, G. Mosca, Physics for scientists and engineers, Macmillan, 2007.

[123] Met One 083E relative humidity sensor, `http://www.metone.com/docs/083e_datasheet.pdf`.

[124] Bronkhorst EL-FLOW, `http://www.bronkhorst.com/en/products/gas_flow_meters_and_controllers/elflow_select/`.

[125] J. Davila, L. Fridman, A. Pisano, E. Usai, Finite-time state observation for non-linear uncertain systems via higher-order sliding modes, International Journal of Control 82 (8) (2009) pp. 1564–1574.

[126] W. Chen, D. Ballance, P. Gawthrop, J. O'Reilly, A nonlinear disturbance observer for robotic manipulators, IEEE Transactions on Industrial Electronics 47 (4) (2000) pp. 932–938.

[127] W. Chen, Nonlinear disturbance observer-enhanced dynamic inversion control of missiles, Journal of Guidance, Control and Dynamics 26 (1) (2003) pp. 161–166.

[128] W. Chen, Disturbance observer based control for nonlinear systems, IEEE/ASME Transactions on Mechatronics 9 (4) (2004) pp. 706–710.

[129] L. Guo, W. Chen, Disturbance attenuation and rejection for systems with nonlinearity via DOBC approach, International Journal of Robust and Nonlinear Control 15 (3) (2005) pp. 109–125.

[130] J. Yang, W. Chen, S. Li, Non-linear disturbance observer-based robust control for systems with mismatched disturbances/uncertainties, IET Control Theory & Applications 5 (18) (2011) pp. 2053–2062.

[131] J. Yang, S. Li, X. Yu, Sliding-mode control for systems with mismatched uncertainties via a disturbance observer, IEEE Transactions on Industrial Electronics 60 (1) (2013) pp. 160–169.

[132] A. Levant, Sliding order and sliding accuracy in sliding mode control, International Journal of Control 58 (6) (1993) pp. 1247–1263.

[133] W. Perruquetti, J. P. Barbot, Sliding mode control in engineering, CRC Press, 2002.

[134] A. Estrada, L. Fridman, Quasi-continuous HOSM control for systems with unmatched perturbations, Automatica 46 (11) (2010) pp. 1916–1919.

[135] A. G. Loukianov, Robust block decomposition sliding mode control design, Mathematical Problems in Engineering 8 (4-5) (2002) pp. 349–365.

[136] S. K. Spurgeon, Sliding mode observers: A survey, International Journal of Systems Science 39 (8) (2008) pp. 751–764.

[137] L. Grüne, J. Pannek, Nonlinear model predictive control, in: Nonlinear Model Predictive Control, Springer, 2011, pp. pp. 43–66.

[138] A. Vahidi, W. Greenwell, A decentralized model predictive control approach to power management of a fuel cell-ultracapacitor hybrid, in: American Control Conference, New York, NY, USA, 2007, pp. pp. 5431–5437.

[139] A. Arce, D. R. Ramirez, A. J. del Real, C. Bordons, Constrained explicit predictive control strategies for PEM fuel cell systems, in: 46th IEEE Conference on Decision and Control, New Orleans, LA, USA, 2007, pp. pp. 6088–6093.

[140] M. Fiacchini, T. Alamo, C. Albea, E. F. Camacho, Adaptive model predictive control of the hybrid dynamics of a fuel cell system, in: IEEE International Conference on Control Applications, Signapore, 2007, pp. pp. 1420–1425.

[141] Q. Chen, S. Quan, C. Xie, Nonlinear predictive control for oxygen supply of a fuel cell system, in: International Joint Conference on Neural Networks, Atlanta, GA, USA, 2009, pp. pp. 518–521.

[142] A. J. del Real, A. Arce, C. Bordons, Hybrid model predictive control of a two-generator power plant integrating photovoltaic panels and a fuel cell, in: 46th IEEE Conference on Decision and Control, New Orleans, LA, USA, 2007, pp. pp. 5447–5452.